ABSTRACT

Title of Document: ORIENTATION DEPENDENCE OF THE PIEZOELECTRIC PROPERTIES OF EPITAXIAL FERROELECTRIC THIN FILMS

Jun Ouyang, Doctor of Philosophy, 2005

Directed By: Professor Alexander. L. Roytburd
Dept. of Materials Science and Engineering

There are both intrinsic piezoelectric response and extrinsic piezoelectric response in ferroelectric materials. The intrinsic piezoelectric response is due to the lattice deformation of a single-domain crystal, which can be characterized by tensors of piezoelectric constants. The extrinsic piezoelectric response depends on extrinsic sources of displacement under the electric field, which can be the movement of domain walls, phase boundaries, or even defects like grain boundaries or dislocations. Due to the elastic interaction between an epitaxial ferroelectric thin film and a substrate, the piezoelectric properties of an epitaxial ferroelectric film are different from those of bulk ferroelectric materials. This work is the first study on the general orientation dependence of the piezoelectric properties of epitaxial ferroelectric thin films, which includes both theoretical and experiment work on intrinsic and extrinsic piezoelectric properties of epitaxial ferroelectric films.

A complete theoretical analysis of intrinsic piezoelectric responses in a single domain ferroelectric film, which are characterized by effective longitudinal, transverse and shear piezoelectric coefficients, is presented in this dissertation.

On the part of extrinsic piezoelectric response, our recent work on the piezoelectric properties of epitaxial thick lead titanate zirconate ($Pb(Zr_xTi_{1-x})O_3$ with x=0.52) films with tetragonal distorted structures will be presented as an example. It is shown that (011) oriented epitaxial films had much enhanced piezoelectric responses as compared with those of (001) and (111) oriented films. Detailed structure analysis showed that instead of an interconnected 3-domain (3-D) architecture that is usually found in a (001) oriented thick film, the (011) films consisted of a dominant 2-domain (2-D) architecture, by which the pinning between neighboring domain walls is much reduced. This study demonstrate the possibility of achieving high extrinsic piezoelectric responses by optimizing the epitaxial relationship between the film and substrate with respect to the domain mobility, and should also be instructive to the design of ferromagnetic and ferroelastic thin film devices used for transducer applications..

ORIENTATION DEPENDENCE OF THE PIEZOELECTRIC PROPERTIES OF EPITAXIAL FERROELECTRIC THIN FILMS

By

Jun Ouyang

Dissertation submitted to the Faculty of the Graduate School of the
University of Maryland, College Park in partial fulfillment
of the requirements for the degree of
Doctor of Philosophy
2005

Advisory Committee:
Professor, Alexander Roytburd, Chair
Professor, John Melngailis
Professor, Manfred Wuttig
Associate Professor, Ichiro Takeuchi
Adjunct Professor, James R. Cullen

Dedication

To My Grandma, Heguan Sheng, a great Chinese woman who best embodies the traditional oriental virtues of diligence, patience, bravery, and dedication to family.

Acknowledgements

I would like to express my sincere gratitude to my advisor, Prof. Alexander L. Roytburd, for giving me the opportunity to work on this interesting and challenging project, and more importantly, his guidance and support throughout the course of my graduate study and research. I benefited from all the discussions we had. It was his wide knowledge in materials science especially on thermodynamics of elastic domains, creative thoughts and sparkling of fresh ideas, dedication to scientific excellence, and most important, his pure love and enthusiasm toward scientific research, that had led to every progress in my Ph.D. research. The same gratitude goes to Prof. R. Ramesh, who served as my co-advisor before and after he left for University of California, Berkeley. It is a great honor for me to have been a part of his team at the Advanced Thin Film Laboratory, which is at the forefront of research in oxide thin film functional materials. His enthusiasm and energy, great instinct on picking up cutting-edge scientific topics, dedication and the drive for academic excellence have been primary motivating factors in this dissertation. I thank both of them for providing me with numerous opportunities to participate in conferences, for these are essential in building confidence and networks.

I would like to thank Prof. Chang-Beom Eom and Dr. Dong Ming Kim at University of Wisconsin, Madison for their support on providing excellent quality epitaxial PZT thick film samples by magnetron sputtering. I am also very grateful to Prof. Susan Trolier-McKinstry and Prof. Wenwu Cao at Penn State University for inspiring and fruitful discussions with them.

I would also like to express my gratitude to Dr. Igor Levin and Dr. Julia Slutsker in National Institute of Standards and Technology, for providing numerous discussions

and suggestions, which has proved to be an indispensable part of this dissertation work. Dr. Levin's expertise in structure analysis and Dr. Slutsker's thermodynamic knowledge and modeling skills have been especially helpful to my understanding of the project.

I would like to thank Prof. John Melngailis, Prof. Manfred Wuttig Prof. I. Takeuchi and Prof. James R. Cullen for taking time out of their busy schedules to review my work.

I specially thank Dr. V. Nagarajan and S. Prasertchoung for leading me into the electrical characterization by scanning probe microscopy; Dr. T. Zhao and Dr. Junling Wang for helping me with the PLD thin film preparation; Ladan Mohaddes-ardabili for introducing me structural analysis by XRD; Zhengkun Ma for numerous times of focus ion beam milling on my samples; S.-Y. Yang for teaching me using ferroelectric tester and impedance-gain phase analyzer; Dr. Haimei Zheng for TEM sample preparation, etc. All the friends and collaborators at University of Maryland, thank you for your support and friendship.

Finally, I want to thank my parents and my fiancée for their love and support. I owe everything I achieved to them. This dissertation is dedicated to them.

TABLE OF CONTENTS

LIST OF FIGURES

LIST OF TABLES

CHAPTER 1, INTRODUCTION

1.1 Piezoelectricity and ferroelectricity

Piezoelectricity

Piezoelectricity was first discovered by Curie brothers in 1880 on the observation of surface charges induced by mechanical deformation of a quartz crystal (direct piezoelectric effect). The converse piezoelectric effect was verified by Curie brothers one year later, following Lippmann's prediction based on the thermodynamic principle of reversible processes.

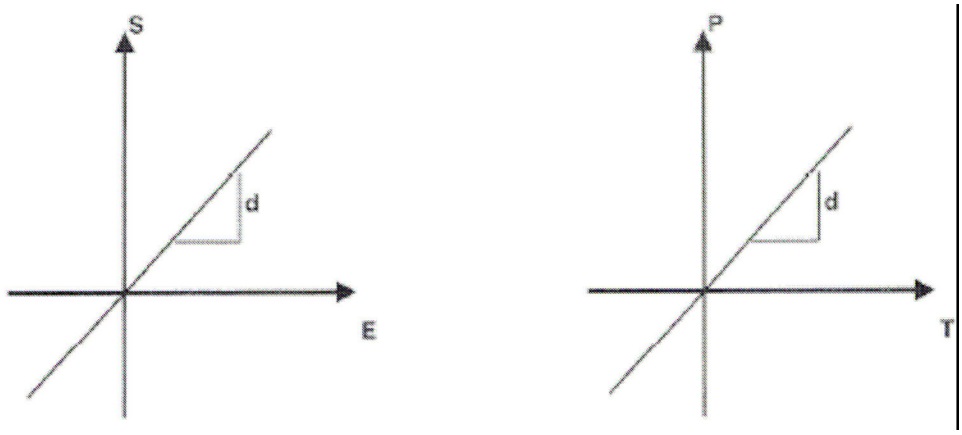

Fig. 1.1 (a) Converse piezoelectricity and (b) direct piezoelectricity. S - mechanical strain, E - electric field strength, P - electrical polarization, T - Mechanical stress.

A piezoelectric crystal may be defined as a crystal in which "electricity or electric polarity" is produced by mechanical deformation, or as one that becomes deformed when in an electric field. Piezoelectricity is different from electrostriction on that the sign of an induced electric polarity/mechanical strain becomes reversed as the sign of an applied mechanical stress/electric field does so. From this point of view, a piezoelectric crystal

must have certain *one-wayness* in its internal structure; in other words, it must have a structural "bias" that determines whether a given region on the surface shall show a positive or negative charge on compression. In the converse effect, the same one-wayness determines the sign of the deformation when an electric field is applied to the crystal.

All crystals can be divided into 32 classes or point groups (from 7 basic crystal systems). The 32 point groups can be further classified into (a) 11 point groups having a centre of symmetry and (b) 21 point groups that do not possess a centre of symmetry. A lack of a centre of symmetry is all-important for the presence of piezoelectricity. As shown in Fig. 1.2, the lack of a centre of symmetry means that a net movement of the positive and negative ions with respect to each other as a result of stress produces an electric dipole, whereas, for the centro-symmetric crystals, the centres of charges of different polarity will still coincide even after the stress inducing a deformation. Of the 21 non-centrosymmetric point groups, 20 are piezoelectric (one class, although lacking a centre of symmetry, is not piezoelectric because of the combination of other symmetry elements) [1]. The basic equations that describe these two effects in regard to electric and elastic properties are:

$$\begin{aligned} D_i &= \varepsilon_{ij}^{T} E_j + d_{ijk} T_{jk} \\ S_{ij} &= d_{ijk} E_k + s_{ijkl}^{E} T_{kl} \end{aligned} \tag{1.1}$$

Here D is the dielectric displacement vector, E is the electric field vector, T is the mechanical stress tensor, S is the mechanical strain tensor, d is the tensor of piezoelectric

constants, ε is the tensor of dielectric constants (superscript T means under constant stress, i.e. mechanically free condition), s is the tensor of mechanical compliance (superscript E means under constant E field, i.e. short-circuit condition) [2].

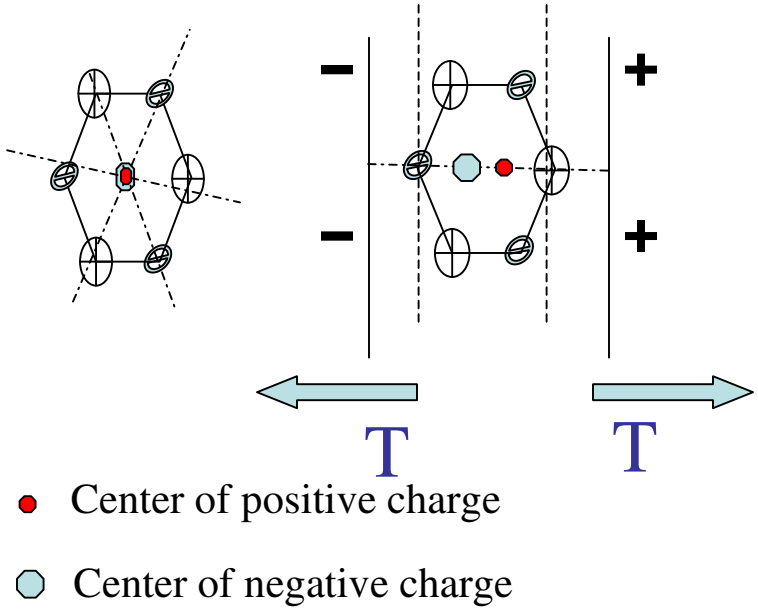

Fig. 1.2. Schematics of a piezoelectric crystal (a) under a tensile stress (b).

Pyroelectricity

Out of the 20 point groups which show the piezoelectric effect, 10 point groups have only a unique polar axis. In absence of any load, they develop a polarization spontaneously and form a permanent dipole within the unit cell. Such kinds of crystals are called polar crystals. The spontaneous polarization (P_{spon}) is defined as the value of dipole moment per unit volume or the value of charge per unit area on the surface perpendicular to the axis of spontaneous polarization. The value of spontaneous polarization depends on the temperature (Θ), this phenomenon is called pyroelectric

effect and the crystals with this effect are called pyroelectrics [3]. The pyroelectric effect can be described in terms of pyroelectric coefficient p as shown in

$$\Delta P_{spon} = p\Delta\Theta \tag{1.2}$$

Ferroelectricity

A subgroup of the spontaneously polarized pyroelectrics is a very special category of materials known as ferroelectrics. By definition, ferroelectrics are polar materials that possess at least two equilibrium orientations of the spontaneous polarization vector in the absence of an external electric field, and in which the spontaneous polarization vector may be switched between those orientations by an electric field.

Among all the ferroelectric materials, the most extensively studied and widely used are the perovskite ferroelectrics. A perfect perovskite structure has a general formula of ABO_3, where A represents a divalent or trivalent cation, and B is typically a tetravalent or trivalent cation. The origin of ferroelectricity in this family of materials can be explained using the well-known example of Barium titanate ($BaTiO_3$). As shown in Figure 1.3, the Ba^{2+} cations are located at the corners of the unit cell. A dipole moment occurs due to relative displacements of the Ti^{4+} and O^{2-} ions from their symmetrical positions. A good introduction to the theories of ferroelectrics and the Laudau-Ginzburg-Devonshire (LGD) equation can be found in [6] and will not be repeated here.

The interrelationship of piezoelectrics and subgroups can be seen in Fig. 1.4. All ferroelectrics are piezoelectrics, but not all piezoelectrics are ferroelectrics. Ferroelectric materials with high piezoelectric constants are widely used in transducer applications.

The direct effect is suitable for sensor applications, and the inverse effect can be exploited for actuator, as shown in Fig. 1.5.

Depending on the symmetry of the crystal, Eq. (1.1) may have a simple or complex full expression. For example, for a tetragonal distorted ferroelectric crystal, there are only three independent piezoelectric constants, d_{33}, d_{31}, and d_{15}. Fig 1.6 illustrates these piezoelectric constants in the converse piezoelectric effects. For a single domain ferroelectric crystal, these piezoelectric constants are correlated with the self-polarization as calculated from LGD phenomenological theory in Eq. (1.3) [6]. Where Q_{ij} and ε_{ij} are the electrostrictive and dielectric constants of the crystal, P_s is the spontaneous polarization, and ε_0 is the vacuum dielectric constant.

$$d_{33} = 2\varepsilon_0\varepsilon_{33}Q_{11}P_s$$

$$d_{31} = d_{32} = 2\varepsilon_0\varepsilon_{33}Q_{12}P_s$$

$$d_{15} = d_{24} = \varepsilon_0\varepsilon_{11}Q_{44}P_s \qquad (1.3)$$

From Eq. (1.3), it can be seen that any process involving a change in polarization or dielectric constant (for example, movement of ferroelectric domain walls, poling of ferroelectric ceramics, phase transition occurred in ferroelectrics which varies the polarization, etc) may affect the magnitude of piezoelectric constants in ferroelectric crystals. In fact, it is where the piezoelectric properties of ferroelectrics differ from those of non-ferroelectric piezoelectric crystals (like quartz). The following sections of this chapter will discuss those extrinsic effects on piezoelectric properties of ferroelectric materials. Due to the equivalence between direct and converse piezoelectric effects, the discussions of piezoelectric effects in bulk materials are limited to converse piezoelectric

effects (section 1.2 and 1.3), while for thin film ferroelectric materials, this equivalence will be “broken” apparently, and we will discuss briefly in this chapter on both direct and converse piezoelectric effects in ferroelectric thin films (section 1.3).

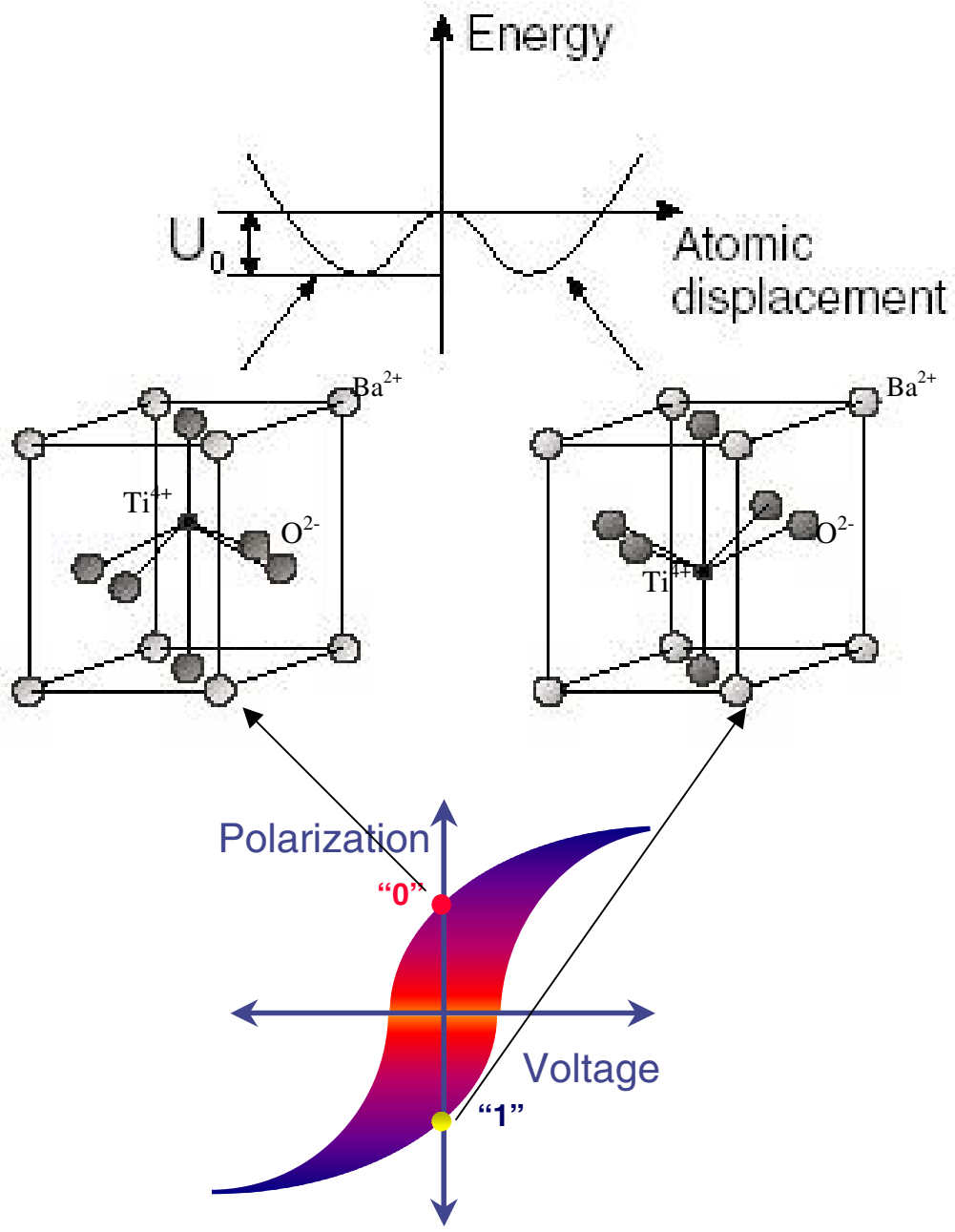

Fig. 1.3 (a) Schematic illustration of the unit cell of perovskite lead titanate ferroelectric crystals. Figure adapted from [4]. (b) Switchable polar states under electric field enable applications for memory devices.

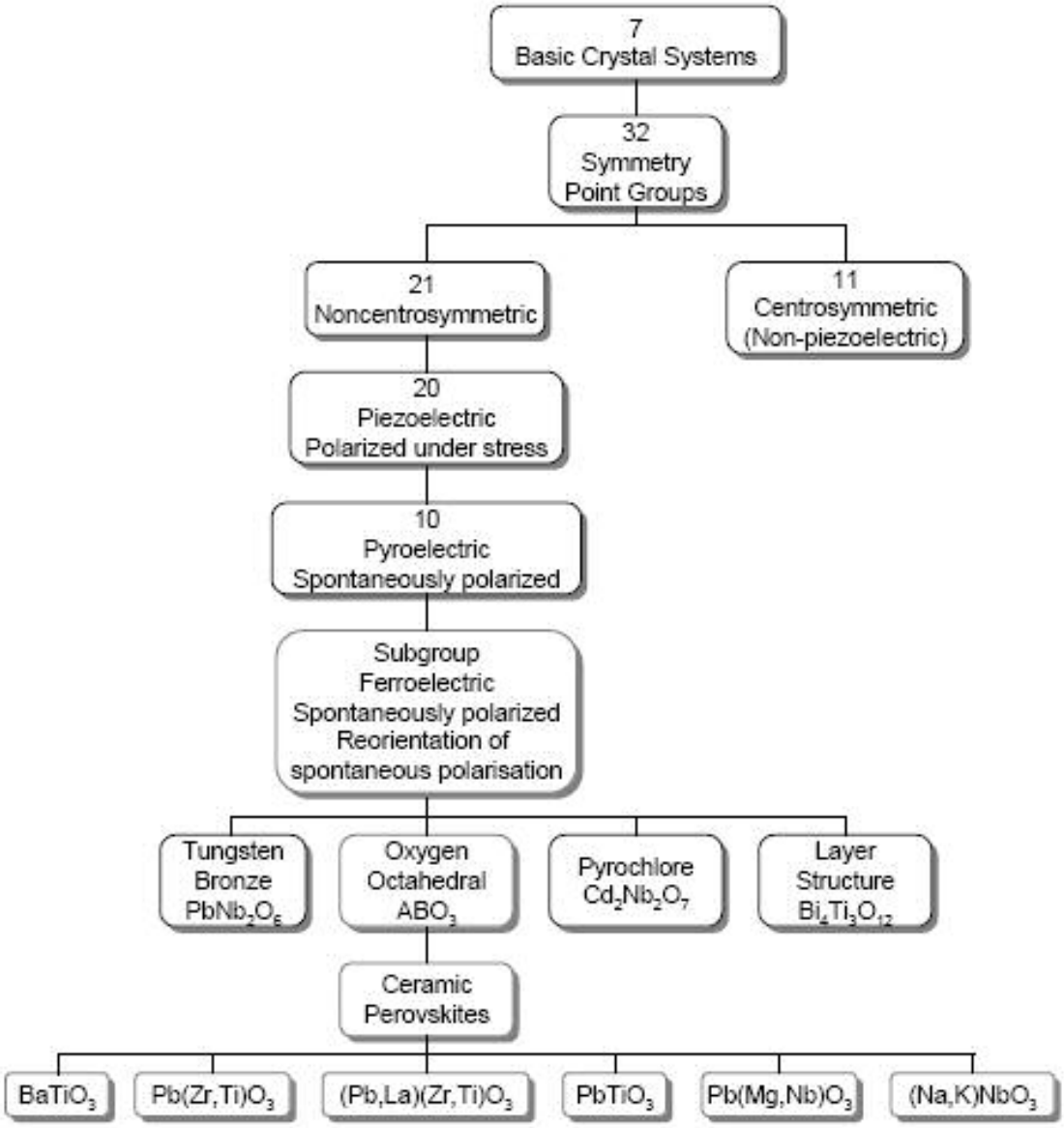

Figure 1.4. Interrelationship of piezoelectrics and subgroups on the basis of symmetry. Figure adapted from [1].

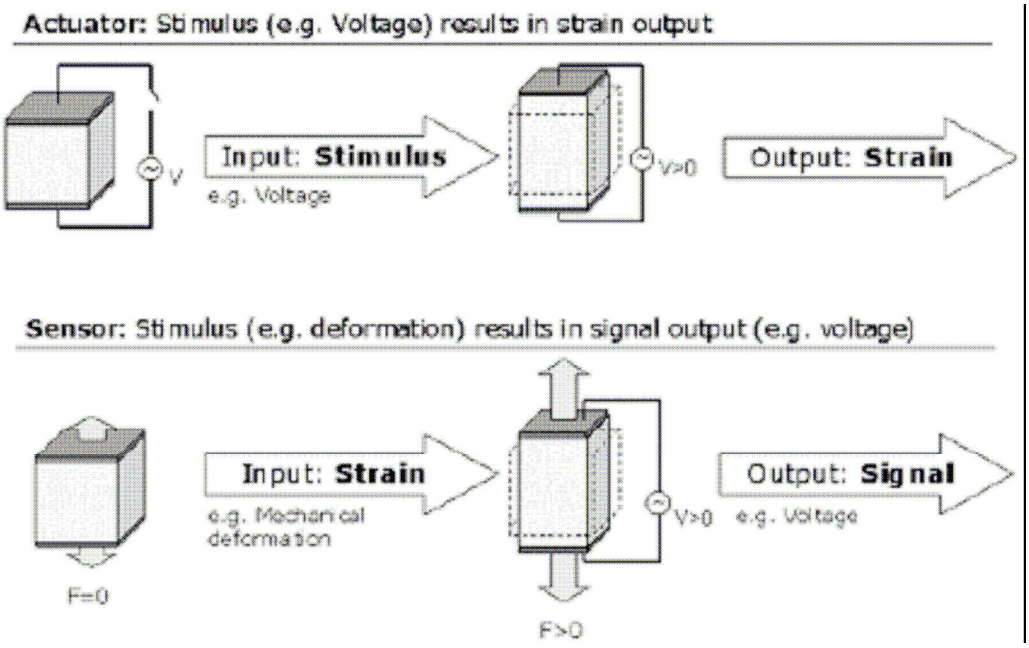

Figure 1.5. Ferroelectric materials used as actuator (top) and sensor (bottom). Figures adapted from [5].

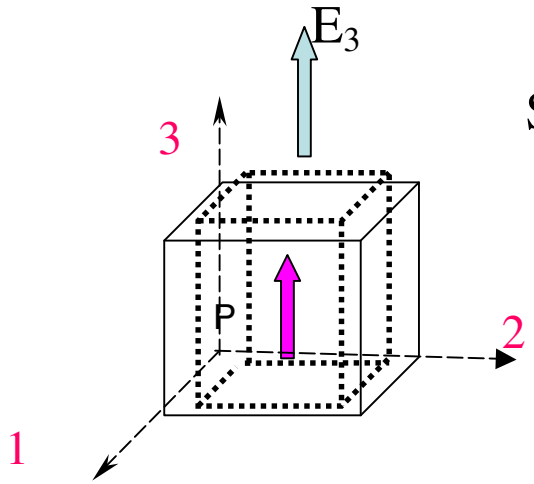

Strain induced by E_3

$$\varepsilon_1 = d_{31}E_3$$

$$\varepsilon_2 = d_{31}E_3$$

$$\varepsilon_3 = d_{33}E_3$$

Strain induced by E_2, E_1: $\varepsilon_4 = d_{15}E_2$ $\varepsilon_5 = d_{15}E_1$

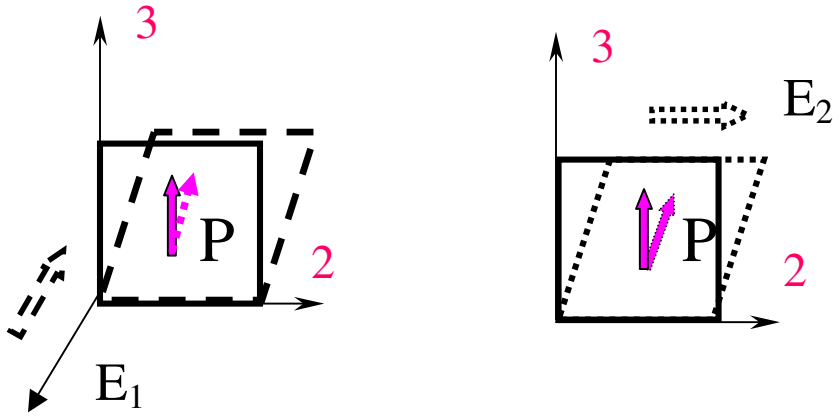

Fig. 1. 6 Equations of converse piezoelectric effects in a tetragonal ferroelectric crystal. P is the self-polarization of the crystal aligned along the tetragonal c-axis (axis 3).

1.2 Intrinsic v.s. extrinsic piezoelectric response

Intrinsic piezoelectric response refers to the piezoelectric deformation of the lattice of a single-domain crystal, which can be characterized by tensors of piezoelectric constants. In this case, the piezoelectric constants described in Eq. 1.3 may be called "intrinsic" piezoelectric constants, which describe piezoelectric effect as an electrostriction biased by the polarization (linearized electrostriction) [6]. The extrinsic piezoelectric response, on the other hand, are from extrinsic sources of displacement under the electric field, which can be movements of domain walls, phase boundaries, or even defects like grain boundaries or dislocations.

Intrinsic piezoelectric response

-Orientation dependence v.s. engineered domain configuration

The expression for a piezoelectric strain of a ferroelectric crystal is presented by Eq. (1.4) in pseudo cubic coordinates. Where d_{kij} are piezoelectric constants of a bulk crystal, E_k are components of the applied electrical field $\boldsymbol{E}$, $E_k = El_k$, and l_k are the direction cosines (the summation is taken over repetitive suffixes).

$$\varepsilon_{ij}^{0} = d_{kij}E_k = d_{kij}l_kE \qquad (i, j, k=1, 2, 3) \tag{1.4}$$

The length change along a normal $\boldsymbol{n}$ is determined by a normal strain $\varepsilon_{ij}^{0}\ n_i n_j$ and it can be characterized by a piezoelectric constant:

$$d_{ln} = d_{kij}l_k n_i n_j \ (i, j, k=1, 2, 3) \tag{1.5}$$

It is reduced to the longitudinal piezoelectric constant $d_{33}(n)=d_{nn}=d_{kij}n_k n_i n_j$ of a single crystal if the field is applied along the same normal n (Fig. 1.8).

The orientation dependence of intrinsic piezoelectric properties for PZT bulk materials near the morphotropic phase boundary (MPB-PZT) was phenomenologically calculated in [7], [8]. As shown in Fig. 1.7, it was found that for tetragonal PZT materials, the effective piezoelectric constant d_{33} has the maximum value in the spontaneous polarization direction [001]. However, for rhombohedral PZT materials, the maximum values of d_{33} can be obtained in the direction 56.7° canted from the polarization direction [111], which is very close to perovskite [001] directions.

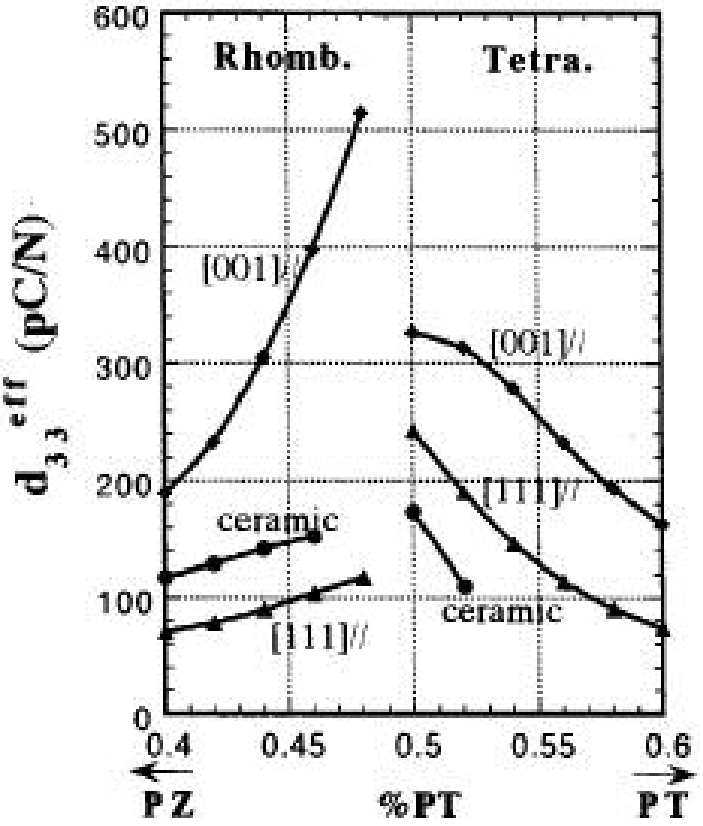

Fig. 1.7 Effective piezoelectric constants d_{33} of PZT with various compositions.

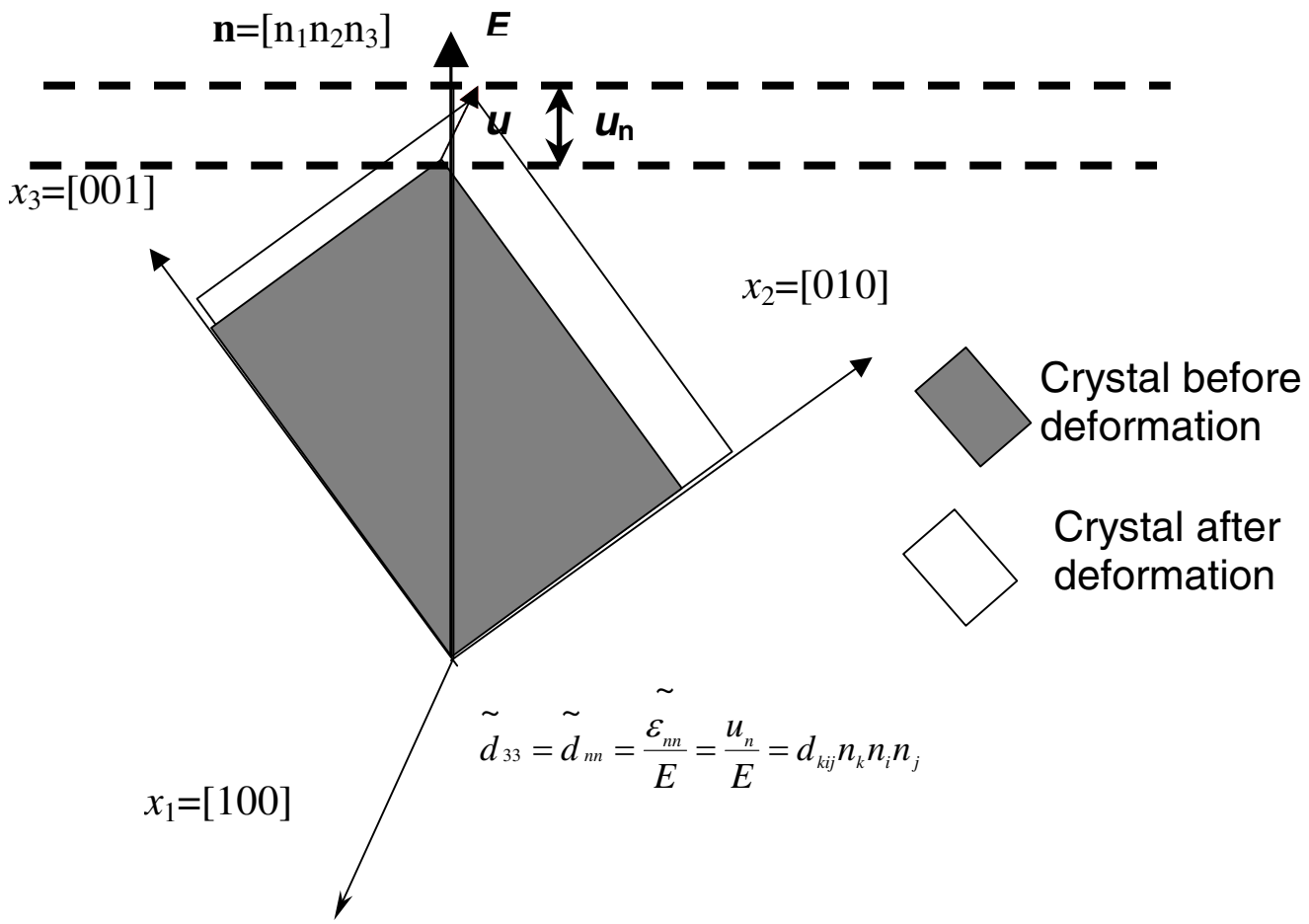

Fig. 1.8 Orientation dependence of longitudinal piezoelectric constants for single crystals

Method of domain engineering, which aims at enhancing the piezoelectric properties of ferroelectric materials by applying the electric field in a non-polar direction across the crystal, has been investigated intensively for the past decade. [9]-[12] The key points of the engineering domain configurations are: [10]

(1) There are crystallographically equivalent domains with inclined polarization to the applied electric field.

(2) Domain wall motion is inhibited, therefore the piezoelectric response is intrinsic. The resulting ε-E curve is hysteresis-free.

(3) Enhanced d_{33} along field direction than along polar direction.

(4) The composition or temperature of the ferroelectric crystal is close to phase transition.

S. Wada et al. [10] investigated piezoelectric properties of barium titanate single crystals at room temperature as a function of crystallographic orientation, and they found that a (111) oriented tetragonal $BaTiO_3$ single crystal, which is in an engineered domain configuration, had a higher longitudinal piezoelectric constant d_{33} (=203pm/V) than that of a (001) oriented one (d_{33} =125pm/V) (Fig. 1.9 a). This has been explained by D. Damjanovic et al. [12], [13] by the contribution to d_{33} from piezoelectric shear effect. Our recent calculation on the orientation dependence of d_{33} for tetragonal $BaTiO_3$ single crystal showed good agreement with the aforementioned experiment results (Fig 1.9 b). [14]. This verifies that the piezoelectric response of a domain engineered tetragonal ferroelectric crystals is "intrinsic".

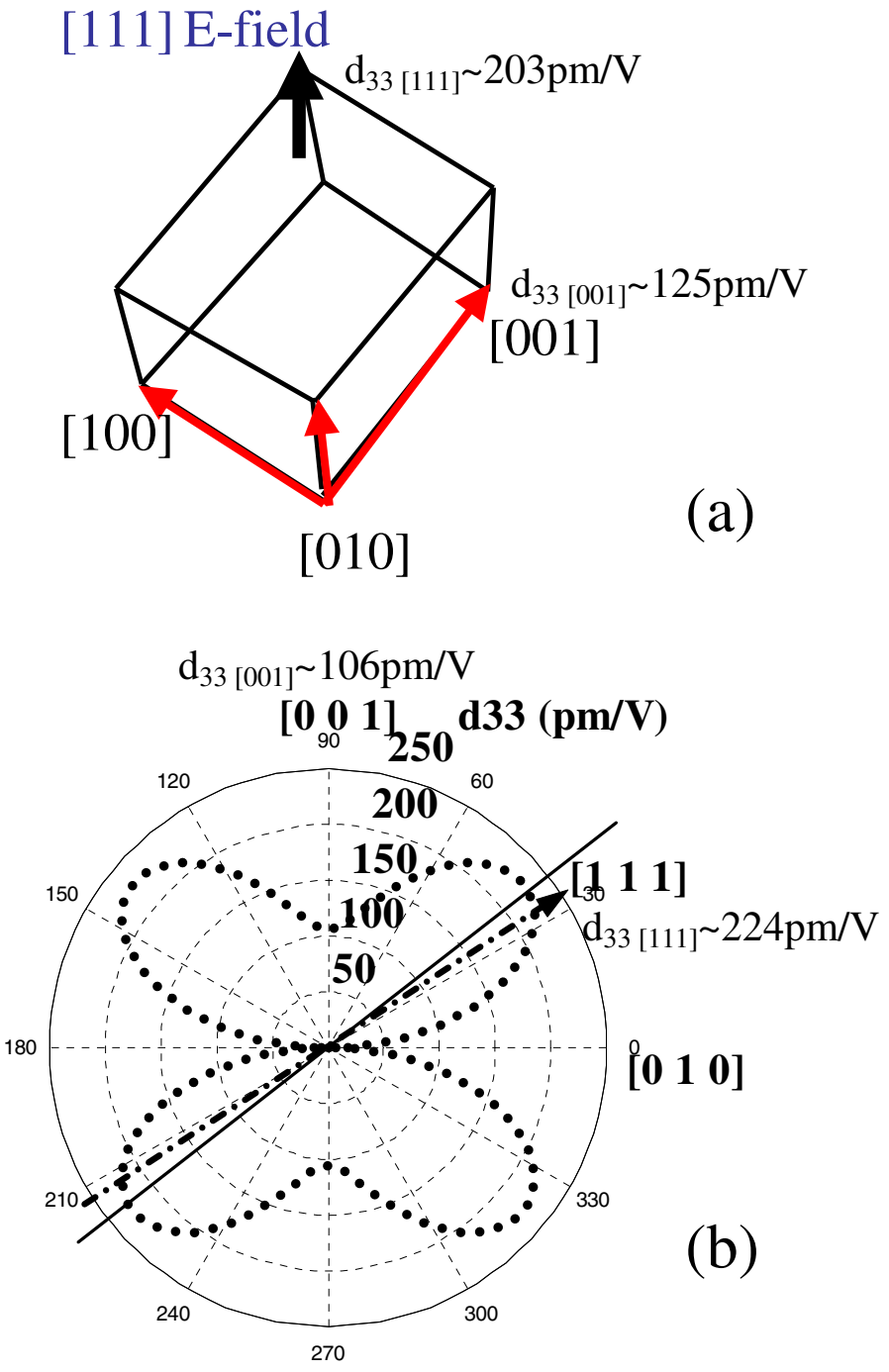

Fig. 1.9 (a) [111] poled 4mm crystal $BaTiO_3$ has measured d_{33} (at room temperature) much larger than d_{33} of [001] poled crystal; [9] (b) Calculated orientation dependence of d_{33} (at room temperature) for 4mm crystal $BaTiO_3$.

For relaxor based ferroelectrics on the rhombohedral side of their morphotropic phase boundaries, such as xPb($Mg_{1/3}Nb_{2/3}$)O_3-(1-x)$PbTiO_3$ (x<0.35), and xPb($Zn_{1/3}Nb_{2/3}$)O_3-(1-x)$PbTiO_3$ (x<0.09), giant piezoelectric constants (>2500 pm/V) can be achieved by poling the crystal in a pseudo-cubic (001) direction (Fig. 1.10).[9] Recently, Cao et al. studied both multi-domain (<001> oriented crystal) and single domain (<111> oriented crystal) properties of 0.67Pb ($Mg_{1/3}Nb_{2/3}$)O_3-0.33$PbTiO_3$ single crystals.[15]-[17] They attributed the origin of the superior electromechanical properties in the (001) direction to the large d_{15} of the single-domain properties, as they reproduced the large piezoelectric constants in multi-domain (001) crystals from single domain properties in the rotated coordinated system (Fig 1.11).[17] Further theoretical study[18], [19] showed that the low field piezoelectric constants for the engineered configuration are very close to those obtained for the corresponding single domain state and the domain wall influence is not significant. This result proves that the piezoelectric response of a domain engineered rhombohedral ferroelectric crystal is "intrinsic".

From the above two examples, it proves to be possible to estimate the effective piezoelectric constants of a multi-domain single crystal with an arbitrary orientation by knowing those calculated in a rotated coordinated system of a single crystal, providing that the domains constitute an engineered domain configuration, i.e, all domains are equivalent under the applied electric field.

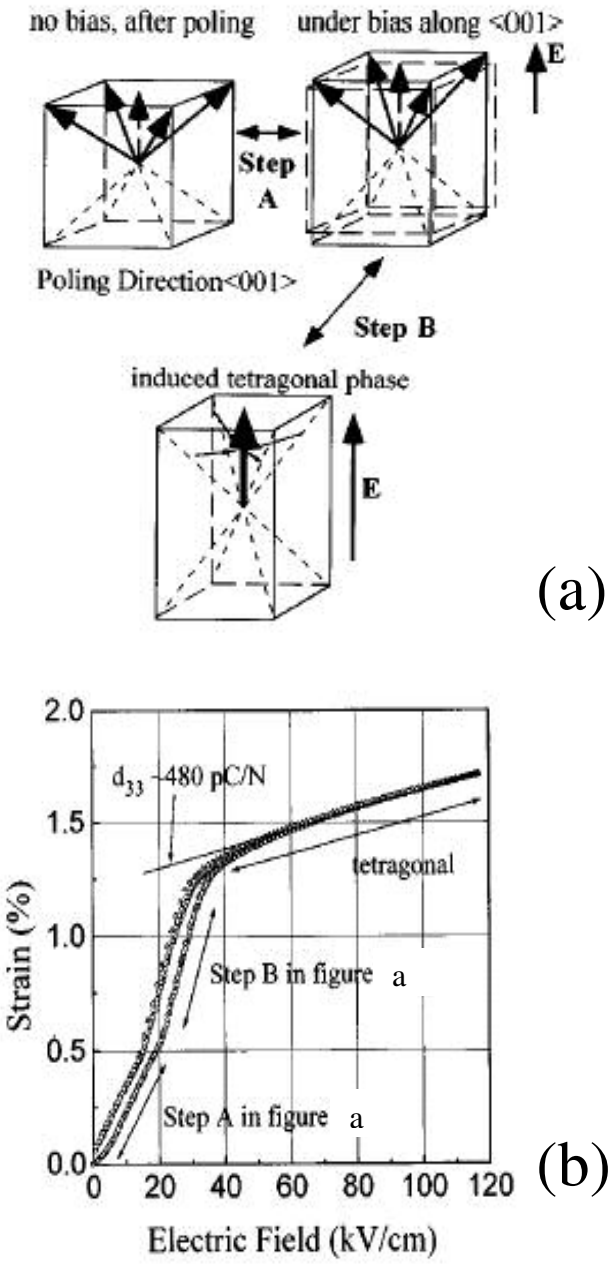

Fig. 1. 10. Ultra-high piezoelectric behavior discovered in PZN-8%PT single crystal in a engineered domain configuration: (a) Schematic diagram of domain configurations in <001)> oriented rhombohedral crystals under bias (step A-piezoelectricity, step B-induced phase transition). (b) Strain vs *E*-field behavior for <001> oriented PZN-8%PT crystal. Maximum field is limited by voltage limit of the apparatus.

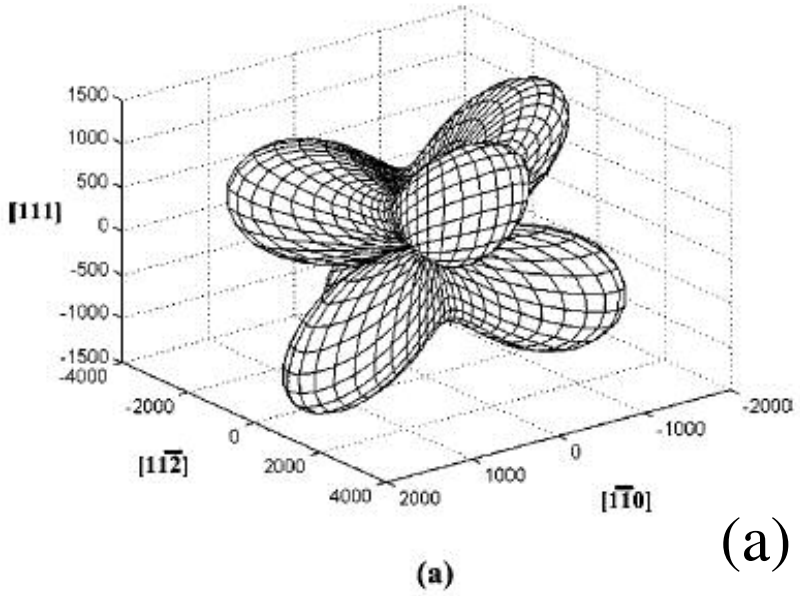

Measured d_{33}=2820 pC/N along (001)

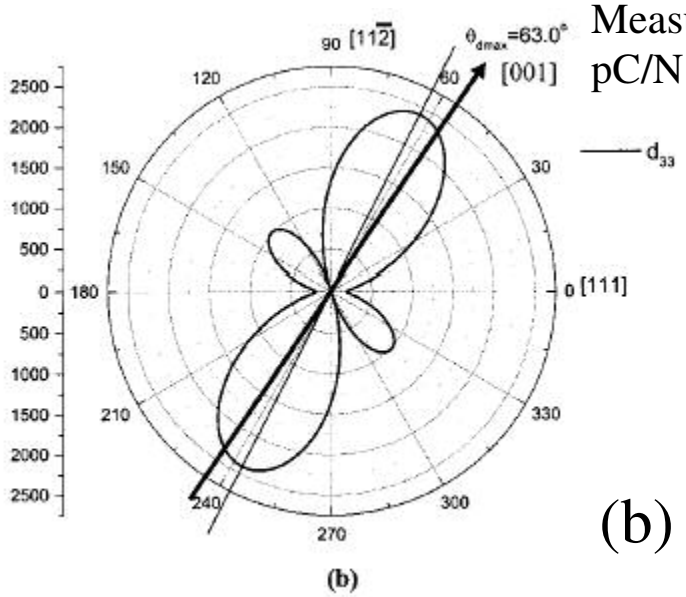

Fig 1.11. (a) Orientation dependence of effective piezoelectric constant d_{33} of PMN-33%PT single crystal with single domain. (b) Cross section plot of (a) in [1 1 1] – [1 1 –2] plane. Figures adapted from [17].

Extrinsic piezoelectric response

180^0 ferroelectric domains

As a consequence of minimization of the depolarization energy [20], ferroelectric 180^o domains are found in ferroelectric crystals with uncompensated surface charges or in unpoled ferroelectric ceramics. On the other hand, elastic non-180^o domains are formed as a consequence of the release of energy of internal stresses.[21] For example, in a tetragonal ferroelectric crystal like $BaTiO_3$, it has six domain variants when it transforms from a high temperature cubic phase (Fig 1.12).

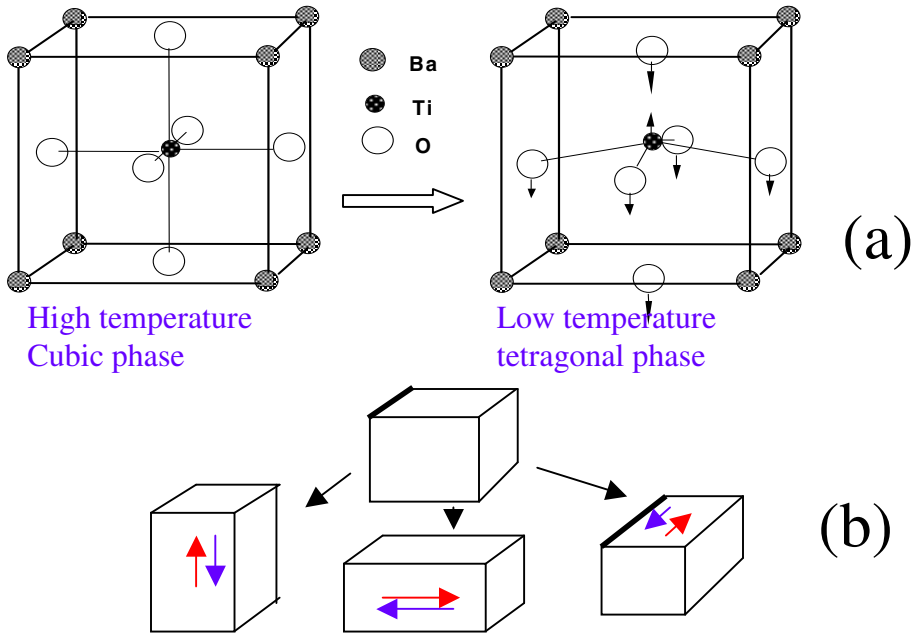

Fig 1.12 (a) Cubic to tetragonal phase transformation in $BaTiO_3$ crystal; (b) The tetragonal ferroelectric phase has six different domains.

In Fig. 1.13, it is illustrated how the surface displacement of an partially poled ferroelectric crystal is affected by the change of fraction of 180° domains α. It can be seen that when there are equivalent fractions of the two sets of 180° domains (α=0.5), which deform in opposite directions under an applied electric field, the apparent d_{33} is zero. When the volume fraction of 180° domains decrease by the movement of domain walls (α goes to 0 or 1), the apparent d_{33} will increase and approach the intrinsic d_{33} value. A detailed investigation on the effect of 180° degree domains on piezoelectric properties of ferroelectric materials (both bulk crystal and film) will be found in [22].

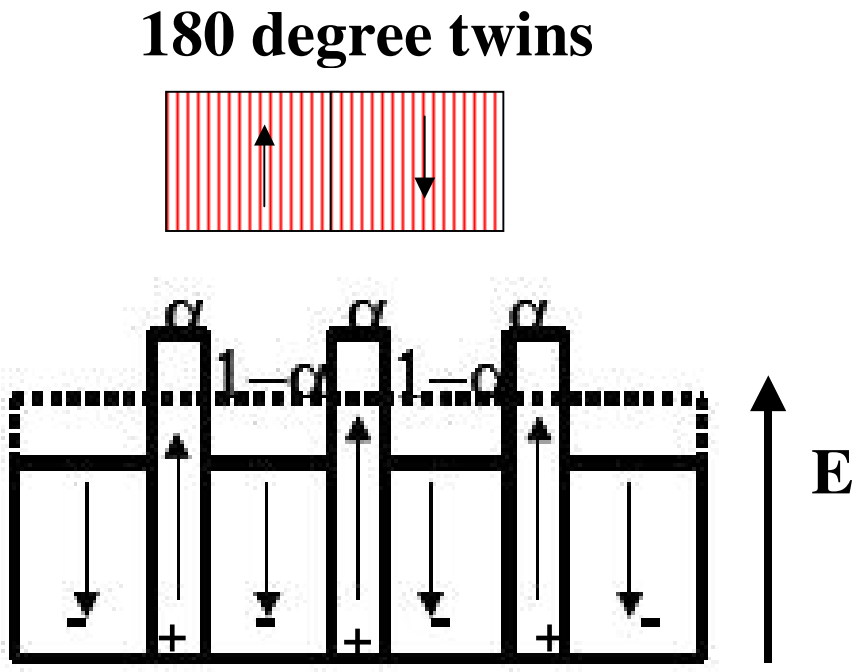

Fig. 1.13: Effect of 180° degree domains on longitudinal d_{33} piezoelectric response. α is the fraction of domains with polarization aligned along the applied electric field ("+" domain), 1-α is the fraction of domains with polarization aligned opposite to the applied electric field ("-" domain). The level of the dashed line is the surface of the crystal when there is no electric field applied.

non-180° elastic domains

Although the switching of 180° domains will affect the apparent piezoelectric constants, it will not substantially increase the piezoelectric strain since the lattice parameters of opposite 180° domains are the same. On the other hand, for non-180° elastic domains, switching between different domain variants will bring large extrinsic piezoelectric strains as shown in Fig 1.14. In the case of a tetragonal ferroelectric crystal, the extrinsic piezoelectric strain can be as high as the tetragonality if the 90° switching between in-plane *a*-domains and out-of-plane *c*- domains takes place. This type of extrinsic piezoelectric response dominates in soft-ferroelectrics like MPB-PZT ceramics.

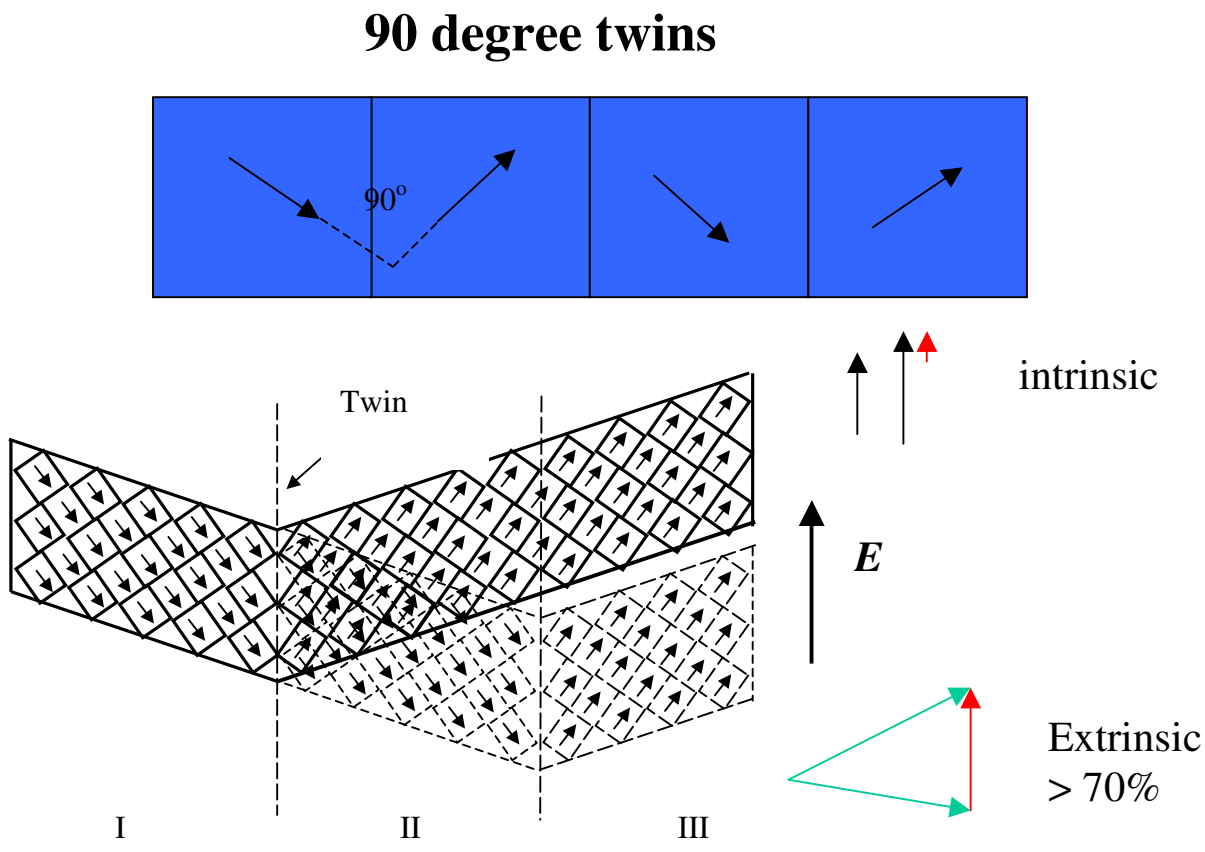

Fig. 1.14: Effect of 90° degree domain wall movement on longitudinal piezoelectric response. It can be seen that the extrinsic contribution dominates the total strain.

Electric field induced phase transitions/polarization rotations

Field-induced phase transitions will significantly change the piezoelectric properties of ferroelectric materials. One such example is illustrated in Fig 1.10. A rhombohedral 3m ferroelectric crystal with its engineered domain configuration (poling along pseudo-cubic <001>) will ultimately transform into a tetragonal 4mm symmetry under an increasing electric field. The piezoelectric strain curve is then characterized by three stages, the initial stage of engineered domain configuration under small electric field, the transition stage, and the final stage of induced tetragonal single domain configuration. While the first and third stage of the piezoelectric response are well characterized by "intrinsic" piezoelectric constants, the transition stage is not.

M. Iwada and Y. Ishibashi's work based on LGD type phenomenological theory has shown the enhancement of d_{33} for engineered domain configurations in both tetragonal and rhombohedral phases, as well as the critical electric fields at which the engineered domains lose their stabilities and phase transitions take place.[23]-[24] However, in order to obtain analytical results, the LGD equation used had to be truncated at 4^{th} order terms, which had undermined the applicability of these results.

Another important piece of research work in this theoretical framework was by M. Budimir and D. Damjanovic et al.[12] They studied the piezoelectric anisotropy–phase transition relations in perovskite single crystals. It was shown that a presence of the ferroelectric–ferroelectric phase transitions in $BaTiO_3$ leads to enhanced effective d_{33} along non-polar directions, while for $PbTiO_3$ which does not exhibit ferroelectric–ferroelectric phase transitions, effective d_{33} has its maximum along the polar axis at all temperatures. This work illustrated the correlation between a large effective d_{33} in a non-

polar direction and a softened lattice in the shear direction. When the ferroelectric lattice is in the vicinity of a phase transition which rotates the polar vector, the shear direction corresponding to this rotation will become "soft", which means a larger compliance for easier shear deformation, no matter this deformation is caused by a temperature driven process or a piezoelectric force. In this case, the shear piezoelectric coefficient will be large enough to vary the orientation dependence of d_{33} ($BaTiO_3$). On the other hand, if the ferroelectric lattice is far from a phase transition, the shear directions are all "stiff", which means easy piezoelectric deformation is not possible and the shear piezoelectric coefficients are low. For $PbTiO_3$ material, it is far from its morphotropic phase boundary and is a very stable tetragonal structure. Consequently, it has very low shear piezoelectric coefficients and the longitudinal piezoelectric coefficients will dominate the effective d_{33}.

Recent study on lead zirconate titanate ($Pb[Zr_{1-x}Ti_x]O_3$, abbreviated as PZT) bulk materials with a composition near its morphotropic phase boundary (abbreviated as MPB, x~0.5, which has a wide variety of applications, such as sensors, actuators and dielectrics, due to its superior electromechanical properties) revealed the presence of a monoclinic phase on the morphotropic phase boundary, which separates the tetragonal phase region on Ti-rich compositions and the rhombohedral phase region on Zr-rich compositions [25]. To account for the unusually high electromechanical constants associated with the morphotropic phase boundary, it was proposed that the monoclinic phase has a polarization vector aligned in a direction between those of the tetragonal phase (pseudo-cubic [001] direction) and the rhombohedral phase (pseudo-cubic [111] direction), and the polarization vector is apt to change its orientation under poling, which can lead to

large piezoelectric responses. According to the general piezoelectric anisotropy–phase transition relations demonstrated in Ref. [12], this special monoclinic phase capable of rotating its polarization vector may be understood as an intermediate phase between tetragonal and rhombohedral phases, which has a very soft shear modulus and consequently, large shear piezoelectric coefficients.

Fu and R. Cohen et al. proposed a polarization rotation mechanism [26] by first principle calculations to explain the ultrahigh electromechanical response discovered on $Pb(Zn_{1/3}Nb_{2/3})O_3$-$PbTiO_3$ (PZN-PT) single crystals[9]. In their calculations, a pevoskite $BaTiO_3$ single crystal was used as the model system to illustrate the rotation of the polarization vector under a canted poling field (Fig 1.15). The key points in this model are:

(1) The ground state of the crystal is rhombohedral phase.

(2) Strain level is high in tetragonal phase;

(3) Large elastic compliance (especially s_{44});

(4) Large effective charges.

They suggested that it might be a general mechanism for other perovskite ferroelectrics to have enhanced piezoelectric response by applying a electric field in a non-polar axis.

Fu's theoretical work and the experiment work on MPB-PZT were supported by the *ab initio* calculation on the poling paths in $PbZr_{1-x}Ti_xO_3$ single crystals. [27] Evolutions of field-induced low energy phases in domain engineered MPB-PZT ferroelectrics were revealed by L. Bellaiche et al. in Ref. [27], which cleared showed that monoclinic phases act as an intermediate "poling state" between tetragonal and rhombohedral phases. Further theoretical investigations were carried out by R. Cohen et

al. on elastic properties of MPB-PZT materials.[28], [29] It was found that the softness of MPB-PZT single crystals with respect to polarization rotation (large shear compliances) is directly responsible for its high electromechanical coupling.[29] Similar conclusions also made for relaxor ferroelectric materials near their MPBs.[28]

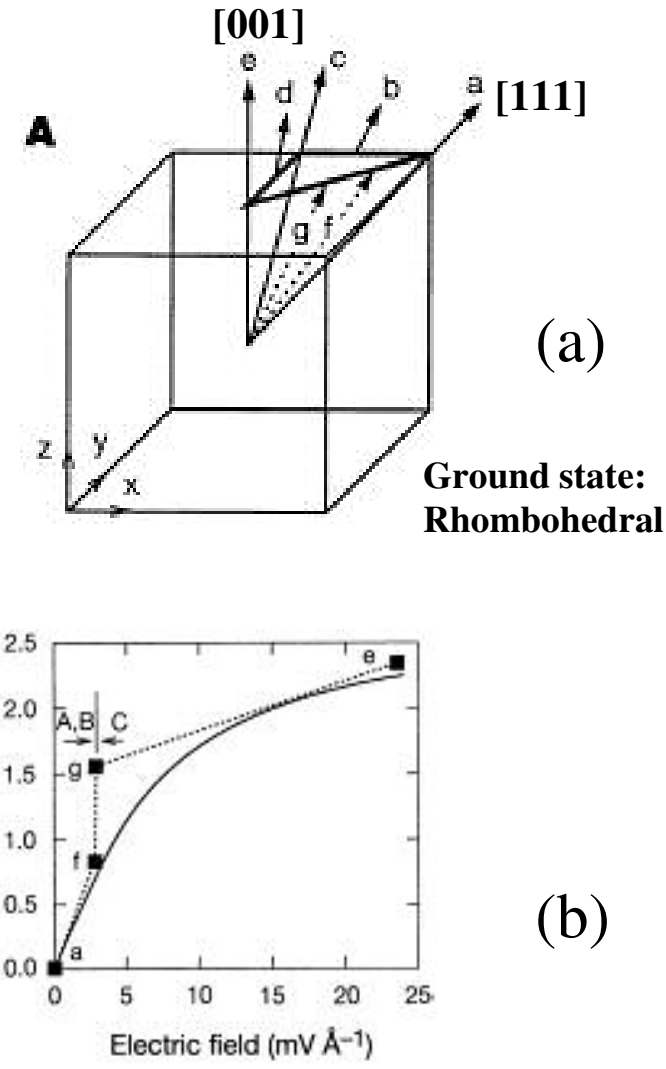

Fig. 1.15. First principle calculations for the longitudinal piezoelectric response of $BaTiO_3$. (a) Possible poling paths indexed by letters for a $BaTiO_3$ single crystal in a rhombohedral ground state, the electric field is applied along the pseudo-cubic [001] direction {e} while the polarization is aligned along [111] {a}. (b) Piezoelectric strain curve associated with the evolution of poling states with lowest energy.

1.3 Bulk ferroelectrics v.s. thin film ferroelectric films

In bulk ferroelectrics (single crystal or ceramics), the "direct" and "converse" piezoelectric effects have the same characteristic constants, which are equivalent thermodynamic potential derivatives.[30] It is convenient for people to characterize the piezoelectric properties of ferroelectric materials based on one of the two effects and use the obtained coefficients in applications based on the other effect.

Recently, there is an increasing number of research works on how to integrate ferroelectric films into MEMS devices, taking advantage of their excellent piezoelectric properties. [31]-[34] There are two major types of piezoelectric-based MEMS devices, microsensors and microactuators. Piezoelectric sensors usually utilize the direct piezoelectric effect of ferroelectric films, namely, to detect an environmental stress or strain by monitoring the piezoelectric charges (Fig 1.16 a). On the other hand, piezoelectric actuators usually utilize the converse piezoelectric effect, namely, to produce strains or stresses under an electric field (Fig 1.16 b, c). Although it is well known that the "direct" and "converse" piezoelectric effects in ferroelectric films can have different characteristic constants, [35]-[40] there is no reported work on why and how the piezoelectric properties of a film differ from those of a single crystal, except for the partial case of a (001) oriented tetragonal film. [35]-[40] The primary goal of this section is to show how clamping of a substrate has broken the equivalence between "direct" and "converse" piezoelectric constants in an ferroelectric thin film.

In various applications of ferroelectric-based transducers, as well as in characterization of piezoelectric properties of ferroelectric films, either an electric stimulus or a electric response is required. On the other hand, since the substrate is usually a piezo-inactive insulator or semiconductor, the film has to be sandwiched by top and bottom electrode layers in order to apply an electric field to the film or have an electric charge output from the film. As compared with a ferroelectric single crystal, which can be considered as a closed system both mechanically and electrically, a ferroelectric film is an electrically closed but mechanically open system to the substrate. This is the reason why the characteristic constants of "direct" and "converse" piezoelectric properties are different for a ferroelectric film.

To illustrate how the mechanical interaction between film and substrate has changed the effective piezoelectric constants, we will start with a discussion on the longitudinal piezoelectric constants. Consider a piezoelectric single crystal plate with a normal **n** placed in an electric field E_3, and at the same time subjected to a mechanical stress σ_{33} ("3" here is the normal direction of the plate **n**). Then there are a longitudinal electric polarization p_3 and a strain ε_{33} induced in the crystal. The change of free energy due to small variations of electric field ΔE_3 and stress $\Delta\sigma_{33}$ can be written in a form of an exact differential:

$$\Delta F \text{ (crystal)} = -p_3 \Delta E_3 + \varepsilon_{33} \Delta\sigma_3 \qquad (1.6)$$

For a thermodynamically reversible process, we can write the Maxwell equation:

$(\frac{\Delta p_3}{\Delta \sigma_3})_E = (\frac{\Delta \varepsilon_{33}}{\Delta E_3})_\sigma = d_{33}^*$. Where d_{33}^* is the effective longitudinal piezoelectric constant, which has a unit of pC/N in the "direct" effect (change in polarization p_3 per applied stress σ_{33}) and a unit of pm/V in the "converse" effect (change in film strain ε_{33} per applied electric field E_3). d_{33}^* can be expressed by Eq. (1.7), [41] where d_{kij} are components of the piezoelectric tensor, which are defined in the Cartesian coordinates of the crystal.[30] n_k, n_i, and n_j are components of the normal vector **n** (the summations are taken over repetitive suffixes in this article, if not otherwise noted).

$$d_{33}^* = d_{kij} n_k n_i n_j \tag{1.7}$$

Consider a piezoelectric film with normal **n** under an electric field E_3 and at the same time subjected to a mechanical stress σ_{33}. Due to the mechanical clamping from the substrate, the in-plane elastic energy contributes to the total free energy, which can be expressed by Eq. (1.8).

$$\Delta F \text{ (film)} = -p_3 \Delta E_3 + \varepsilon_{33} \Delta \sigma_{33} + \varepsilon_{11} \Delta \sigma_{11} + \varepsilon_{22} \Delta \sigma_{22} + \varepsilon_{12} \Delta \sigma_{12} \tag{1.8}$$

Where σ_{11}, σ_{12} and σ_{22} are in-plane stresses due to clamping of substrate, ε_{11}, ε_{22}, and ε_{12} are the elastic strains, and hence $\varepsilon_{11}\Delta\sigma_{11}+\varepsilon_{22}\Delta\sigma_{22}+\varepsilon_{12}\Delta\sigma_{12}$ are the in-plane elastic energy. All these quantities aforementioned after Eq. (1.8) are functions of applied stress σ_{33} and electric field E_3. In this case, p_3 and ε_{33} are not partial derivatives of the free energy. Therefore, the Maxwell equation $(\frac{\Delta p_3}{\Delta \sigma_3})_E = (\frac{\Delta \varepsilon_{33}}{\Delta E_3})_\sigma = d_{33}^*$ valid for the case of a single crystal plate does not hold true here, which explains why the effective "direct"

piezoelectric constant $d_{33}^{f,D} = (\frac{\Delta p_3}{\Delta \sigma_3})_{E_3}$ (subscript "*f*" denotes "film") is different from the effective "converse" constant $d_{33}^{f,C} = (\frac{\Delta \varepsilon_{33}}{\Delta E_3})_{\sigma_{33}}$. Here subscript "D" and "C" denote "direct" and "converse" piezoelectric effects, respectively.

In some of the characterization methods for converse longitudinal piezoelectric constant, such as piezoelectric force microscopy[42] and single beam interferometer,[43] the total longitudinal displacement of the film/substrate couple is measured for calculation of the field induced strain. In these cases, a contribution from substrate deformation is added to the apparent longitudinal piezoelectric constant of the film $\bar{d}_{33}^{f,C} = (\frac{\Delta \bar{\varepsilon}_{33}}{E_3})_{\sigma_{33}}$. [44]

Here $\Delta \bar{\varepsilon}_{33} = \frac{\Delta h_{33}}{t}$ is the effective piezoelectric strain with Δh_{33} being the total surface displacement and *t* the film thickness. Taking the film/substrate couple as the objective thermodynamic system, the change of free energy of this system due to piezoelectric effect can be written in a form of an exact differential: $\Delta \mathbb{F} = -p_3 \Delta V_3 + h_{33} \Delta \sigma_{33}$, where $\Delta \mathbb{F}$ is the free energy per area for the film/substrate couple, p_3 is the induced longitudinal polarization, V_3 is the voltage drop across the film thickness t ($\Delta V_3 = E_3 t$), h_{33} is the displacement along the normal direction, and σ_{33} is the stress applied along the normal of the system. The Maxwell relation gives $d_{33}^{f,D} = (\frac{\Delta P_3}{\Delta \sigma_3})_{V_3} = (\frac{\Delta h_{33}}{\Delta V_3})_{\sigma_3} = (\frac{\Delta \bar{\varepsilon}_{33}}{E_3})_{\sigma_3} = \bar{d}_{33}^{f,C}$.

It should be noted that the non-epitaxial ferroelectric films like polycrystalline and textured films behave differently in piezoelectric properties. Factors other than clamping of substrate, like grain size and distributions, degrees and orientations of

texture, etc., will require additional concerns in quantifying the effective piezoelectric coefficients. There have been long discussed in literature, and therefore are not included in this dissertation. Instead, intrinsic and extrinsic piezoelectric effects in epitaxial ferroelectric films are the main focus of this dissertation.

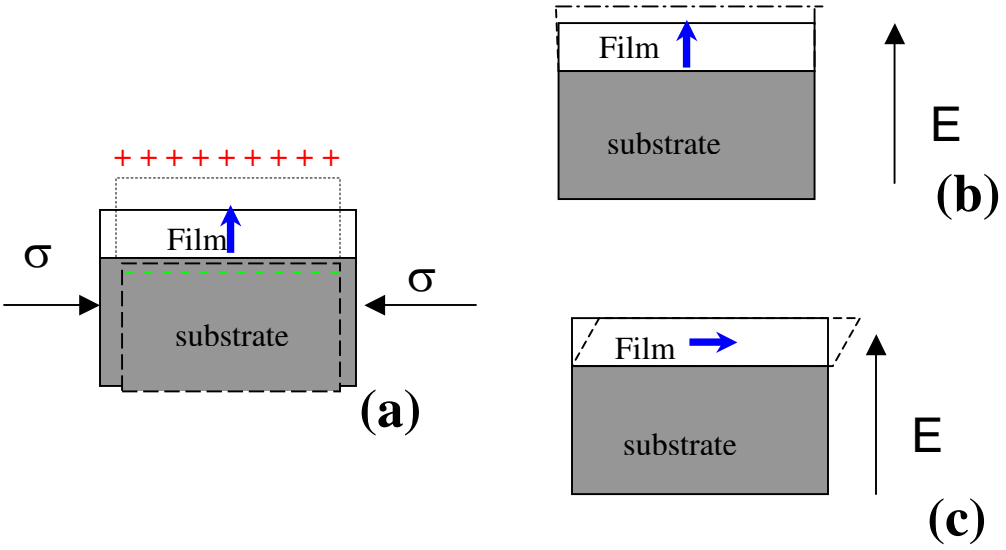

Fig. 1.16 (a) Microsensor based on the direct piezoelectric effect of ferroelectric films. (b) longitudinal, (c) shear microacuators based on the converse piezoelectric effect of ferroelectric films. The blue arrows inside the films indicate the alignment of the polar vectors in the film.

1.4 Conclusion

The main points in this chapter are summarized here:

(1). Piezoelectricity originates from lack of centro-symmetry in a crystalline structure. Ferroelectric materials is a sub-group of piezoelectric materials. It is characterized by a switchable remnant polarization.

(2). Due to their large piezoelectric coefficients, many ferroelectric materials are being used in piezoelectric transducer applications. The converse piezoelectric effects are utilized in piezoelectric actuators, where a output mechanical strain can be produced and controlled by an input electric field. On the other hand, a piezoelectric sensor will utilize the direct piezoelectric effects to transform input mechanical stimulus to output electric signals.

(2). Intrinsic piezoelectric response refers to the piezoelectric deformation of the lattice of a single-domain crystal, which can be characterized by tensors of piezoelectric constants. Intrinsic piezoelectric constants in ferroelectric materials describe piezoelectric effect as an electrostriction biased by the polarization (linearized electrostriction) [6].

(3). The extrinsic piezoelectric response, on the other hand, are from extrinsic sources of displacement under the electric field. Processes involving changes in polarization or dielectric constant (for example, movement of ferroelectric domain walls, poling of ferroelectric ceramics, phase transition occurred in ferroelectrics which varies the polarization, etc) will add “extrinsic” piezoelectric response to the “intrinsic” one.

(4) The domain engineering method, which aims at enhancing piezoelectric response by poling the ferroelectric material in a non-polar direction, will lead to two possible consequences. One is that the domains are equivalent under the poling field and the piezoelectric response is intrinsic, the enhanced piezoelectric responses can be evaluated by calculating the effective piezoelectric constants of a single-domain single crystal - $d_{\ln} = d_{kij} l_k n_i n_j$ (Eq. 1.5), in the domain engineered orientation (pseudo cubic <001> for rhombohedral crystals and pseudo cubic <111> for tetragonal crystals). The other possible consequence is a field-induced phase transition, which may lead to large extrinsic piezoelectric responses.

(5) Another important source of extrinsic piezoelectric response comes from domain wall movement. Both 180^o domain wall and non-180^o domain wall movements can affect the piezoelectric properties. However, while 180^o domain wall movement does not substantially increase the piezoelectric strain, switching between non-180^o domains will bring large extrinsic piezoelectric strains.

(6). Due to clamping from the substrate, a ferroelectric film has different apparent "direct" and "transverse" piezoelectric constants.

CHAPTER 2, INTRINSIC PIEZOELECTRIC RESPONSE IN THIN EPITAXIAL FERROELECTRIC FILMS

2.1 Converse piezoelectric properties for ferroelectric thin films

It is well known that the field-induced strain of piezoelectric films is strongly modified by their elastic interaction with substrates. The relation between an intrinsic converse piezoresponse of a single crystal or a free standing film and that of a film clamped by a substrate is of a great interest for many applications of piezoelectric thin films. However, this relation is obtained only for one partial case: a (001) oriented tetragonal film clamped by a rigid or a thick substrate under electric field normal to the film.[37] The goal of this section is to calculate the effective piezoelectric coefficients of a substrate-constrained single domain film as a function of its crystallographic orientation and a direction of applied electric field. This information will set up a framework of reference for evaluating converse piezoelectric properties of clamped thin films growing in arbitrary orientation and help to separate intrinsic properties from extrinsic effects[45] (domain wall motion, incomplete clamping, substrate bending, etc.). Knowledge of the orientation dependence of piezoelectric coefficients of constrained films will allow one to optimize their electromechanical performance. In the section, the general expressions for characterization of the piezoelectric strain of a clamped film with an arbitrary orientation is obtained, and, as typical examples, converse longitudinal piezoelectric coefficients of films with tetragonal and rhombohedral crystallographic structure are calculated for three orientations- (001), (011) and (111).

We start with an expression for a piezoelectric strain of a free standing film, which is presented by Eq. (2.1) in pseudo cubic coordinates. Where d_{kij} are piezoelectric

coefficients of a bulk crystal, E_k are components of the applied electrical field $\boldsymbol{E}$, $E_k = El_k$, and l_k are the direction cosines (the summation is taken over repetitive suffixes).

$$\varepsilon_{ij}^{0} = d_{kij}E_k = d_{kij}l_kE \qquad (i, j, k=1, 2, 3) \qquad (2.1)$$

The change of the thickness of a film with a normal $\boldsymbol{n}$ is determined by a normal strain $\varepsilon_{ij}^{0}\ n_i n_j$ and it can be characterized by an effective piezoelectric coefficient: $d_{ln} = d_{kij}l_k n_i n_j$ (i, j, k=1, 2, 3). It is reduced to the longitudinal piezoelectric coefficient $d_{nn} = d_{kij}n_k n_i n_j$ of a single crystal or a free standing film if the field is normal to the film.

If the film is clamped by a rigid substrate or if a substrate is much thicker than the film, then the components of the strain in the film plane are equal to zero. The piezoelectric strain is so-called an invariant plane strain: all planes parallel to film remain undistorted and its displacement is proportional to the distance of the plane from the film-substrate interface. The invariant plane strain is expressed by a dyadic tensor $\varepsilon_{ij} = s_i n_j$, where s_i is a characteristic vector. There is no displacement normal to the plane containing the vectors $\boldsymbol{s}$ and $\boldsymbol{n}$. Therefore the piezoelectric strain of a completely clamped film is characterized by only two parameters: a normal piezoelectric coefficient $d_{ln}^{f} = s_i n_i / E$ and a tangential piezoelectric coefficient $d_{l\tau}^{f} = s_i \tau_i / E$, where $\boldsymbol{\tau}$ is a unit vector along the projection of $\boldsymbol{s}$ on a film plane and can be determined by $\boldsymbol{\tau} = \boldsymbol{n} \times (\boldsymbol{s} \times \boldsymbol{n})/|\mathbf{s}|$.

To determine the effective piezoelectric coefficients $d_{\ln}^{f}$ and $d_{l\tau}^{f}$, it is necessary to find the vector ***s***. Taking into account that the stress in the film is $\sigma_{ij} = C_{ijkl}(\varepsilon_{kl} - \varepsilon_{kl}^{0})$ and there is no force normal to the ($\sigma_{ij}n_j$=0), it is possible to show that:

$$s_i = \Pi_{ik}\, n_t C_{kt\alpha\beta}\, d_{\gamma\alpha\beta}\, l_\gamma E \tag{2.2}$$

where $C_{kt\alpha\beta}$ is the tensor of elastic moduli of the film, $\Pi_{ik} = (\Lambda_{ik})^{-1}$, a Green tensor $\Lambda_{ik} = n_m C_{mikp} n_p$.[46]-[48] Then $d_{\ln}^{f}$ and $d_{l\tau}^{f}$ can be expressed as follows:

$$d_{\ln}^{f} = \Pi_{ik}\, C_{kt\alpha\beta}\, d_{\gamma\alpha\beta}\, n_t n_i l_\gamma \quad (2.3a)$$

$$d_{l\tau}^{f} = \Pi_{ik}\, C_{kt\alpha\beta}\, d_{\gamma\alpha\beta}\, n_t \tau_i l_\gamma \quad (2.3b)$$

As two typical examples, we calculate the intrinsic longitudinal piezoelectric coefficients for tetragonal and rhombohedral films in an usual set up with bottom and top electrodes. In this case, the electrostatic field is directed along the film normal ***n***. The effective longitudinal piezoelectric coefficient can be written as: [41]

$$d_{33,f} = d_{nn}^{f} = \Pi_{ik}\, C_{kt\alpha\beta}\, d_{\gamma\alpha\beta}\, n_t n_i n_\gamma \tag{2.4}$$

where $C_{kt\alpha\beta}$ and $d_{\gamma\alpha\beta}$ are the tensor of elastic moduli and piezoelectric coefficients of the film; $\Pi_{ik} = (\Lambda_{ik})^{-1}$, a Green tensor $\Lambda_{ik} = n_m C_{mikp} n_p$;[46]-[48] n_t and n_i are the direction cosines of the film normal ***n***. The electric field **E** is applied along **n**.

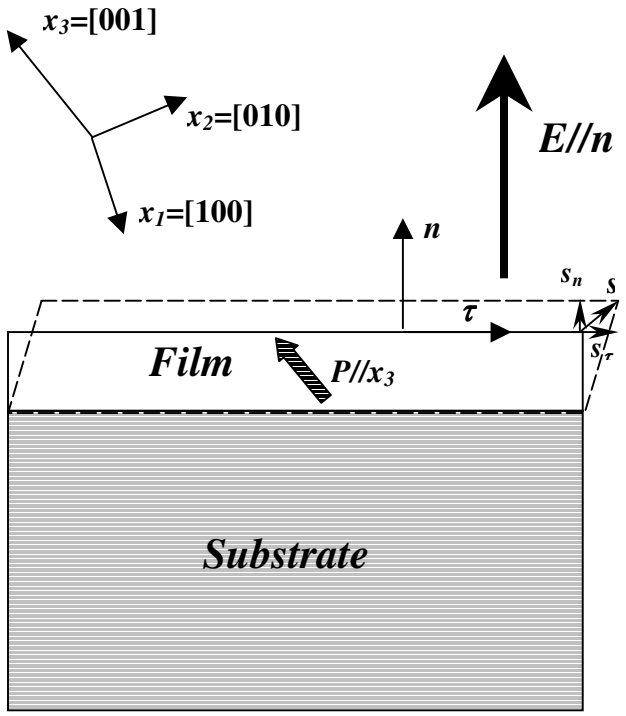

Figure 2. 1. A single domain tetragonal ferroelectric film with normal ***n*** under electric field ***E (E//n)***. x_1, x_2, x_3 are the crystalline coordinates. ***P*** is the polarization vector, ***P*** is parallel to x_3. The deformation is exaggerated here for illustration.

In a tetragonal phase with 4mm symmetry, $P_1=P_2=0$, $P_3=P\neq 0$. There are 7 non-zero piezoelectric coefficients, out of which only 3 are independent. $d_{311}=d_{322}=d_{31}$, $d_{333}=d_{33}$, $d_{223}=d_{232}(=\frac{1}{2}d_{24})=d_{113}=d_{131}=\frac{1}{2}d_{15}$. The coordinates of the tetragonal phase are pseudo-cubic coordinates. For a rhombohedral PZT phase, there are 11 non-zero piezoelectric coefficients, out of which only 4 are independent due to the 3m symmetry: $d_{113}=d_{131}=\frac{1}{2}d_{15}$, $d_{112}=d_{121}=\frac{1}{2}d_{16}=-d_{22}$, $d_{211}=-d_{22}$, $d_{222}=d_{22}$, $d_{223}=d_{232}=\frac{1}{2}d_{24}=\frac{1}{2}d_{15}$,

$d_{311}=d_{322}=d_{31}$, $d_{333}=d_{33}$. It should be noted that, the above piezoelectric coefficients are referred to a rhombohedral coordinate system, which is defined as follows:[49]

Pseudo-cubic axis $[1\bar{1}\ 0]\leftrightarrow$ rhombohedral axis x_1 [100]

Pseudo-cubic axis $[11\bar{2}\ ]\leftrightarrow$ rhombohedral axis x_2 [010]

Pseudo-cubic axis [111] $\leftrightarrow$ rhombohedral axis x_3 [001]

The tensors Π_{ik} are shown in Table 2.1 and Table 2.2 for three typical orientations (001), (011) and (111) in tetragonal and rhombohedral films, respectively . The longitudinal piezo-electric coefficients d_{nn}^{f} and d_{nn} of a free standing film are presented in Table 2.3 and Table 2.4 for comparison.

Table 2.1 Calculated orientation prefactors Π_{ik} for (001), (011) and (111) oriented single-domain tetragonal films. $\Delta=(C_{11}+C_{44})(C_{33}+C_{44})-(C_{13}+C_{44})^2$, $\Omega=(C_{11}+C_{44}-C_{12})[C_{33}+2C_{44})*(C_{11}+C_{44}+C_{12}+2C_{66})-2(C_{13}+C_{44})^2]$

Orientations $\boldsymbol{n}$	$\Pi_{ik}=(\Lambda_{ik})^{-1}=(n_m C_{mikp} n_p)^{-1}$
(001)	$\begin{bmatrix} C_{44}^{-1} & 0 & 0 \\ 0 & C_{44}^{-1} & 0 \\ 0 & 0 & C_{33}^{-1} \end{bmatrix}$
$(1/\sqrt{2})(011)$	$2\Delta^{-1}\begin{bmatrix} \Delta(C_{66}+C_{44})^{-1} & 0 & 0 \\ 0 & (C_{33}+C_{44}) & -(C_{13}+C_{44}) \\ 0 & -(C_{13}+C_{44}) & (C_{11}+C_{44}) \end{bmatrix}$
$(1/\sqrt{3})(111)$	$\frac{3}{\Omega}\begin{bmatrix} (C_{11}+C_{44}+C_{66})(C_{33}+2C_{44})-(C_{13}+C_{44})^2 & (C_{13}+C_{44})^2-(C_{12}+C_{66})(C_{33}+2C_{44}) & (C_{12}-C_{11}-C_{44})(C_{13}+C_{44}) \\ (C_{13}+C_{44})^2-(C_{12}+C_{66})(C_{33}+2C_{44}) & (C_{11}+C_{44}+C_{66})(C_{33}+2C_{44})-(C_{13}+C_{44})^2 & (C_{12}-C_{11}-C_{44})(C_{13}+C_{44}) \\ (C_{12}-C_{11}-C_{44})(C_{13}+C_{44}) & (C_{12}-C_{11}-C_{44})(C_{13}+C_{44}) & (C_{11}+C_{44}+C_{66})^2-(C_{12}+C_{66})^2 \end{bmatrix}$

Table 2.2. Calculated orientation prefactors Π_{ik} for epitaxial single-domain rhombohedral films with pseudo cubic orientations of (001), (110) and (111).

$$\Delta = (C_{11} - 2\sqrt{2}C_{14} + 2C_{44})(2C_{33} + C_{44}) - [\sqrt{2}(C_{13} + C_{44}) - C_{14}]^2$$

$$\Omega = (2C_{11} + 2\sqrt{2}C_{14} + C_{44})(C_{33} + 2C_{44}) - [2C_{14} + \sqrt{2}(C_{13} + C_{44})]^2$$

Orientations ***n*** (pseudo-cubic)	$\Pi_{ik} = (\Lambda_{ik})^{-1} = (n_m C_{mikp} n_p)^{-1}$
(001)	$\begin{bmatrix} \frac{1}{C_{44}} & 0 & 0 \\ 0 & \frac{1}{C_{44}} & 0 \\ 0 & 0 & \frac{1}{C_{33}} \end{bmatrix}$
$(1/\sqrt{2})$ (011)	$\begin{bmatrix} \frac{3}{C_{66}+2\sqrt{2}C_{14}+2C_{44}} & 0 & 0 \\ 0 & \frac{3(C_{44}+2C_{33})}{\Delta} & \frac{3[\sqrt{2}(C_{44}+C_{13})-C_{14}]}{\Delta} \\ 0 & \frac{3[\sqrt{2}(C_{44}+C_{13})-C_{14}]}{\Delta} & \frac{3[C_{11}-2\sqrt{2}C_{14}+2C_{44}]}{\Delta} \end{bmatrix}$
$(1/\sqrt{3})$ (111)	$\begin{bmatrix} \frac{3}{2C_{66}-2\sqrt{2}C_{14}+C_{44}} & 0 & 0 \\ 0 & \frac{3(C_{33}+2C_{44})}{\Omega} & \frac{3[2C_{14}+\sqrt{2}(C_{13}+C_{44})]}{\Omega} \\ 0 & \frac{3[2C_{14}+\sqrt{2}(C_{13}+C_{44})]}{\Omega} & \frac{3[2C_{11}+C_{44}+2\sqrt{2}C_{14}]}{\Omega} \end{bmatrix}$

Table 2.3. The longitudinal converse piezoelectric coefficients for different orientations of constrained tetragonal films d_{nn}^{f} and free standing films d_{nn}. d_{ij} are the piezoelectric coefficients of single crystals in pseudo cubic coordinates.

$\kappa=\Pi_{22}^{(011)}+\Pi_{23}^{(011)}$, $\lambda=\Pi_{33}^{(011)}+\Pi_{23}^{(011)}$

$\psi=\Pi_{11}^{(111)}+2\Pi_{12}^{(111)}+\Pi_{22}^{(111)}+\Pi_{31}^{(111)}+\Pi_{32}^{(111)}=6\Omega^{-1}(C_{33}-C_{13}+C_{44})\,(C_{11}-C_{12}+C_{44})$

$\phi=\Pi_{13}^{(111)}+\Pi_{23}^{(111)}+\Pi_{33}^{(111)}=3\Omega^{-1}(C_{11}+C_{12}-2C_{13}+2C_{66}-C_{44})(C_{11}-C_{12}+C_{44})$

Orientation **n**	Bulk d_{nn}	Film d_{nn}^{f}
(001)	d_{33}	$d_{33}+2C_{13}d_{31}/C_{33}$
$1/\sqrt{2}$ (011)	$(d_{33}+d_{31}+d_{15})/(2\sqrt{2})$	$\{(\kappa C_{13}+\lambda C_{33})d_{33}+(\kappa+\lambda)C_{44}d_{15}+[\kappa(C_{11}+C_{12})+2\lambda C_{13}]d_{31}\}/2\sqrt{2}$
$1/\sqrt{3}$ (111)	$(d_{33}+2d_{31}+2d_{15})/(3\sqrt{3})$	$\{(\Psi C_{13}+\Phi C_{33})d_{33}+(\Psi+2\Phi)C_{44}d_{15}+[\Psi(C_{11}+C_{12})+2\Phi C_{13}]d_{31}\}/(3\sqrt{3})$

Table 2.4. The converse longitudinal piezoelectric coefficients for different orientations of constrained rhombohedral films (d_{nn}^{f}) and bulk crystals (d_{nn}). d_{ij} are the piezoelectric coefficients of single-domain rhombohedral single crystals defined in rhombohedral coordinates. d_{ij}^{m} are the pseudo-tetragonal piezoelectric coefficients of a (001) oriented multi-domain rhombohedral single crystal.[15] $q_1=\sqrt{2}\Pi_{22}^{(001)}-\Pi_{32}^{(001)}$, $q_2=\sqrt{2}\Pi_{23}^{(001)}-\Pi_{33}^{(001)}$, $k_1=\Pi_{22}^{(110)}+\sqrt{2}\Pi_{32}^{(110)}$, $k_2=\Pi_{23}^{(110)}+\sqrt{2}\Pi_{33}^{(110)}$.

Orientation **n**	Bulk d_{nn}	Film d_{nn}^{f}
(001)	$\frac{1}{3\sqrt{3}}[2(d_{15}+d_{31})$ $-2\sqrt{2}d_{22}+d_{33})$	(1) $\frac{1}{3\sqrt{3}}\{(\sqrt{2}C_{13}q_1-C_{33}q_2)d_{33}+[\sqrt{2}(C_{11}+C_{12})$ $q_1-2C_{13}q_2]d_{31}+[2(C_{12}-C_{11}-\sqrt{2}C_{14})q_1+$ $4C_{14}q_2]d_{22}+[(\sqrt{2}C_{44}+2C_{14})q_1-2C_{44}q_2]d_{15}\}$ (2) $d_{33}^{m}+\frac{2C_{13}^{m}}{C_{33}^{m}}d_{31}^{m}$
$1/\sqrt{2}$ (110)	$\frac{1}{3\sqrt{3}}[\sqrt{2}(d_{15}+d_{31})$ $+d_{22}+2\sqrt{2}d_{33})$	$\frac{1}{3\sqrt{3}}\{(\sqrt{2}C_{13}k_1+2C_{33}k_2)d_{33}+[\sqrt{2}(C_{11}+C_{12})k_1+$ $4C_{13}k_2]d_{31}+[(C_{11}-C_{12}-2\sqrt{2}C_{14})k_1-2C_{14}k_2]d_{22}$ $+[(\sqrt{2}C_{44}-C_{14})k_1+C_{44}k_2]d_{15}\}$
$1/\sqrt{3}$ (111)	d_{33}	$d_{33}+\frac{2C_{13}}{C_{33}}d_{31}$

2.2 Direct piezoelectric properties for ferroelectric thin films

The orientation dependence of the direct piezoelectric coefficients $d_{33,f}^{D}$, $d_{31,f}^{D}$ and $e_{31,f}^{D}$ ("D" denotes "direct piezoelectric effect", "*f*" denotes "film") are generally formulated in this chapter, which can help to predict and optimize the performance of piezoelectric MEMS sensor devices based on ferroelectric thin films. Numerical results are obtained and discussed for $Pb(Zr_xTi_{1-x})O_3$ thin films grow on Si substrates with various compositions and structures.

Recently, there is an increasing number of research works on ferroelectric films as sensor components in micro-electric-mechanical system (MEMS), which aims at realizing direct piezoelectric functions by capacitive sensing in a reduced length scale. [32], [34], [50], [51] In a general configuration for a piezoelectrically driven MEMS sensor, a ferroelectric thin film is grown on top of a thick substrate, a stress or a strain field from the surrounding environment is applied to the substrate and sensed by the ferroelectric film through "direct" piezoelectric effect (via the lateral constraint imposed by the substrate). The primary goal of this section is to calculate the effective direct piezoelectric coefficients $d_{33,f}^{D}$, $d_{31,f}^{D}$ and $e_{31,f}^{D}$ of a substrate-constrained single domain ferroelectric film as a function of its crystallographic structure and orientation. This information will provide a framework of reference for evaluating direct piezoelectric properties of clamped ferroelectric films.

The widely used piezoelectric coefficients characterizing piezoelectric sensing processes are the longitudinal $d_{33,f}^{D}$ coefficient and the transverse $d_{31,f}^{D}$ and $e_{31,f}^{D}$ coefficients. A piezoelectric sensor is said to be in a longitudinal sensing mode when a

longitudinal force is applied along the normal of the device and a charge is generated on the surface of the ferroelectric film and then is collected and analyzed. On the other hand, a transverse sensing mode is when in-plane stresses or strains are applied to the device to induce the charge. For a (001) oriented tetragonal film, $d_{33,f}^{D}$, $d_{31,f}^{D}$ and $e_{31,f}^{D}$ coefficients are expressed in Eq (2.5):[36],[37]

$$d_{33}^{f,D} = Q_3^E / \sigma_{33} = d_{33} + 2(s_{13}^{E,sub} - s_{13}^{E,f})d_{31} / (s_{11}^{E,f} + s_{12}^{E,f}) \quad (2.5.1)$$

$$d_{31}^{f,,D} = Q_3^E / (\sigma_{11}^{sub} + \sigma_{22}^{sub}) = d_{31}(s_{11}^{E,sub} + s_{12}^{E,sub}) / (s_{11}^{E,f} + s_{12}^{E,f}) \quad (2.5.2)$$

$$e_{31}^{f,D} = Q_3^E / (\varepsilon_{11}^{sub} + \varepsilon_{22}^{sub}) = d_{31} / (s_{11}^{E,f} + s_{12}^{E,f}) \quad (2.5.3)$$

Where Q_3^E is the piezoelectrically induced charge ("E" denotes "at constant electric field"), σ_{33} is the longitudinal stress from the surrounding environment applied to the device, d_{ij} (i, j=1~3) are the piezoelectric coefficients of the ferroelectric single crystal. σ_{11}^{sub}, σ_{22}^{sub} and ε_{11}^{sub}, ε_{22}^{sub} are the in-plane stresses and strains applied to the substrate in transverse sensing processes. $s_{ij}^{E,sub}$ ("sub" denotes "substrate") and $s_{ij}^{E,f}$ (i, j=1~3) are the elastic compliances under constant electric field for substrate and film material, respectively.

As can be seen from Eq. (2.5), the direct piezoelectric coefficients for a ferroelectric film are functions not only of its own electromechanical properties, but also of the substrate's mechanical properties. $e_{31}^{f,D}$ is always larger than the single crystal piezoelectric coefficient e_{31}, while $d_{33}^{f,D}$ and $d_{31}^{f,D}$ can be smaller or larger than single crystal coefficients depending on the mechanical properties of the substrate

with respect to the film material. However, to quantitatively evaluate the direct piezoelectric effect, Eq. (2.5) is good only for [001] tetragonal or pseudo-tetragonal epitaxial films. Therefore, in order to find optimal orientations and structures for piezoelectric sensing performance, it is important to know how much the effective direct piezoelectric coefficients will change as we vary the orientation and/or structure of the film.

We start with a general expression for the in-plane stress components of an epitaxial film with a normal **n** in the longitudinal sensing mode, where a longitudinal stress σ_{NN} is applied to the device (the subscript "N" denotes the longitudinal direction **n**, it is NOT a suffix number throughout this article). The strain tensors induced due to σ_{NN} are $\varepsilon_{pq}^{f} = s_{pqij}^{E,f}\,\sigma_{NN}\,n_i n_j$ and $\varepsilon_{pq}^{sub} = s_{pqij}^{*,sub}\sigma_{NN}\,n_i n_j$ (p, q, i, j=1~3; the summations are taken over repetitive suffixes if not otherwise noted), for the film and substrate, respectively. $s_{pqij}^{*,sub} = s_{efgh}^{sub}\,a_{pe}a_{qf}a_{ig}a_{jh}$ is the effective elastic compliance tensor of the substrate defined in the Cartesian coordinates of the film and s_{efgh}^{sub} is the elastic compliance tensor of the substrate defined in its own Cartesian coordinates (x_k^{sub}, k=1-3), a_{lm} is the direction cosines between $\boldsymbol{x}_\mathbf{l}$ and x_m^{sub} (l, m=1-3).[49]

The difference between the two strain tensors is the self strain $\varepsilon_{pq}^{0} = \varepsilon_{pq}^{f} - \varepsilon_{pq}^{sub}$

$=(s_{pqij}^{E,f} - s_{pqij}^{*,sub})\,\sigma_{NN}\,n_i n_j$. The in-plane stresses in the film are expressed in Eq. (2.6):[46]-[48]

$$\sigma_{lm} = -G_{lmpq}^{E,f}(n)\;\varepsilon_{pq}^{0} = (C_{lmpq}^{E,f} - C_{lm\alpha\beta}^{E,f} n_\alpha \Pi_{\beta\delta}\, n_\varepsilon C_{\delta\varphi q}^{E,f})\;(s_{pqij}^{*,sub} - s_{pqij}^{E,f})\;\sigma_{NN}\,n_i n_j \qquad (2.6)$$

Where $G_{lmpq}^{E,f}(n)$ is the planar elastic modulus for a fully clamped film with a normal **n** at constant electric field. $G_{lmpq}^{E,f}(n) = C_{lmpq}^{E,f} - C_{lm\alpha\beta}^{E,f} n_\alpha \Pi_{\beta\delta} n_\varepsilon C_{\delta\varepsilon pq}^{E,f}$.[43]-[45] $\boldsymbol{C}^{\mathbf{E,f}}$ ($C_{lmpq}^{E,f}$, $C_{lm\alpha\beta}^{E,f}$, and $C_{\delta\varepsilon pq}^{E,f}$) is the tensor of elastic moduli of the film at constant electric field, $\Pi_{\beta\delta} = (\Lambda_{\beta\delta})^{-1}$, a Green tensor $\Lambda_{\beta\delta} = n_\gamma C_{\gamma\beta\delta\zeta}^{E,f} n_\zeta$.[43]-[45] Therefore, the piezoelectric charge induced by the stress σ_{NN} and σ_{lm} are: $Q_N^E = d_{NN}\sigma_{NN} + d_{klm}\sigma_{lm}n_k = \sigma_{NN}[d_{NN} + d_{klm}G_{lmpq}^{E,f}(n)\,(s_{pqij}^{*,sub} - s_{pqij}^{E,f})\,n_k n_i n_j]$. The effective direct piezoelectric coefficient $d_{33,f}^D$ is shown in Eq. (2.7):

$$\begin{aligned} d_{33}^{f,D} &= Q_N^E / \sigma_{NN} = d_{NN} + d_{klm}G_{lmpq}^{E,f}(n)\,(s_{pqij}^{*,sub} - s_{pqij}^{E,f})n_i^{(3)}n_j^{(3)} \\ &= [d_{kij} + d_{klm}G_{lmpq}^{E,f}(n)\,(s_{pqij}^{*,sub} - s_{pqij}^{E,f})]\,n_k^{(3)}n_i^{(3)}n_j^{(3)} \end{aligned} \tag{2.7}$$

Where $d_{NN} = d_{kij}n_k n_i n_j$ is the intrinsic longitudinal piezoelectric coefficient for the film.[41]

The film's in-plane axies are labeled as $\mathbf{n^{(1)}}$, $\mathbf{n^{(2)}}$ and normal as $\mathbf{n^{(3)}}$ (previous as **n**) in the case of transverse piezoelectric effects (Fig. 2.2). In a $d_{31}^{f,D}$ sensing mode, a stress field $\sigma_{UV}^{'}$ is applied to the substrate laterally (the prime in the superscript denotes that the stress components are expressed in the coordinate system of the film where the subscript *U, V* stand for direction of $\mathbf{n^{(U)}}$ and $\mathbf{n^{(V)}}$, *U, V*=1,2). In the crystalline coordinate system defined by symmetry of the film structure, this stress field can be written as

$\sigma_{ij} = \sigma'_{UV} n_i^{(U)} n_j^{(V)}$ (i, j=1-3).[49] The self strain $\varepsilon_{pq}^0 = - s_{pqij}^{*,sub} \sigma_{ij} = -s_{pqij}^{*,sub} \sigma'_{UV} n_i^{(U)} n_j^{(V)}$ and the in-plane stresses in the film are shown in Eq. (2.8): [46]-[48]

$$\sigma_{lm} = - G_{lmpq}^{E,f} (n^{(3)}) \varepsilon_{pq}^0 = (C_{lmpq}^{E,f} - C_{lm\alpha\beta}^{E,f} n_\alpha^{(3)} \Pi_{\beta\delta} n_\varepsilon^{(3)} C_{\delta pq}^{E,f}) \; s_{pqij}^{*,sub} \sigma'_{UV} n_i^{(U)} n_j^{(V)} \tag{2.8}$$

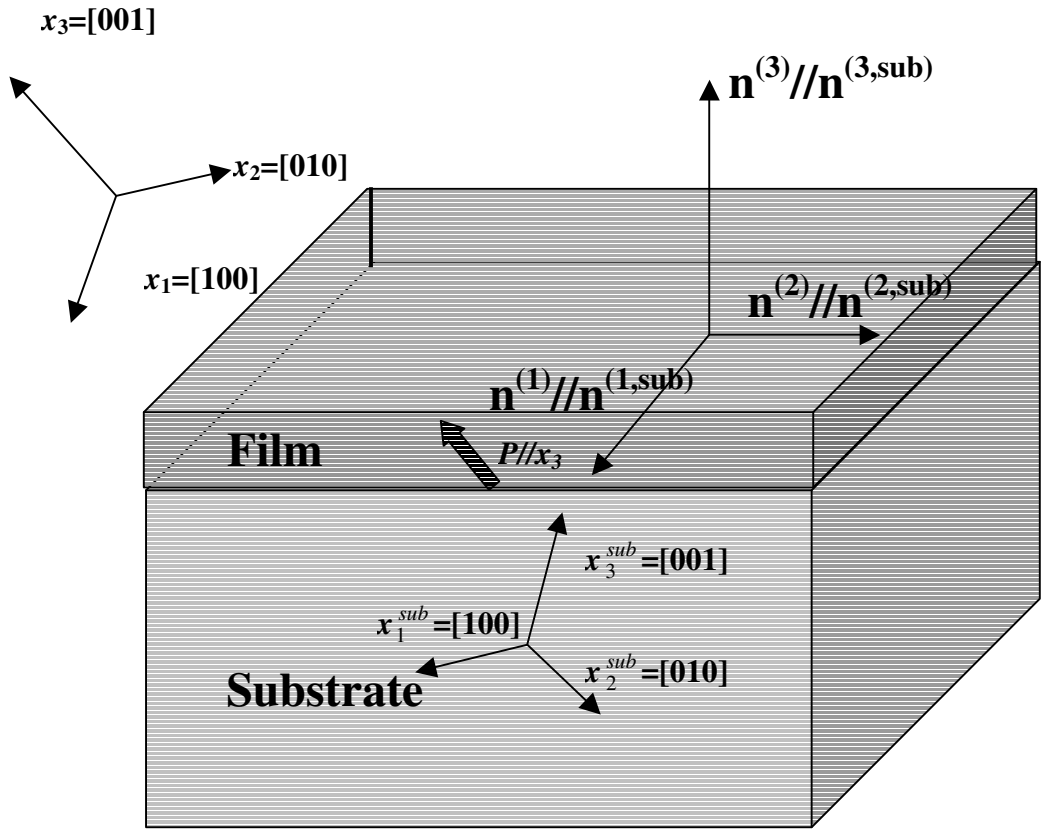

Figure 2.2. The epitaxial relation between a ferroelectric film and substrate with arbitrary orientations. x_i and $x_{i,sub}$ are the Cartesian coordinates of the crystalline structures of the film and substrate, respectively.

Therefore, the longitudinal piezoelectric charge induced by σ_{lm} is: $Q_3^E = d_{klm}\sigma_{lm}n_k^{(3)}$ $= d_{klm}G_{lmpq}^{E,f}(n^{(3)}) - s_{pqij}^{*,sub}\sigma_{UV}^{'} n_k^{(3)}n_i^{(U)}n_j^{(V)}$. Usually, the stress $\sigma_{UV}^{'}$ has two components $\sigma_{11}^{'}$ and $\sigma_{22}^{'}$, which are applied along $\mathbf{n^{(1)}}$ and $\mathbf{n^{(2)}}$, respectively. Then $Q_3^E = -d_{klm}G_{lmpq}^{E,f}(n^{(3)})$ $s_{pqij}^{*,sub}[\sigma_{11}^{'} n_i^{(1)}n_j^{(1)} + \sigma_{22}^{'} n_i^{(2)}n_j^{(2)}]n_k^{(3)}$. The effective direct piezoelectric coefficient $d_{31,f}^{D}$ can be expressed as in Eq. (2.9):

$$d_{31}^{f,D} = Q_3^E/(\sigma_{11}^{'}+\sigma_{22}^{'}) = -d_{klm}G_{lmpq}^{E,f}(n^{(3)})s_{pqij}^{*,sub}[\sigma_{11}^{'} n_i^{(1)}n_j^{(1)} + \sigma_{22}^{'} n_i^{(2)}n_j^{(2)})n_k^{(3)}]/(\sigma_{11}^{'}+\sigma_{22}^{'})$$

$$= -d_{klm}G_{lmpq}^{E,f}(n^{(3)})s_{pqij}^{*,sub}[n_i^{(1)}n_j^{(1)} + n_i^{(2)}n_j^{(2)}]n_k^{(3)}/2 \qquad (\sigma_{11}^{'} = \sigma_{22}^{'}) \qquad (2.9)$$

On the other hand, in the case of a $e_{31}^{f,D}$ sensing mode, biaxial in-plane strains ε_{11} and ε_{22} are applied to the substrate and hence the substrate-constrained film. The total film strain can be written as $\varepsilon_{pq} = \varepsilon_{11}n_p^{(1)}n_q^{(1)} + \varepsilon_{22}n_p^{(2)}n_q^{(2)} + \varepsilon_{33}n_p^{(3)}n_q^{(3)}$ in the Cartesian coordinates of the film (p, q=1-3), where ε_{33} is the normal strain due to Poison effect. The in-plane stresses in the film induced by the applied strains are $\sigma_{lm} = G_{lmpq}^{E,f}(n^{(3)})*$ $\varepsilon_{pq} = G_{lmpq}^{E,f}(n^{(3)})[\varepsilon_{11}n_p^{(1)}n_q^{(1)} + \varepsilon_{22}n_p^{(2)}n_q^{(2)}]$ (ε_{33} does not contribute to in-plane stresses since $G_{lmpq}^{E,f}(n^{(3)})\, n_p^{(3)}n_q^{(3)} = 0$). [43]-[45] The induced longitu-dinal charge is $Q_3^E = d_{klm}\sigma_{lm}n_k^{(3)} =$ $d_{klm}G_{lmpq}^{E,f}(n^{(3)})[\varepsilon_{11}n_p^{(1)}n_q^{(1)} + \varepsilon_{22}n_p^{(2)}n_q^{(2)}]n_k^{(3)}$. The effective direct piezoelectric coefficient $e_{31,f}^{D}$ is expressed in Eq. (2.10):[52]

$$e_{31}^{f,D} = Q_3^E/(\varepsilon_{11}+\varepsilon_{22}) = d_{klm}G_{lmpq}^{E,f}(n^{(3)})[\varepsilon_{11}n_p^{(1)}n_q^{(1)} + \varepsilon_{22}n_p^{(2)}n_q^{(2)}]n_k^{(3)}/(\varepsilon_{11}+\varepsilon_{22})$$

$$= d_{klm} G^{E,f}_{lmpq} (n^{(3)})[n^{(1)}_p n^{(1)}_q + n^{(2)}_p n^{(2)}_q] n^{(3)}_k / 2 \text{ (when } \varepsilon_{11} = \varepsilon_{22}) \quad (2.10)$$

Equations (2.7) (2.9) and (2.10) will allow one to compute the effective direct piezoelectric coefficients for an arbitrary orientation of a film with a variable crystalline structure, if the intrinsic piezoelectric coefficients of the film and the elastic moduli of the film and substrate are known. It can be seen that Eqs. (2.7) (2.9) and (2.10) will reduce to Eqs. (2.5), if we take $\mathbf{n^{(1)}=[100]}$, $\mathbf{n^{(2)}=[010]}$, $\mathbf{n^{(3)}=[001]}$, and the crystalline structure of the film is tetragonal.

In summary, the effective piezoelectric coefficients for epitaxial ferroelectric films as components of piezoelectric MEMS sensors are generally formulated in this article. It is demonstrated how the direct piezoelectric properties of a ferroelectric film are affected by the film/ substrate interface stresses, which are induced by clamping of substrate.

2.3 Summary of the intrinsic piezoelectric properties in ferroelectric thin films

In this section, the effective piezoelectric coefficients of an epitaxial ferroelectric film are generally formulated by taking into account of clamping from a substrate. It is illustrated how the equivalent converse and direct piezoelectric coefficients in a single crystal differ from each other in an epitaxial film, which may serve as an example showing how the film-substrate interactions have modified properties of functional thin film materials.

Piezoelectric materials can be used as functional components in a wide variety of applications, such as sensors, actuators, ultrasonic and solar systems. Piezoelectric properties can be either characterized by “direct” piezoelectric effects, where electric

responses (induced charge/voltage) are induced by mechanical stimulus (stress /strain field), or "converse" piezoelectric effects, where mechanical response (stresses/strains) are induced by electric stimulus (electric field). In single crystals, these two kinds of effects have the same characteristic coefficients, which are equivalent thermodynamic potential derivatives.[30] For example, the effective longitudinal piezoelectric coefficient d_{33}^{*}, which has a unit of pC/N in the "direct" effect (change in polarization p_3 per applied stress σ_{33}) and a unit of pm/V in the "converse" effect (change in film strain ε_{33} per applied electric field E_3), can be expressed by Eq. (2.11),[44] where d_{kij} are components of the piezoelectric tensor, which are defined in the Cartesian coordinates of the crystal.[49] $n_k^{(3)}, n_i^{(3)}$, and $n_j^{(3)}$ are components of the normal vector $\mathbf{n^{(3)}}$.

$$d_{33}^{*} = d_{kij} n_k^{(3)} n_i^{(3)} n_j^{(3)} \tag{2.11}$$

However, for ferroelectric films, from the discussion presented in Section 1. 3 and the results obtained in Sections 2.1 and 2.2, the "direct" and "converse" piezoelectric coefficients are characteristically different from each other.

For a single domain (001) oriented tetragonal piezoelectric film, $d_{33,}^{f,D}$ is larger than $d_{33}^{f,C}$. They can be characterized by the following formula:[36]-[37]

$$d_{33}^{f,D} = d_{33} + 2(s_{13}^{sub} - s_{13}^{E,f}) * d_{31} / (s_{11}^{E,f} + s_{12}^{E,f}) = d_{33}^{f,C} + \Delta d_{33} \tag{2.12.1}$$

$$d_{33}^{f,C} = d_{33} - 2s_{13}^{E,f} d_{31} * (s_{11}^{E,f} + s_{12}^{E,f}),\ \Delta d_{33} = 2s_{13}^{sub} d_{31} / (s_{11}^{E,f} + s_{12}^{E,f}) \tag{2.12.2}$$

Where d_{31}, d_{33} are the piezoelectric coefficients and s_{ij}^{sub}, $s_{ij}^{E,f}$ (i, j=1~3) are the elastic compliances defined in a matrix notation.[30] Subscript "sub" and "*f*" denote substrate and film, respectively, while subscript "E" denotes "at constant electric field". Δd_{33} is the difference between the direct coefficient $d_{33,}^{f,D}$ and the converse coefficient $d_{33}^{f,C}$. The in-plane piezoelectric coefficients are found to be:[35]

$$d_{31}^{f,C} = 0 \quad \text{(due to in-plane clamping)}$$

$$d_{31}^{f,D} = \Delta P_3 \,/(\sigma_{11} + \sigma_{22}) = d_{31}(s_{11}^{E,sub} + s_{12}^{E,sub})/(s_{11}^{E,f} + s_{12}^{E,f}) \tag{2.12.3}$$

$$e_{31}^{f,D} = \Delta P_3 \,/(\varepsilon_{11} + \varepsilon_{22}) = d_{31}/(s_{11}^{E,f} + s_{12}^{E,f}) \tag{2.12.4}$$

$$e_{31}^{f,C} = \sigma_{11}^{f}/E_3 = d_{31}/(s_{11}^{E,f} + s_{12}^{E,f}) = e_{31}^{f,D} \tag{2.12.5}$$

In a general case, an epitaxial ferroelectric film with a normal $\mathbf{n^{(3)}}$ bounded by a thick substrate is shown in Fig. 2.2. It is assumed that the substrate is a piezoelectrically inactive single crystal. The substrate is much thicker than the film and it has a fixed bottom surface.[53] The epitaxial relationship for the film/substrate couple are $\mathbf{n^{(1)}//n^{(1,\,sub)}}$, $\mathbf{n^{(2)}//n^{(2,\,sub)}}$ in plane and $\mathbf{n^{(3)}//n^{(3,\,sub)}}$ along the normal, where $\mathbf{n^{(i)}}$ and $\mathbf{n^{(i,\,sub)}}$ (i=1-3) are unit vectors representing the three orthorhombic axes of the film/substrate couple, and they are indexed in the Cartesian coordinates of the crystalline structure of the film ($\boldsymbol{x}_{\mathbf{k}}$) and substrate ($\boldsymbol{x}_k^{sub}$), respectively.[49] Since a substrate usually has different electro-mechanical properties from those of a film, stresses will arise on the film/substrate interface when the couple undergoes a piezoelectric driven process. As illustrated in the previous chapter, it is these in-plane stresses that will modify the piezoelectric properties of a ferroelectric film and make them deviate from those of a single crystal.

The in-plane stresses will be concentrated on the film if it is grown on a thick

substrate. It can be written as: [46-48]

$$\sigma_{lm} = -G^{E,f}_{lmpq}(n^{(3)})\ \varepsilon^{0}_{pq} \tag{2.13}$$

Where $G^{E,f}_{lmpq}(n^{(3)})$ is the planar elastic modulus tensor at constant electric field of a film with a normal $\mathbf{n^{(3)}}$, which is presented by Eq. (2.14). ε^{0}_{pq} is the self-strain between film and substrate which is induced by the applied mechanical or electrical stimulus.

$$G^{E,f}_{lmpq}(n^{(3)}) = C^{E,f}_{lmpq} - C^{E,f}_{lm\alpha\beta}\ n^{(3)}_{\alpha}\ \Pi_{\beta\delta}(n^{(3)})\ n^{(3)}_{\varepsilon} C^{E,f}_{\delta\varepsilon pq} \tag{2.14}$$

$C^{E,f}_{lmpq}$, $C^{E,f}_{lm\alpha\beta}$, and $C^{E,f}_{\delta\varepsilon pq}$ are the tensor of elastic moduli of the film (at constant electric field), $\Pi_{\beta\delta}(n^{(3)}) = (\Lambda_{\beta\delta}(n^{(3)}))^{-1}$, a Green tensor $\Lambda_{\beta\delta}(n^{(3)}) = n^{(3)}_{\gamma} C^{E,f}_{\gamma\beta\delta\zeta}\ n^{(3)}_{\zeta}$.[46-48] The in-plane stresses will induce a longitudinal polarization Δp_3 in a direct piezoelectric mode or a longitudinal strain $\Delta\varepsilon_{33}$ in a converse piezoelectric mode:

$$\Delta p_3 = d_{klm}\sigma_{lm} n^{(3)}_{k} \quad \text{or} \quad \Delta\varepsilon_{33} = s^{E,f}_{ijpq}\ \sigma_{pq} n^{(3)}_{i} n^{(3)}_{j} \tag{2.15}$$

Where $s^{E,f}_{ijpq}$ is the tensor of elastic compliance of the piezoelectric crystal.

2.3.1 Direct piezoelectric coefficients for a clamped ferroelectric film

As can be seen in Fig 2.3 (a), in a transverse piezoelectric mode, in-plane stresses (σ_{11}, σ_{22}) or strains ($\varepsilon_{11}, \varepsilon_{22}$) are applied to a substrate. An in-plane stress field σ^{f} will arise in the film due to clamping from the substrate. A longitudinal polarization Δp_3 in the form of Eq. (2.15) will be induced, and it can be characterized by a direct transverse

piezoelectric coefficient $d_{31}^{f,D} = \Delta p_3 /(\sigma_{11} + \sigma_{22})$ or $e_{31}^{f,D} = \Delta p_3 /(\varepsilon_{11} + \varepsilon_{22})$. For a longitudinal piezoelectric mode ($d_{33}^{f,D}$) as is shown in Fig 2.3 (b), a normal stress σ_{33} is applied to the film/ substrate couple, and in-plane stresses will arise in the film due to the discontinuity of elastic properties across the film/substrate interface. A polarization induced by these in-plane stresses in the form of Eq. (2.15) will add to the longitudinal charge $d_{33}^{*}\ \sigma_{33}$ characterized by Eq. (2.11). The effect of in-plane stresses on the direct piezoelectric responses and the resulting effective piezoelectric coefficients are tabulated in Table 2.5 and Table 2.6, respectively.

2.3.2 Converse piezoelectric coefficients for a clamped ferroelectric film

On the other hand, for a film under an normal electric field E_3 (Fig. 2.4), there are three converse piezoelectric effects-a transverse effect characterized by $e_{31}^{f,C} = (\sigma_{11}^{f} + \sigma_{22}^{f})/2E_3$, a longitudinal effect characterized by $d_{33}^{f,C} = \varepsilon_{33}/E_3$, and a shear effect characterized by $d_{3\tau}^{f,C} = \varepsilon_{3\tau}/E_3$ (τ is the shear direction). It should be noted here that all these strains calculated here are strains of the film.

The in-plane stresses are: $\sigma_{pq} = -G_{lmpq}^{E,f}(n^{(3)})\ \varepsilon_{lm}^{0} = -G_{lmpq}^{E,f}(n^{(3)}) d_{klm}\, n_k^{(3)} E_3$. Which is $\sigma_{uv}^{f} = \sigma_{pq} n_p^{(u)} n_q^{(v)} = -G_{lmpq}^{E,f}(n^{(3)}) d_{klm}\, n_k^{(3)} n_p^{(u)} n_q^{(v)} E_3$ when expressed in the orthorhombic coordinates of $\mathbf{n^{(1)}}$, $\mathbf{n^{(2)}}$ and $\mathbf{n^{(3)}}$. The effective converse piezoelectric coefficient $e_{31}^{f,C}$ can be obtained by taking the average of the in-plane stresses σ_{11}^{f} and σ_{22}^{f} over the applied field E_3:

$$e_{31}^{f,C} = -[(\sigma_{11}^{f} + \sigma_{22}^{f})/2]/E_3 = d_{klm}\, n_k^{(3)}\, G_{lmpq}^{E,f}(n^{(3)})[n_p^{(1)} n_q^{(1)} + n_p^{(2)} n_q^{(2)}]/2 \qquad (2.16)$$

The longitudinal and shear converse piezoelectric coefficients have been formulated in Section 2.1. Here we can find another identical expression for $d_{33}^{f,C}$ by considering the contribution to a longitudinal strain by the in-plane film stresses, which is characterized by Eq. (2.15) as $\Delta\varepsilon_{33} = s_{ijpq}^{E,f}\ \sigma_{pq} n_i^{(3)} n_j^{(3)}$. By doing this, we can find a general quantitative relationship between the single crystal piezoelectric coefficient d_{33}^{*} (which has equivalent values for direct and converse coefficients), the direct piezoelectric coefficient $d_{33}^{f,D}$ and the converse piezoelectric coefficient $d_{33}^{f,C}$, which is presented in Eq. (2.17).

$$d_{33}^{f,D} = d_{33}^{*} + \Delta d_{33}^{f,D} = d_{33}^{*} + \Delta d_{33}^{f,C} + \Delta d_{33}^{D-C} = d_{33}^{f,C} + \Delta d_{33}^{D-C} \qquad (2.17)$$

Where $d_{33}^{*} = d_{kij} n_k^{(3)} n_i^{(3)} n_j^{(3)}$ is the longitudinal piezoelectric coefficient for a single crystal plate with normal $\mathbf{n^{(3)}}$, $\Delta d_{33}^{f,D} = -d_{klm} G_{lmpq}^{E,f}(n^{(3)}) n_k^{(3)} (s_{pqij}^{E,f} - s_{pqij}^{*,sub}) n_i^{(3)} n_j^{(3)}$ is the change of direct longitudinal piezoelectric coefficient due to substrate clamping, $s_{pqij}^{*,sub}$ is the effective elastic compliance tensor of the substrate defined in the Cartesian coordinates of the film, $\Delta d_{33}^{f,C} = -d_{klm} s_{pqij}^{E,f}\ G_{lmpq}^{E,f}(n^{(3)}) n_k^{(3)} n_i^{(3)} n_j^{(3)}$ is the change of converse longitudinal piezoelectric coefficient due to substrate clamping, $\Delta d_{33}^{D-C} = \Delta d_{33}^{D} - \Delta d_{33}^{C}$

$= d_{klm} n_k^{(3)} G_{lmpq}^{E,f}(n^{(3)})\ s_{pqij}^{*,sub} n_i^{(3)} n_j^{(3)}$ is the characteristic of the difference between $d_{33}^{f,D}$ and $d_{33}^{f,C}$. The effect of in-plane stresses on the converse piezoelectric responses and the

effective converse piezoelectric coefficients are tabulated in Table 2.5 and Table 2.6, respectively.

From Table 2.6, it is not difficult to see that expressions for $d_{33}^{f,D}$, $d_{33}^{f,C}$ $d_{31}^{f,D}$, $e_{31}^{f,D}$ and $e_{31}^{f,C}$ will reduce to Eq. (2.12), for the case of an epitaxial tetragonal film grown on a (001) cubic substrate. This set of formula in Table 2.6 will allow one to compute the effective piezoelectric coefficients for arbitrary crystalline structures and orientations of a film and its supporting substrate, if the intrinsic piezoelectric coefficients of the film and the elastic moduli of the film and substrate are known.

In summary, the effective piezoelectric coefficients for an epitaxial ferroelectric film were generally formulated in this section. It was demonstrated how the piezoelectric behavior of a ferroelectric film is affected by the film/substrate interface stresses, which are induced by the clamping of substrate. Our result for the effective piezoelectric coefficients of a clamped ferroelectric film will be equally applicable to piezoelectric films which are not ferroelectrics.

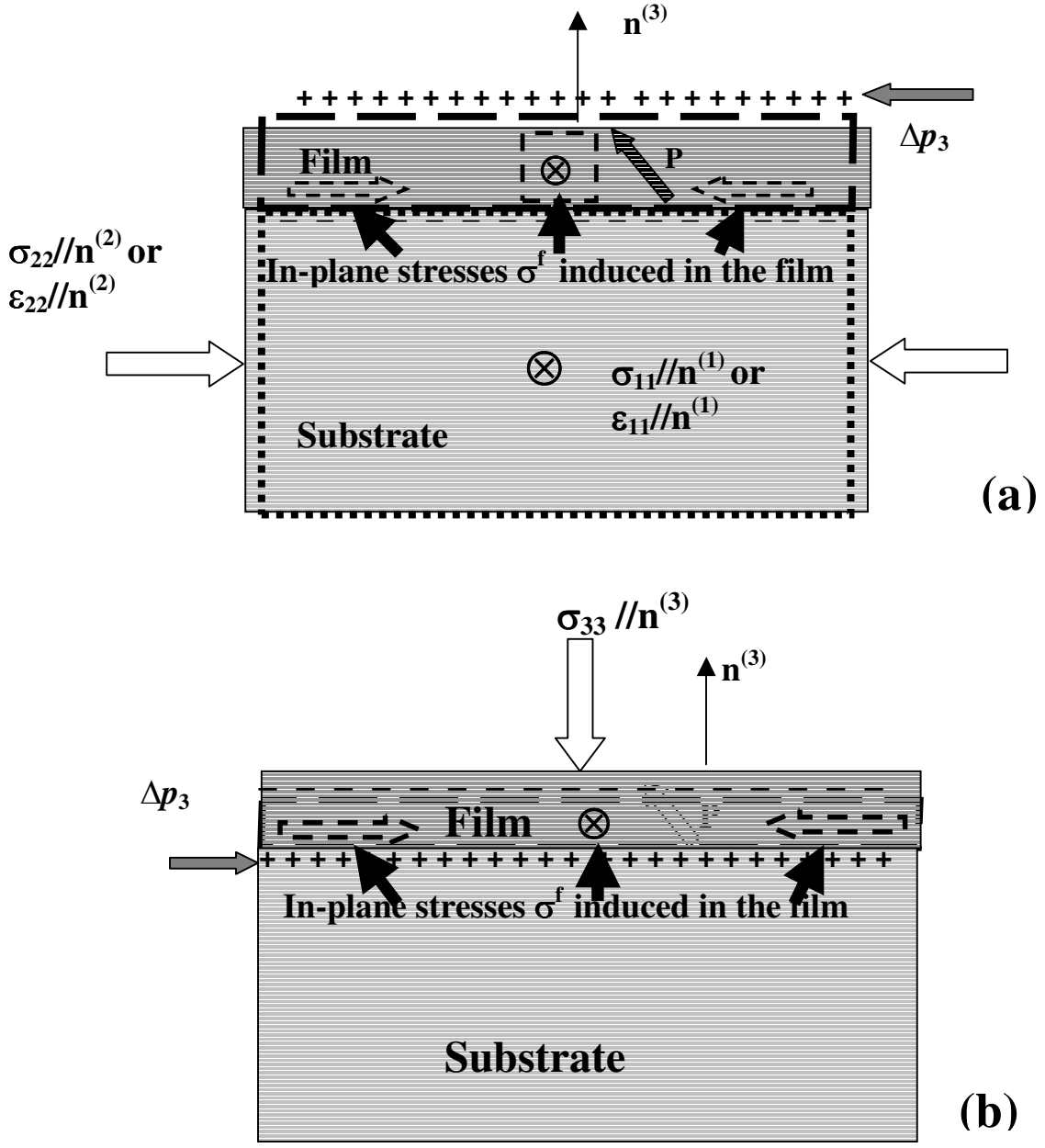

Fig. 2.3 Direct piezoelectric effect: (a) d_{31}/e_{31} mode- a longitudinal charge is produced by applying in-plane stresses/strains to the substrate. (b) d_{33} mode- a longitudinal charge is produced in the film by applying a stress normal to the film/substrate couple.

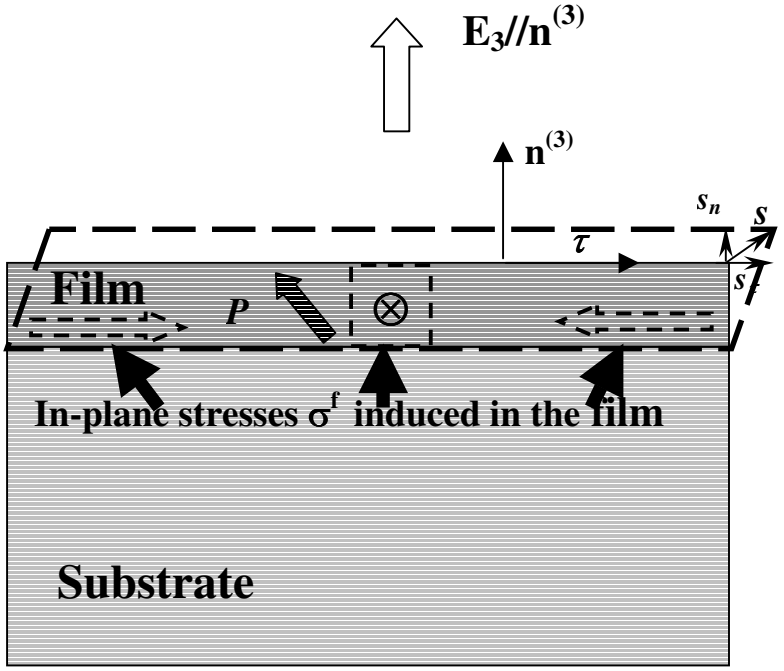

Fig. 2.4 Converse piezoelectric effect –A longitudinal strain and a shear strain are produced by applying an electric field normal to the film[44]; in-plane stresses are also produced under the electric field as a result of substrate clamping. The deformation is exaggerated here for illustration.

Table 2.5. Effect of the film-substrate interface in-plane stresses on the piezoelectric behavior of a clamped ferroelectric film.

Piezoelectric Mode		Stimulus	Response	Self-strain $\overline{\varepsilon^0}$ between film and substrate induced by the applied stimulus	piezoelectric response due to in-plane stresses $-\overline{\overline{G}}(n^{(3)})*\overline{\varepsilon^0}$
"Direct" effect under constant electric field	d_{33}	Longitudinal stress σ_{33}	Longitudinal polarization Δp_3	$\varepsilon^0_{pq} = (s^{E,f}_{pqij} - s^{*,sub}_{pqij})\ n_i^{(3)}\ n_j^{(3)}\ \sigma_{33}$	$\Delta p_3 = -d_{klm} G^{E,f}_{lmpq}(n^{(3)})\ \varepsilon^0_{pq}\ n_k^{(3)}$ will add to intrinsic response $d_{kij} n_k^{(3)} n_i^{(3)} n_j^{(3)}\ \sigma_{33}$
	d_{31}	In-plane stresses σ_{11}, σ_{22}	Longitudinal charge Δp_3	$\varepsilon^0_{pq} = -s^{*,sub}_{pqij}[\sigma_{11}\ n_i^{(1)} n_j^{(1)} + \sigma_{22}\ n_i^{(2)} n_j^{(2)}]$	$\Delta p_3 = -d_{klm} G^{E,f}_{lmpq}\ (n^{(3)}) \varepsilon^0_{pq} n_k^{(3)}$
	e_{31}	In-plane strains ε_{11}, ε_{22}	Longitudinal charge Δp_3	$\varepsilon^0_{pq} = \varepsilon_{11} n_p^{(1)} n_q^{(1)} + \varepsilon_{22} n_p^{(2)} n_q^{(2)}$	$\Delta p_3 = -d_{klm} G^{E,f}_{lmpq}\ (n^{(3)}) \varepsilon^0_{pq} n_k^{(3)}$
"Converse" effect under constant mechanical stress	d_{33}	Longitudinal electric filed E_3	Longitudinal strain ε_{33}	$\varepsilon^0_{lm} = d_{klm} n_k^{(3)} E_3$	$\Delta\varepsilon_{33} = -s^{E,f}_{ijpq} G^{E,f}_{lmpq}(n^{(3)}) \varepsilon^0_{lm} n_i^{(3)} n_j^{(3)}$ will add to intrinsic response $d_{kij} n_k^{(3)} n_i^{(3)} n_j^{(3)} E_3$
	e_{31}	Longitudinal electric filed E_3	In-plane stresses σ_{11}^f, σ_{22}^f	$\varepsilon^0_{lm} = d_{klm} n_k^{(3)} E_3$	$\sigma_{11}^f = -G^{E,f}_{lmpq}(n^{(3)}) \varepsilon^0_{lm} n_p^{(1)} n_q^{(1)}$ $\sigma_{22}^f = -G^{E,f}_{lmpq}(n^{(3)}) \varepsilon^0_{lm} n_p^{(2)} n_q^{(2)}$

Table 2.6. The effective piezoelectric coefficients for a clamped ferroelectric film with an orientation shown in Fig. 2.2, in comparison with those of a single crystal plate with the same orientation.

Piezoelectric coefficients	Single crystal	Film	
		Direct coefficients	Converse coefficients
Longitudinal	$d_{33}^{*}=d_{kij}n_k^{(3)}n_i^{(3)}n_j^{(3)}$	$d_{33}^{f,D}=d_{33}^{*}-d_{klm}G_{lmpq}^{E,f}(n^{(3)})(s_{pqij}^{E,f}-s_{pqij}^{*,sub})n_k^{(3)}n_i^{(3)}n_j^{(3)}$	$d_{33}^{f,C}=d_{33}^{*}-d_{klm}G_{lmpq}^{E,f}(n^{(3)})\ s_{pqij}^{E,f}n_k^{(3)}n_i^{(3)}n_j^{(3)}$ $\overline{d}_{33}^{f,C}$ (measured by total surface displacement) $=d_{33}^{f,D}$
Transverse	$d_{31}^{*}=d_{kij}n_k^{(3)}n_i^{(1)}n_j^{(1)}$ $d_{32}^{*}=d_{kij}n_k^{(3)}n_i^{(2)}n_j^{(2)}$ $e_{31}^{*}=\sum_{i=1}^{6}d_{3i}^{*}C_{i1}^{*}$ † $e_{32}^{*}=\sum_{i=1}^{6}d_{3i}^{*}C_{i2}^{*}$	$d_{31}^{f,D}=d_{klm}\ G_{lmpq}^{E,f}\ (n^{(3)})\ s_{pqij}^{*,sub}[n_i^{(1)}n_j^{(1)}+n_i^{(2)}n_j^{(2)}]n_k^{(3)}/2$ (when $\sigma_{11}=\sigma_{22}$) $e_{31}^{f,D}=d_{klm}\ G_{lmpq}^{E,f}\ (n^{(3)})n_k^{(3)}[n_p^{(1)}n_q^{(1)}+n_p^{(2)}n_q^{(2)}]/2$ (when $\varepsilon_{11}=\varepsilon_{22}$)	$d_{31}^{f,C}=0$ $e_{31}^{f,C}=d_{klm}G_{lmpq}^{E,f}(n^{(3)})n_k^{(3)}\ [n_p^{(1)}n_q^{(1)}+n_p^{(2)}n_q^{(2)}]/2$
Shear	$d_{34}^{*}=2\,d_{kij}n_k^{(3)}n_i^{(2)}n_j^{(3)}$ $d_{35}^{*}=2d_{kij}n_k^{(3)}n_i^{(1)}n_j^{(3)}$ $d_{36}^{*}=2d_{kij}n_k^{(3)}n_i^{(1)}n_j^{(2)}$	N/A	$d_{3\tau}^{f,C}=\Pi_{ik}(n^{(3)})\ C_{kt\alpha\beta}^{E,f}\ d_{\gamma\alpha\beta}n_t^{(3)}n_\gamma^{(3)}\tau_i$ [14]

†: C_{ij}^{*} are the effective elastic constants of the film. If $C_{\alpha\beta\delta\theta}^{*}$ is the full tensor notation of C_{ij}^{*}, it can be obtained by $C_{\alpha\beta\delta\theta}^{*}=C_{ghuv}n_g^{(\alpha)}n_h^{(\beta)}n_u^{(\delta)}n_v^{(\theta)}$, where C_{ghuv} is the elastic tensor of the single crystal.[49] $\mathbf{n^{(k)}}$ (k=1-3) are the orientation vectors of the film (Fig. 1)

2.4 Theoretical prediction for various thin film material systems

Based on the available piezoelectric coefficients and mechanical properties for bulk materials, the orientation dependences of the converse longitudinal piezoelectric coefficient $d_{33,f}$ and piezoelectric force coefficient $e_{31}^{f,D}$ are calculated for ferroelectric film materials like lead zirconate titanate solid solution system, barium titanate, and some relaxor ferroelectrics. To compare the direct piezoelectric coefficients with converse ones, direct piezoelectric coefficients $d_{33,f}^{D}$ and $d_{31,f}^{D}$ are also calculated for lead zirconate titanate materials with silicon and strontium titanate substrates.

2.4.1 Lead Zirconate Titanate solid solution

Lead zirconate titanate ($PbZr_xTi_{1-x}O_3$, abbreviated as PZT) bulk ceramics have a wide range of applications in electromechanical systems due to their excellent piezoelectric properties. Recently, there is an increasing number of research works on PZT in thin film form due to the success of its epitaxial growth and its potential for micro-electro-mechanical applications. By using different measurement techniques, people obtained piezoelectric coefficients $d_{33,f}$ ranging from ~50pm/V (pC/N) to ~800pm/V (pC/N) for PZT films.[38], [45], [54], [55] Despite the substrate clamping effect, which deteriorates the piezo-electric properties of the film, some of these reported values were even larger than phenomenologically predicted bulk values.[6] Therefore, a clear understanding of the intrinsic piezoelectric properties in a clamped PZT film will help us to tell if a measured effective piezoelectric coefficient has extrinsic contributions, such as domain wall motion, incomplete clamping, substrate bending[37],[43], or even experiment fraud.

Based on the phenomenologically calculated piezoelectric coefficients and available mechanical properties for bulk materials, the orientation dependences of the converse longitudinal piezoelectric coefficient $d_{33,f}$ and piezoelectric force coefficient $e_{31}^{f,D}$ are calculated for epitaxial $Pb(Zr_xTi_{1-x})O_3$ films with different compositions. The calculations indicate that both tetragonal and rhombohedral $Pb(Zr_xTi_{1-x})O_3$ films have their maximum $d_{33,f}$ and $e_{31}^{f,D}$ values along an axis close to the pseudo-cubic [001] direction, which are similar to the orientation dependence results for $Pb(Zr_xTi_{1-x})O_3$ bulk materials. However, the calculated maximum intrinsic $d_{33,f}$ value (~330pm/V), which is in a [001] oriented $Pb(Zr_{0.52}Ti_{0.48})O_3$ film (on the rhombohedral side of the morphotropic phase boundary), is only about half of the result for bulk crystals (624pm/V); On the other hand, the calculated maximum intrinsic $e_{31}^{f,D}$, which is also in a [001] oriented rhombohedral $Pb(Zr_{0.52}Ti_{0.48})O_3$ film, is about twice as much as that for the corresponding bulk material. This calculation showed that the substrate clamping plays an important role on determining the piezoelectric properties of lead zirconate titanate ferroelectric thin films.

In principle, we can calculate the longitudinal piezoelectric coefficients for arbitrary orientations and here for three typical orientations (001), (011) and (111). The expressions for Π_{ik} and $d_{33,f}$ of these three orientations are calculated and shown in Table 2.1 through 2.4.

The elastic compliance data for PZT film near the PT composition (x=0, 0.2) were taken from J. D. Freire et al. [56] For PZT films with compositions near the MPB (x~0.5), the elastic compliance data were taken from T. Mitsui et al., [57] since there is no single

crystal data reported. The quantitative values of these three piezoelectric coefficients were given by phenomenological calculations.[6] For tetragonal $PbZr_xTi_{1-x}O_3$ films with x=0 ($PbTiO_3$, d_{31}=-23.1pm/V, d_{33}=79.2pm/V, d_{15}=56.1pm/V) and x=0.48 (PZT 48/52, d_{31}=-135pm/V, d_{33}=313pm/V, d_{15}=530pm/V), the orientation dependence of $d_{33,f}$ are presented in Fig. 2.5 and Fig 2.6, respectively.

The quantitative values of the piezoelectric coefficients were given by phenomenological calculations in the pseudo-cubic coordinate system.[6] By the standard transformation law for tensor quantities given by J. F. Nye, [49] the piezoelectric coefficients defined in a rhombohedral coordinate system can be obtained for rhombohedral $PbZr_xTi_{1-x}O_3$ material ($x \geq 0.52$). For rhombohedral $PbZr_xTi_{1-x}O_3$ films with x=0.52 (PZT 52/48, d_{31}=-62pm/V, d_{33}=107pm/V, d_{15}=1244pm/V, d_{22}=-273pm/V) and x=0.6 (PZT60/40, d_{31}=-11.3pm/V, d_{33}=70.8pm/V, d_{15}=359.9pm/V, d_{22}=-75.2pm/V), the orientation dependence of $d_{33,f}$ are presented in Fig. 2.7 and Fig 2.8, respectively.

The calculation results showed that:

(1) Both tetragonal and rhombohedral $Pb(Zr_xTi_{1-x})O_3$ films have similar orientation dependence as those of their bulk materials.[7] The maximum $d_{33,f}$ is in a direction close to pseudo cubic (001) in both tetragonal and rhombohedral structures.

(2) In films with a rhombohedral structure, $d_{33,f}$ values are much more reduced in non-polar directions than in the polar direction [111], as compared with the bulk properties. It is the opposite in tetragonal films where the $d_{33,f}$ value is much more reduced in the polar direction [001] than in a non-polar direction;

(3) The calculated maximum intrinsic $d_{33,f}$ (327.5pm/V) for $Pb(Zr_xTi_{1-x})O_3$ material, which is for a [001] oriented $Pb(Zr_{0.52}Ti_{0.48})O_3$ film (on the rhombohedral side of the morphotropic phase boundary), is only about half of the result for bulk crystals (624pm/V). This calculation showed that the substrate clamping plays an important role on determining the piezoelectric properties of ferroelectric thin films.

In addition, Fig. 2.9 (a) shows $d_{33,f}$ for [001], [011] [111] oriented PZT films as function of the composition and Fig 2.9 (b) compares $d_{33,f}$ for a [001] oriented epitaxial film and that of a [001] poled polycrystalline film (calculated by using material constants from T. Mitsui et al. [57]). It is seen that the order of magnitude for $d_{33,f}$ is [001]>[011] >[111] in PZT epitaxial films with compositions $x \leq 0.6$, and an epitaxial film always has larger intrinsic $d_{33,f}$ than that of a polycrystalline one at the same composition.

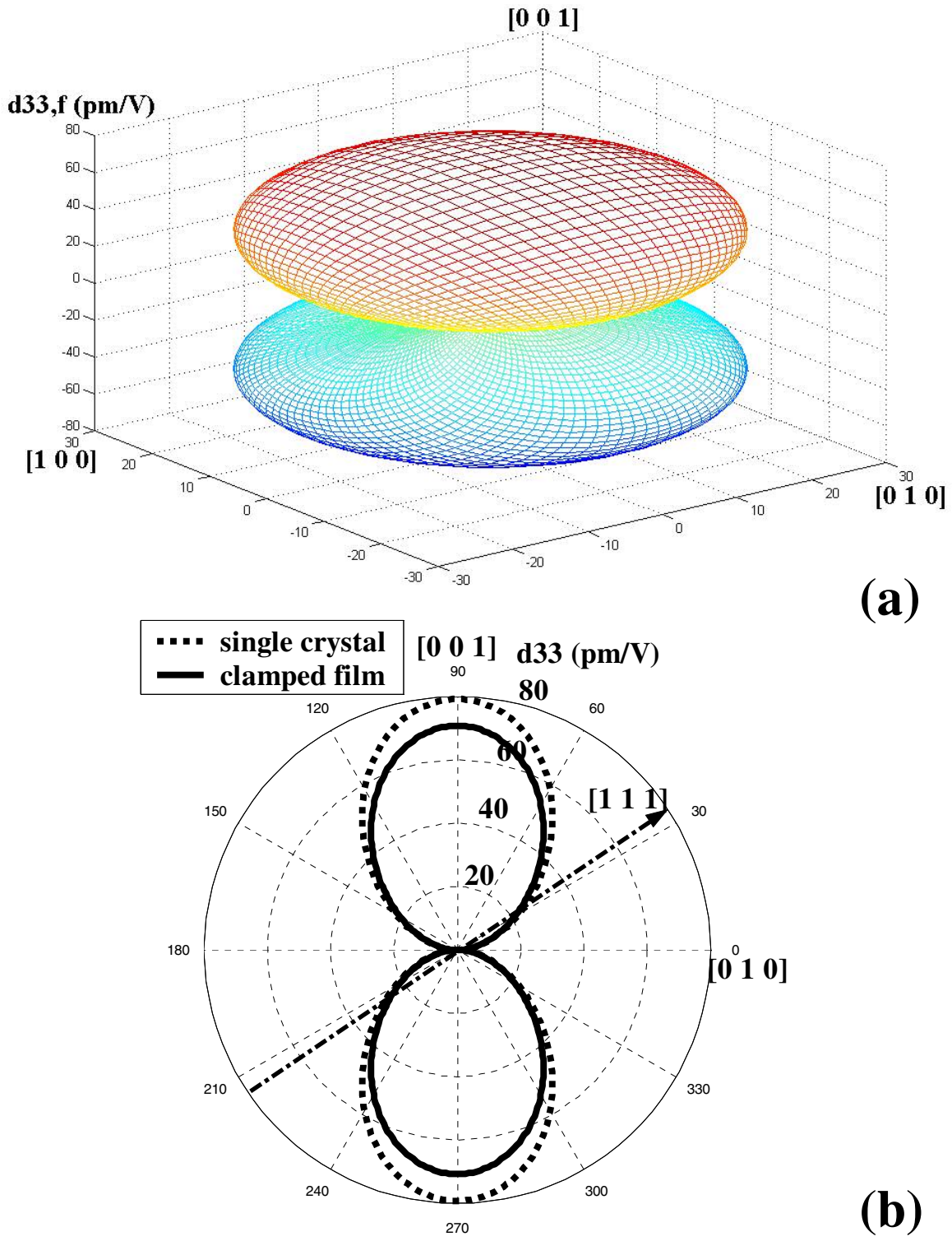

Figure 2.5 (a) Orientation dependence of the intrinsic longitudinal converse piezoelectric coefficient $d_{33,f}^{C}$ of $PbTiO_3$ films; (b) The cross section curve when the figure in (a) is cut by the (1 0 0) plane.

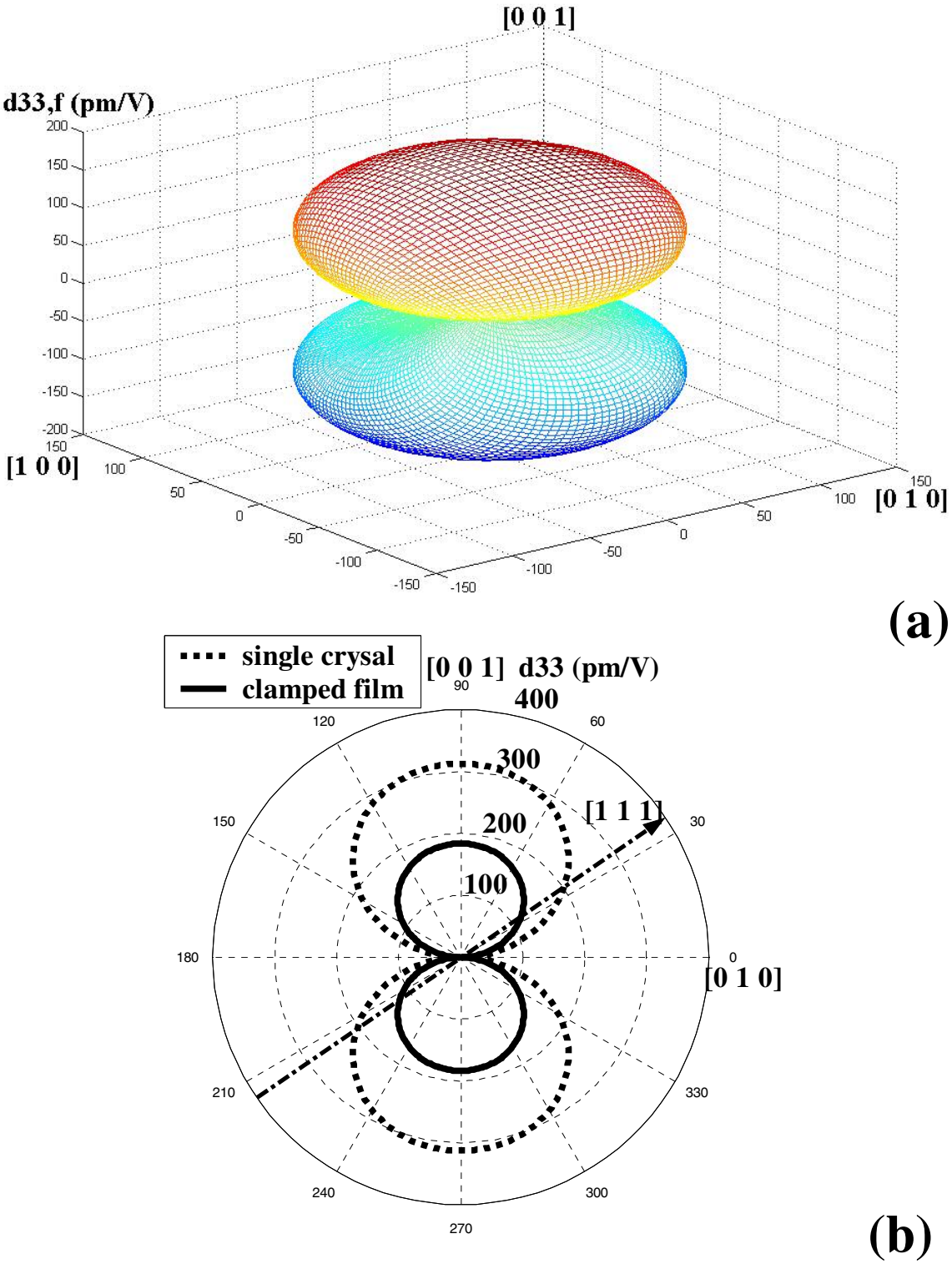

Figure 2.6 (a) Orientation dependence of the intrinsic longitudinal converse piezoelectric coefficient $d_{33,f}^{C}$ of $Pb(Zr_{0.48}\ Ti_{0.52})O_3$ films; (b) The cross section curve when the figure in (a) is cut by the (1 0 0) plane.

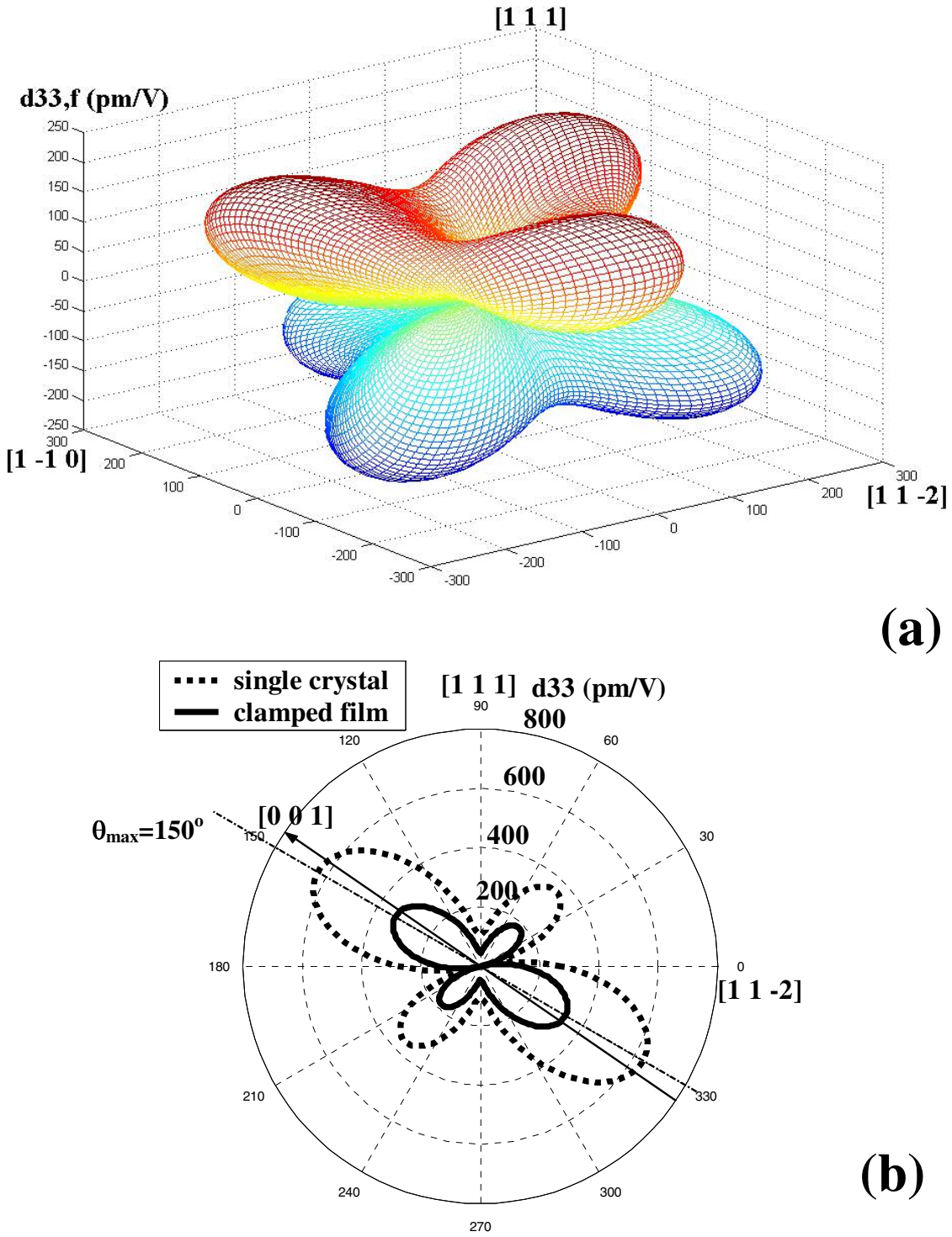

Figure 2.7. (a) Orientation dependence of the intrinsic longitudinal converse piezoelectric coefficient $d_{33,f}^{C}$ of $Pb(Zr_{0.52}\ Ti_{0.48})O_3$ films; (b) The cross section curve when the figure in (a) is cut by the (1 -1 0) plane.

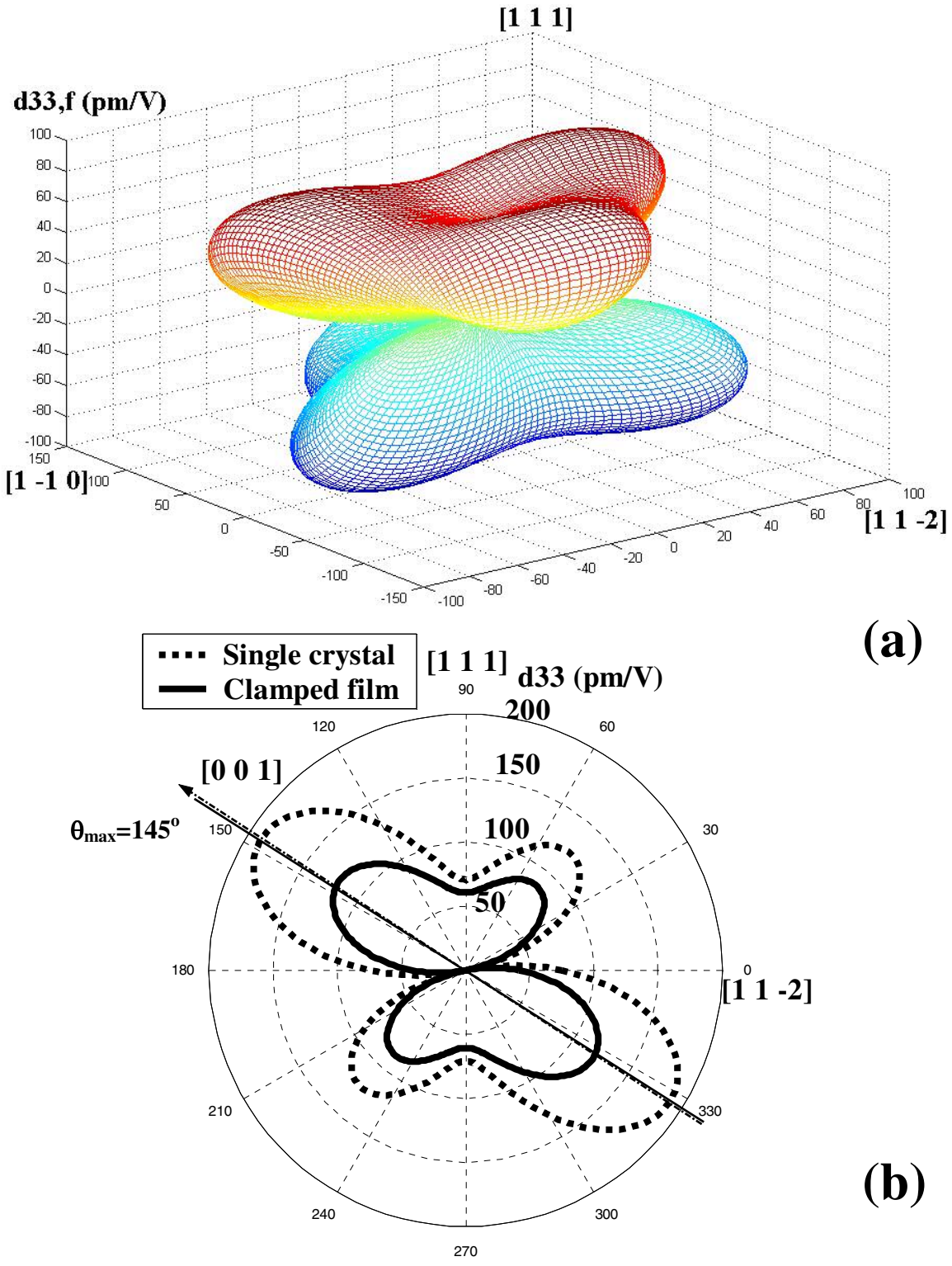

Figure 2.8. (a) Orientation dependence of the intrinsic longitudinal converse piezoelectric coefficient $d_{33,f}^{C}$ of $Pb(Zr_{0.6}\ Ti_{0.4})O_3$ films; (b) The cross section curve when the figure in (a) is cut by the (1 -1 0) plane.

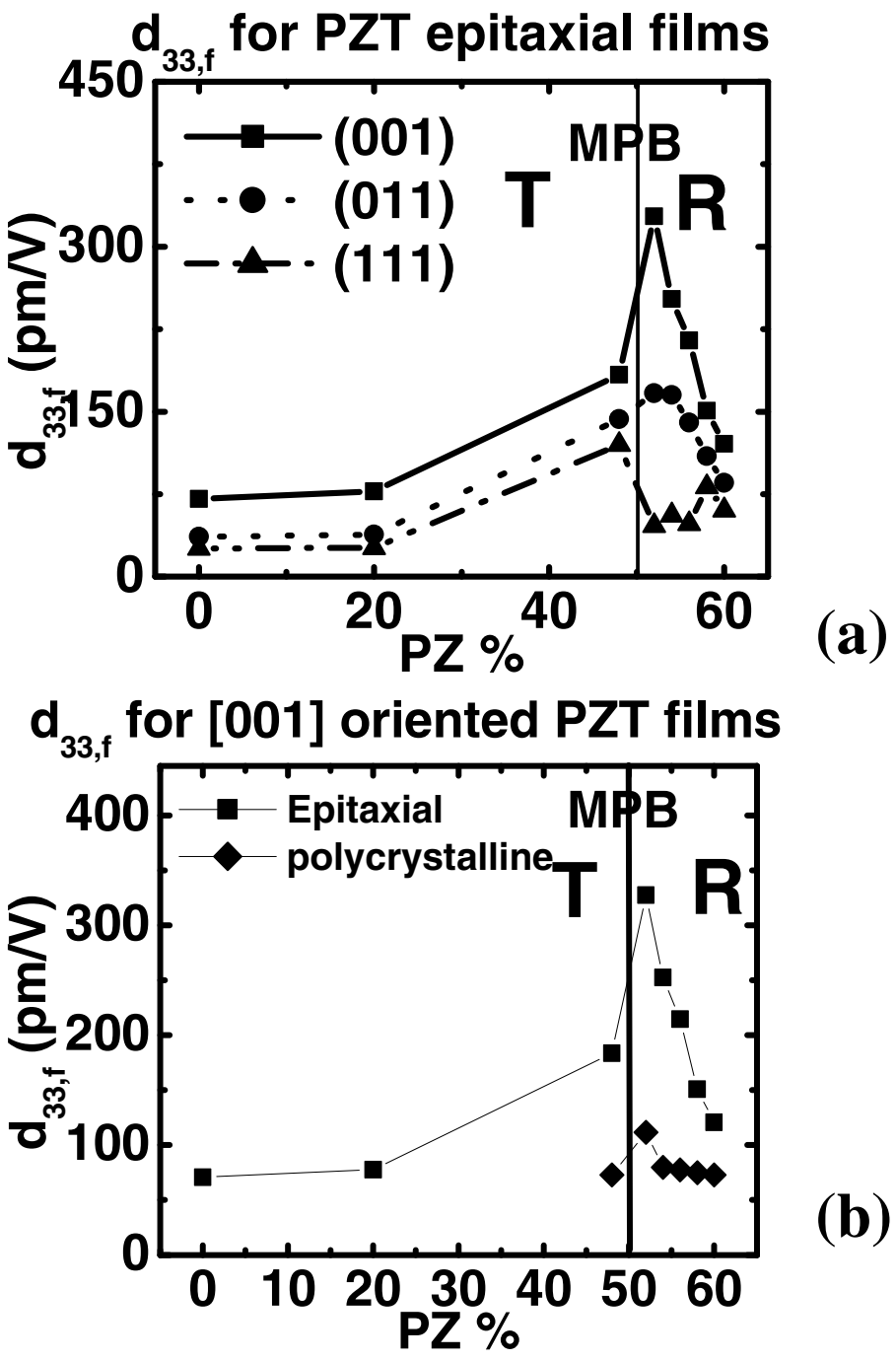

Figure 2.9 (a) $d_{33,f}^{C}$ for [001], [011], [111] oriented PZT epitaxial films as function of film composition; (b) $d_{33,f}^{C}$ for [001] oriented epitaxial and polycrystalline films as function of film composition.

Calculations for transverse piezoelectric coefficients $e_{31}^{f,D}$ (=$e_{31}^{f,C}$) based on the results in Table 2.6 are performed for MPB-PZT thin films - x=0.50 for a tetragonal structure and x=0.52 for a rhombohedral structure. The piezoelectric coefficients (in a pseudo cubic coordinate system) for PZT bulk materials were calculated by using a phenomenological method developed by Haun et al. [6] The elastic modulus of PZT materials were taken from T. Mitsui et al.[57].

The orientation dependence of $e_{31}^{f,D}$ with respect to the film normal $\mathbf{n}^{(3)}$ for a tetragonal PZT 50/50 film is visualized in Fig 2.10 (a), where the distance between the surface of the graph and the origin represents the magnitude of $e_{31}^{f,D}$ for that orientation. Fig. 2.10 (b) shows the cross section curve of (100) plane for $e_{31}^{f,D}$ and e_{31} (for single crystal) of PZT 50/50. It shows that both e_{31} and $e_{31}^{f,D}$ have their maximum values for a film orientation $\mathbf{n}^{(3)}$ =[001].

Similarly, the orientation dependence of $e_{31}^{f,D}$ in a rhombohedral PZT 52/48 film is visualized in Fig. 2.11 (a), and Fig. 2.11 (b) shows the cross section curve of a pseudo-cubic (1 -1 0) plane (rhombohedral (010) plane) for $e_{31}^{f,D}$ and e_{31}. It shows that both e_{31} and $e_{31}^{f,D}$ has minima for the pseudo-cubic [111] orientation, which is the polarization direction. The maximum value of $e_{31}^{f,D}$ (~30C/m^2), as well as that of e_{31}, is in an orientation $\mathbf{n}^{(3)}$ very close to [001] axis, which is 54.7^o away from [1 1 1].

Fig. 2.12 shows the effective piezoelectric coefficient $e_{31,f}$ in [001], [111] oriented epitaxial PZT films with respect to compositions (denoted as $e_{31,f[001]}$ and $e_{31,f[111]}$, respectively). For both tetragonal and rhombohedral PZT films, $e_{31,f[001]}$ is

larger than $e_{31,f[111]}$. However, the difference between $e_{31,f[001]}$ and $e_{31,f[111]}$ is remarkably large for rhombohedral PZT films and it increases as the composition approaches the morphotropic phase boundary. On the rhombohedral side of the MPB (x=0.52), $e_{31,f[001]}$ has the maximum value of -30.2 C/m^2 while $e_{31,f[111]}$ is only -5.7 C/m^2. It should be noted that the highest $e_{31,f}$ reported for PZT materials is around -26 C/m^2 in a (001) orientation[58], which agrees well with our calculation.

As a comparison, $e_{31,f}$ values for PZT polycrystalline films ($e_{31,f\ poly}$, calculated by using Eq. 2.10 with material constants taken from Ref. [57] and experiment measured $e_{31,f}$ for textured PZT films ($e_{31,f\ textu.}$)[35] are also plotted in Fig. 2.12. On the rhombohedral side of the MPB (x≥0.52), $e_{31,f\ poly}$ have the maximum value at x=0.52, which is about -10C/m^2 and agrees well with the data reported in Ref. [34]. For the (001) oriented films on the same side, it can be seen that $e_{31,f[001]} > e_{31,f\ textu.}(001) > e_{31,f\ poly}$. While for the (111) oriented films, it is $e_{31,f[111]} < e_{31,f\ textu.}(111) < e_{31,f\ poly}$. This can be understood if $e_{31,f}$ increases as the film orientation is canted away from the polar direction [111] toward the [001] orientation, just like in the case of d_{33}[8]. Thus, even in a fully poled poly-crystalline film, some PZT grains canted away from the poling direction will enhance $e_{31,f}$,. This may explain why $e_{31,f}$ for polycrystalline films are larger than $e_{31,f[111]}$, which is calculated by assuming that the [111] film has a single domain structure.

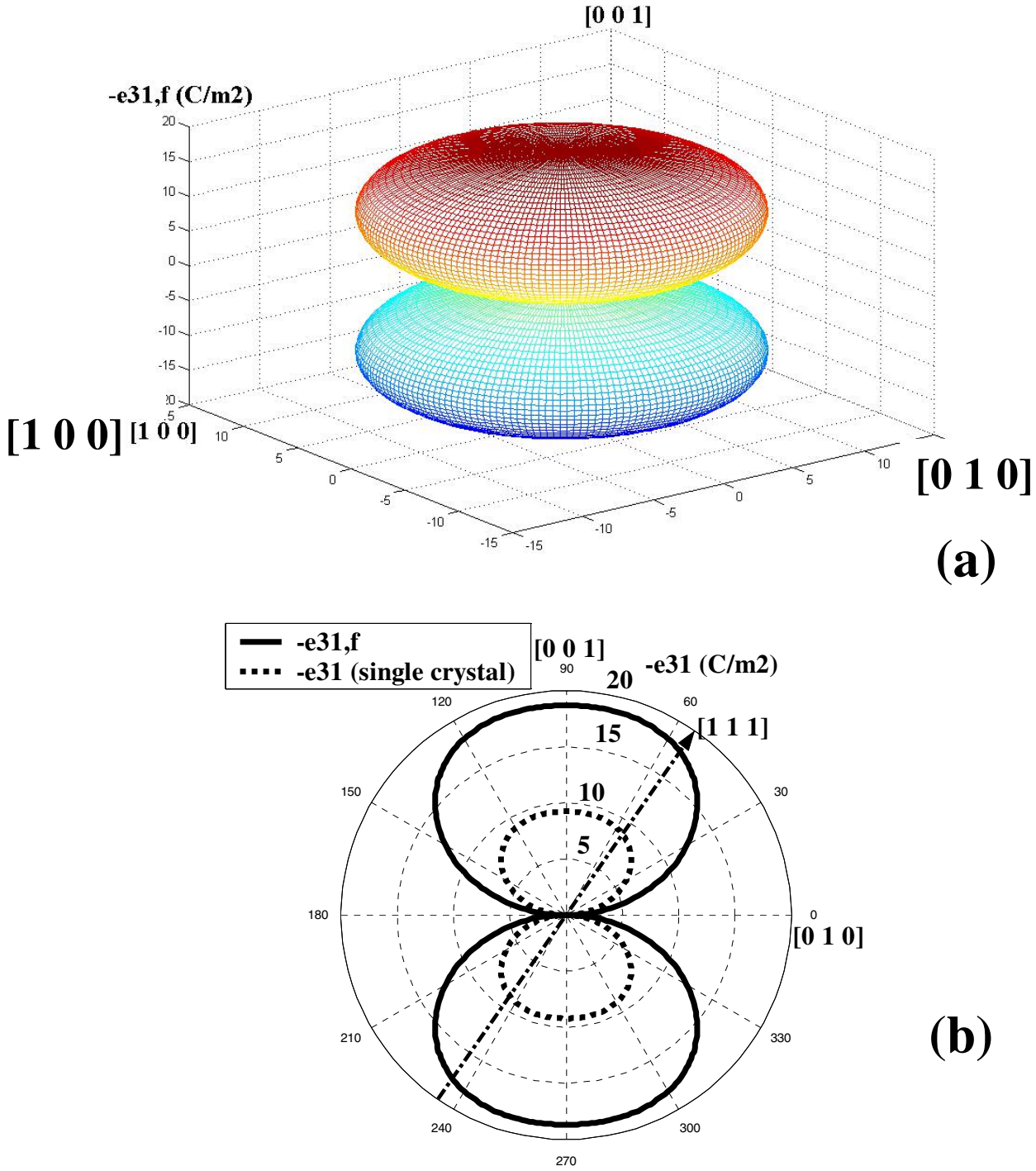

Fig. 2.10 (a) Effective piezoelectric coefficient $e_{31}^{f,D}$ of a tetragonal PZT 50/50 film as function of film orientation. (b) The cross section curve of (a) cut by the (1 0 0) plane.

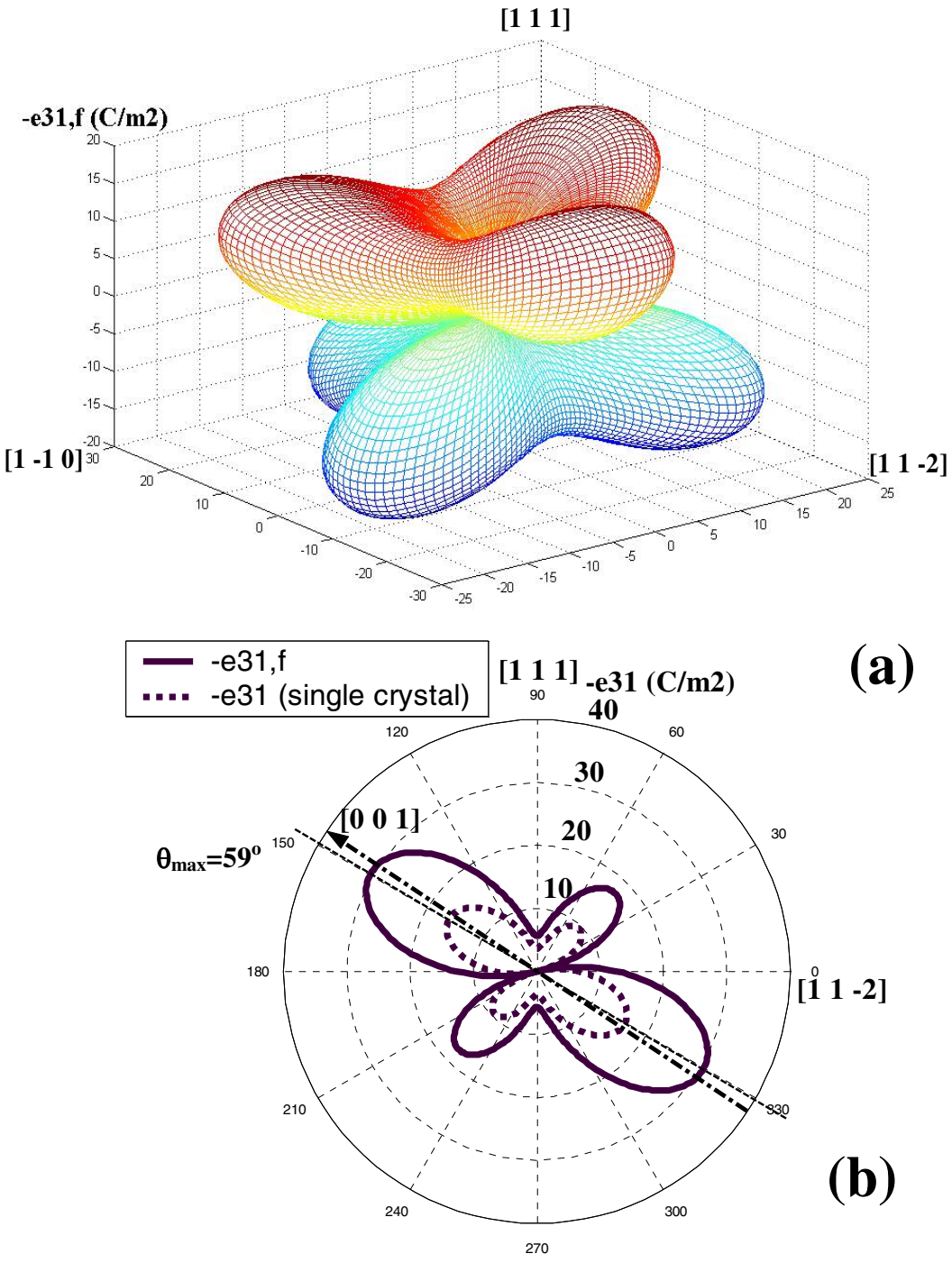

Fig. 2.11 (a) Effective piezoelectric coefficient $e_{31}^{f,D}$ of a rhombohedral PZT 52/48 film as function of film orientation.. (b) The cross section curve of (a) cut by the pseudo-cubic (1 -1 0) plane.

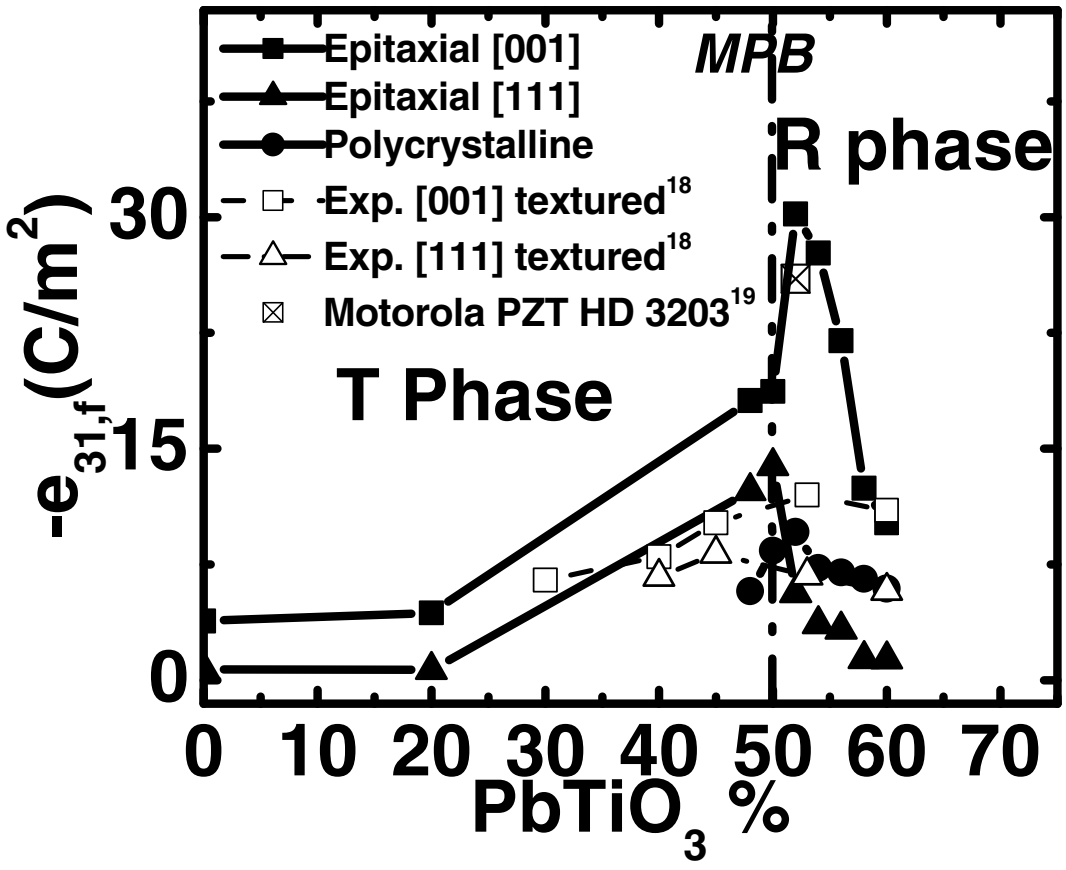

Figure 2.12 Effective piezoelectric coefficient $e_{31,f}$ of PZT films with various compositions.

$d_{33,f}^{D}$, $d_{31,f}^{D}$ and $e_{31,f}^{D}$ values are also numerically calculated for three typical orientations (001), (101) and (111) in Fig. 2.13 as functions of composition x for $Pb(Zr_x Ti_{1-x})O_3$ single domain ferroelectric thin films epitaxially grown on Si substrate. Piezoelectric and elastic constants for $Pb(Zr_x Ti_{1-x})O_3$ materials necessary for calculations are taken from Ref. [6] and [56]-[57], respectively. The elastic constants for single crystal Si are taken from Ref. [59].

From Figures 2.13, it can be seen that $Pb(Zr_x Ti_{1-x})O_3$ films have their maximum direct piezoelectric coefficients in a pseudo cubic [0 0 1] orientation, regardless of the film composition and structure. Optimum $d_{33,f}^{D}$, $d_{31,f}^{D}$ and $e_{31,f}^{D}$ values for $Pb(Zr_x Ti_{1-x})O_3$ films as MEMS sensor components maybe realized in a pseudo-cubic [001] orientation on the rhombohedral side of the morphotropic boundary (x=0.52). The calculated $d_{33,f}^{D}$ and $e_{31,f}^{D}$ are about ~450pC/N and -30 C/m^2, respectively, for this (001) oriented MPB-PZT film grown on a Si substrate, which agree well with the reported experiment data in Ref [36] and Ref [58]. The results suggested that PZT epitaxial thin films used for MEMS sensor applications should adopt the rhombohedral composition on the morphotropic phase boundary with a pseudo-cubic [001] orientation.

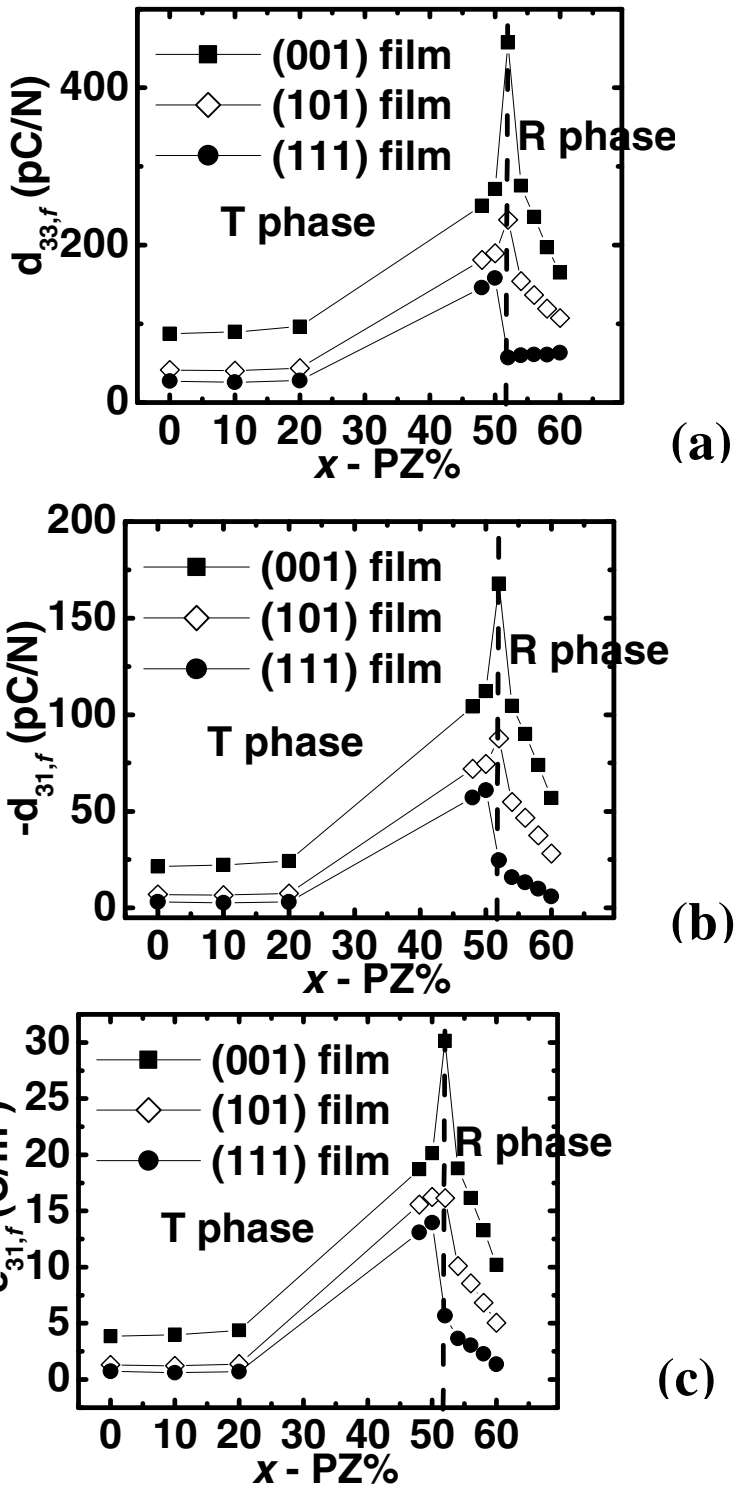

Figure 2.13. (a) Longitudinal piezoelectric coefficient $d_{33,f}^{D}$; (b) transverse piezoelectric coefficient $d_{31,f}^{D}$ and (c) transverse piezoelectric coefficient $e_{31,f}^{D}$ for PZT films grown on Si.

It is more convenient to look at the cross section curves for comparison of substrate-clamping and orientation effects between $d_{33}^{f,D}$ and $d_{33}^{f,C}$. Fig 2.14 shows the cross section curves of $d_{33}^{f,D}$ and $d_{33}^{f,C}$ as a function of the film orientation $\mathbf{n}^{(3)}$, in comparison with that of the intrinsic piezoelectric coefficient d_{33}^{*} given by Eq. (2.11). In the calculation, Si and $SrTiO_3$ (STO) were chosen as the substrates and their elastic constants were also taken from Refs. [59] and [60], respectively. Both films have their maximum longitudinal piezoelectric coefficients in a direction along or very close to the pseudo cubic [0 0 1] direction. It can be seen that $d_{33}^{f,D}$ is always larger than $d_{33}^{f,C}$. Moreover, as the converse coefficient $d_{33}^{f,C}$ does not have substrate dependence, the direct coefficient $d_{33}^{f,D}$ shows a larger value for a film on a relatively soft substrate (Si) than the same film on a relatively rigid substrate ($SrTiO_3$).

The results indicate that, PZT film based transducers can have enhanced longitudinal and transverse piezoelectric responses by choosing a rhombohedral composition near the morphotropic phase boundary, a pseudo-cubic [001] orientation, and a soft substrate.

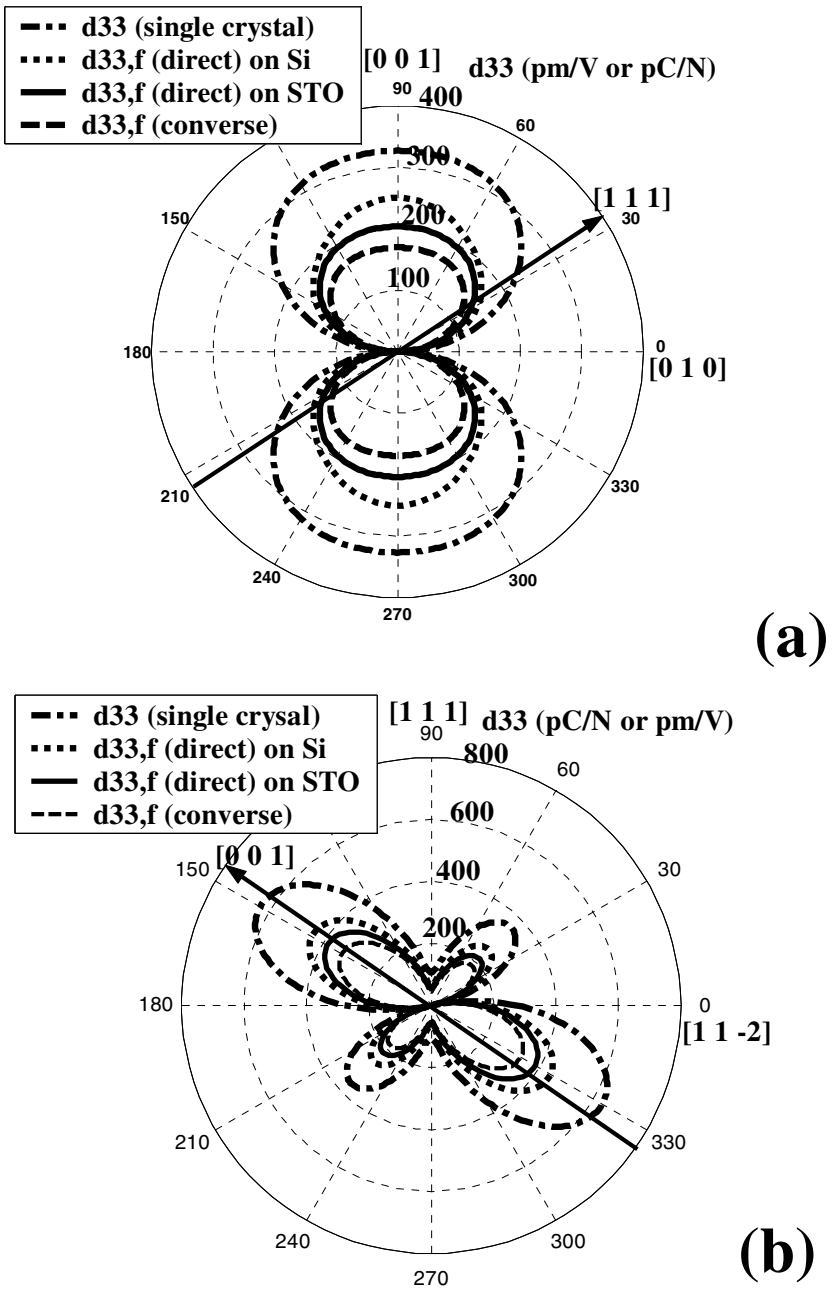

Fig. 2.14 (a). The cross section curve (cut by the (100) plane) of the longitudinal piezoelectric coefficients for a tetragonal $Pb(Zr_{0.5}Ti_{0.5})O_3$ film as function of film orientation. (b) The cross section curve (cut by the pseudo-cubic (1 -1 0) plane) of the longitudinal piezoelectric coefficients for a rhombohedral $Pb(Zr_{0.52}Ti_{0.48})O_3$ film as function of film orientation.

In summary, both tetragonal and rhombohedral PZT epitaxial films have largest piezoelectric coefficients along an axis close to the pseudo-cubic [001] direction, which are similar to the orientation dependence results for PZT bulk materials.[7], [8] However, the calculated maximum intrinsic $d_{33,f}$ (327.5pm/V) for PZT material, which is in a [001] oriented $Pb(Zr_{0.52}Ti_{0.48})O_3$ epitaxial film on the rhombohedral side of the morphotropic phase boundary, is only about half of the result for its bulk crystals (624 pm/V); while the maximum intrinsic $e_{31}^{f,D}$ (~30C/m^2) is about twice as much as that for the corresponding bulk material (~15C/m^2). Our calculations showed quantitatively how the clamping of a substrate can vary the intrinsic longitudinal converse piezoelectric coefficients and gives numerical results for PZT films with various compositions.

2.4.2 Barium Titanate material

The orientation dependences of the converse longitudinal piezoelectric coefficient $d_{33}^{f,C}$, and the in-plane converse piezoelectric coefficient $e_{31,f}$ ($e_{31}^{f,C} = e_{31}^{f,D} = e_{31,f}$), are calculated for tetragonal barium titanate epitaxial films. The calculations demonstrate that both $e_{31,f}$ and $d_{33}^{f,C}$ have their maximum values along an axis close to the (111) direction of the pseudo-cubic system, which are similar to the orientation dependence results for a tetragonal $BaTiO_3$ single crystal. The calculated piezoelectric coefficients for a (111) oriented $BaTiO_3$ epitaxial film ($e_{31,f}$ =-23C/m^2, $d_{33}^{f,C}$ =124pm/V) suggest that it is a good candidate material for lead-free MEMS applications.

Barium Titanate ($BaTiO_3$) is one of the most intensively studied ferroelectric materials. It has an ABO_3 type perovskite cubic structure at high temperature, which is paraelectric, and a ferroelectric tetragonal structure at room temperature. Recently, due to the discovery of the large piezoelectric effect in relaxor-ferroelectric single crystals with non-polar orientations, [9], [15],[61] there has been a renewed interest on the investigation of piezoelectric properties in classic ferroelectrics with simpler structures such as $BaTiO_3$. [6], [10], [12], [13], [62]-[64] S. Wada et al. investigated piezoelectric properties of barium titanate single crystals at room temperature as a function of crystallographic orientation [10] , and they found that a (111) oriented tetragonal $BaTiO_3$ single crystal had a higher longitudinal piezoelectric coefficient d_{33} (=203pm/V) than that of a (001) oriented one (d_{33} =125pm/V). This has been explained by D. Damjanovic et al. [12],[13] by the contribution to d_{33} from piezoelectric shear effect.

In an effort to realize variable functions of $BaTiO_3$ in integrated devices, there have been several methods in growing epitaxial $BaTiO_3$ films with good qualities.[65]-[70] However, despite the fact that $BaTiO_3$ is a lead-free material with large bulk piezoelectric coefficients, there have been very few experiment results on its piezoelectric properties in thin film form. In this section we will calculate the intrinsic piezoelectric coefficients of tetragonal $BaTiO_3$ epitaxial films as function of crystalline orientation and find the optimal conditions for its piezoelectric performance.

On evaluating piezoelectric properties of ferroelectric films for applications in MEMS transducers,[35] the two most important coefficients are the longitudinal piezo-electric coefficient $d_{33,f}$, and the in-plane piezoelectric coefficient $e_{31,f}$. $d_{33}^{f,C}$ is the ratio between a longitudinally generated mechanical strain ε_{33} and a longitudinally applied

electric field E_3, while $e_{31,f}$ is the ratio between an induced longitudinal polarization ΔP_3 (electric charge density) and the sum of laterally applied mechanical strains ε_{11} and ε_{22} (subscripts "1" and "2" indicate the in-plane axies while "3" the longitudinal axis). Excellent piezoelectric transducers either can produce large electric charge signal at small mechanical strains (large $e_{31,f}$) or large mechanical strains at a small electric field (large $d_{33}^{f,C}$), therefore $e_{31,f}$ and $d_{33}^{f,C}$ are essential quantities describing the performance of ferroelectric-film based MEMS transducers. Due to the clamping from substrate, these two piezoelectric coefficients for ferroelectric films can be very different from their counterparts in bulk materials.[44], [52]

The previous results on evaluation of these two piezoelectric coefficients in lead zirconate titanate (abbreviated as PZT) films[44], [52], [71] have shown that a (001) oriented film have larger piezoelectric coefficients than those of a (111) oriented film of the same material in both tetragonal and rhombohedral ferroelectric phases; therefore, it is interesting to see if the orientation dependences of $e_{31,f}$ and $d_{33}^{f,C}$ in $BaTiO_3$ films can match those of PZT films.

From Eq. 2.4 and 2.10, it is seen that $d_{33}^{f,C}$ and $e_{31,f}$ are functions of elastic moduli and piezoelectric moduli, as well as the crystallographic orientation of the epitaxial film. In literature, there are a few sets of elastic moduli and piezoelectric moduli data obtained by different research groups, [72]-[74] which all give qualitatively similar results when used to calculate $e_{31,f}$ and $d_{33}^{f,C}$, as can be seen in Fig 2.15. Here we employ the electromechanical constants reported by Z. Li et al., [74] which is the most

recent experiment data obtained on high-quality $BaTiO_3$ single crystals and gives about average values in calculated piezoelectric coefficients among the three sets of data.

The orientation dependence of $d_{33}^{f,C}$ in a single domain $BaTiO_3$ film is visualized in Fig. 2.16 (a), where the distance between the surface of the graph and the origin represents the magnitude of $d_{33}^{f,C}$ in that orientation. Fig. 2.16 (b) shows the orientation dependence of $e_{31,f}$ in a similar manner as Fig 2.16 (a), while Fig. 2.17 (a) (b) shows the cross sectional curve of a (100) plane for $d_{33}^{f,C}$ and $e_{31,f}$, respectively. The orientation dependence of single crystal d_{33} and e_{31} are also shown in Fig 2.17 (a) and (b) for comparison with thin film data and evaluation of clamping effect. It can be seen that $d_{33}^{f,C}$ and $e_{31,f}$ each has a similar orientation dependence as that of its bulk counterpart. The calculated orientations for maximum $d_{33}^{f,C}$ and $e_{31,f}$ are 50^o and 48^o away from the polar direction [001] (denoted in Fig. 2.17 as 40^o and 42^o away from the [010] direction), close to those calculated for bulk d_{33} (50^o) and e_{31} (52^o). However, the maximum piezoelectric coefficients for $d_{33}^{f,C}$ and $e_{31,f}$ are 127.5 pm/V and -24.7 C/m^2, respectively, while those for d_{33} and e_{31} are –228 pm/V and -13.0C/m^2, respectively. The differences in piezoelectric coefficients demonstrate the influence of substrate clamping on the piezoelectric properties of thin film barium titanate materials.

The piezoelectric anisotropy reflected on Fig. 2.16 and Fig. 2.17 may be used to explain the large differences observed in piezoelectric properties of [001] and [111] oriented $BaTiO_3$ films or bulk materials. It can be seen from Fig. 2.17 that all the piezoelectric coefficients (d_{33}, e_{31}, $d_{33}^{f,C}$ and $e_{31,f}$) have their maximum in an orientation

close to [111] (which is 54.7° away from the polar direction - [001]). For $BaTiO_3$ single crystals, d_{33} along [111] direction is about twice large (224pm/V) as that along the polar direction [001] (106pm/V), which agrees well with the experiment observations [10] (125 pm/V and 203pm/V for [001] and [111] oriented $BaTiO_3$ single crystals, respectively). While for the in-plane piezoelectric coefficient, a (111) oriented $BaTiO_3$ single crystal has a e_{31} value (=-12.9 C/m^2) about four times large as that of a (001) oriented crystal (-3.82 C/m^2). Moreover, the calculations on $d_{33}^{f,C}$ and $e_{31,f}$ showed similar anisotropies as those of the single crystal. The calculated $d_{33}^{f,C}$ and $e_{31,f}$ are 124 pm/V and -23C/m^2 for a (111) oriented epitaxial $BaTiO_3$ film, while they are only 34.8 pm/V and -7.8 C/m^2 for a (001) oriented film. From our calculations, it is suggested that a (111) oriented tetragonal $BaTiO_3$ epitaxial film has superior piezoelectric properties, as compared with those of a (001) oriented tetragonal $BaTiO_3$ epitaxial film. The calculated $d_{33}^{f,C}$ (124 pm/V) and $e_{31,f}$ (-23C/m^2) for a (111) oriented epitaxial $BaTiO_3$ film are even comparable to those for PZT films near the morphotropic phase boundary[71], which makes it a good candidate material for lead-free transducer applications.

In summary, two important parameters characterizing piezoelectric performance of ferroelectric films, $d_{33}^{f,C}$ and $e_{31,f}$, have been calculated for epitaxial tetragonal $BaTiO_3$ films. It is found that although $d_{33}^{f,C}$ and $e_{31,f}$ are quantitatively different from those of a single crystal due to clamping of substrate, they have qualitatively similar orientation dependences as those of a single crystal. A (111) oriented epitaxial $BaTiO_3$ film has $d_{33}^{f,C}$ (124 pm/V) and $e_{31,f}$ (-23C/m^2) much larger than those of a (001) oriented film, and may serve as an alternative to PZT ferroelectric films in MEMS applications.

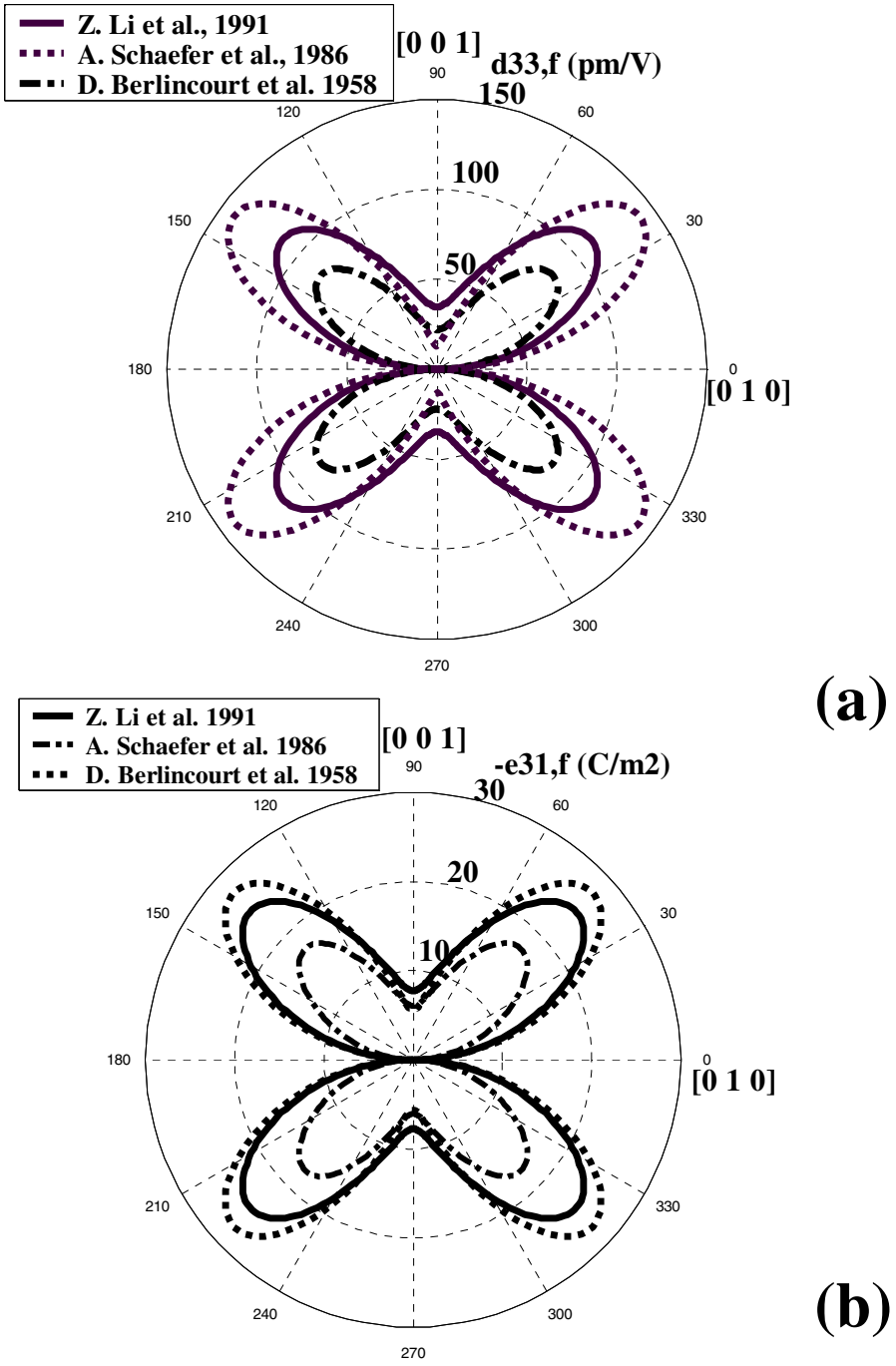

Figure 2.15. (a) Calculated piezoelectric coefficients $d_{33}^{f,C}$ and (b) $e_{31,f}$ by using different sets of electromechanical data.

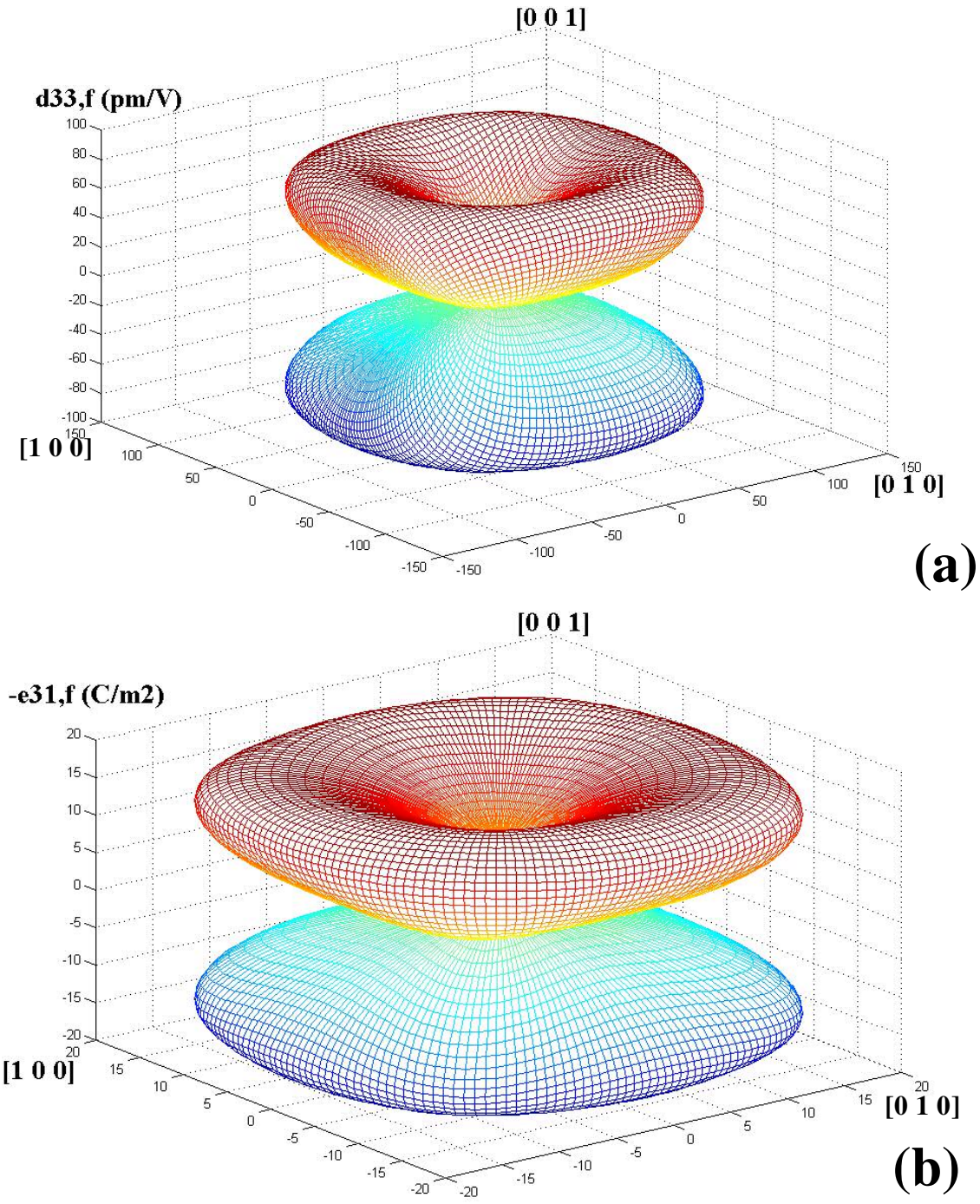

Figure 2.16 (a) Calculated piezoelectric coefficients $d_{33}^{f,C}$ and (b) $e_{31,f}$ of single domain tetragonal $BaTiO_3$ films as function of crystalline orientation of the film normal.

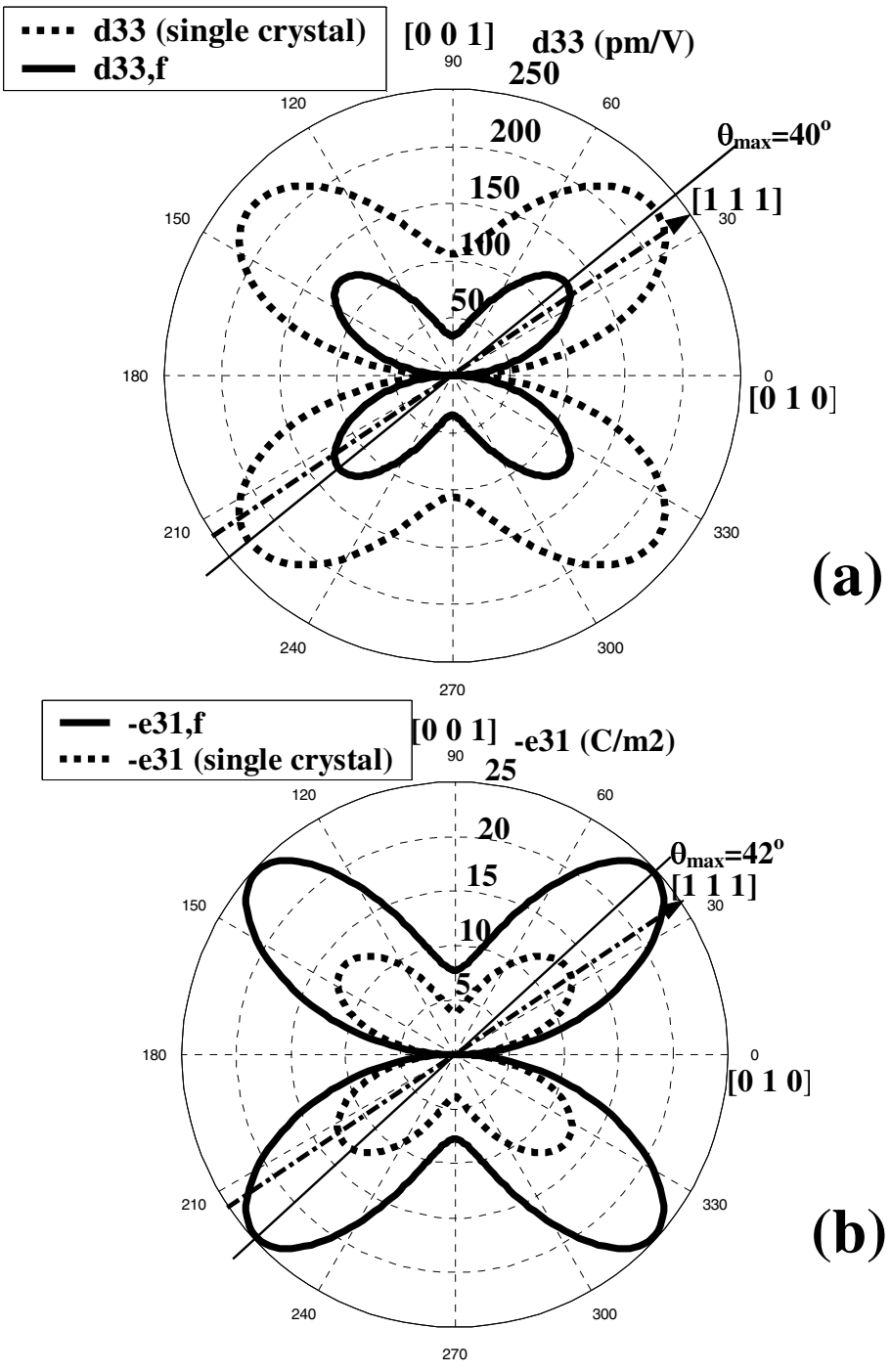

Figure 2.17 (a) Cross section curves of piezoelectric coefficients $d_{33}^{f,C}$ and (b) $e_{31,f}$ of single domain tetragonal $BaTiO_3$ films when Fig. 2.17 (a), (b) are cut by the (1 0 0) plane.

2.4.3 Relaxor ferroelectric films

Recently, there have been intensive research works on relaxor-lead titanate (abbreviated as PT) type ferroelectric single crystals, among which xPb($Mg_{1/3}Nb_{2/3}$)O_3-(1-x)$PbTiO_3$ (abbreviated as PMN-PT) and xPb($Zn_{1/3}Nb_{2/3}$)O_3-(1-x)$PbTiO_3$ (abbreviated as PZN-PT) are centers of attentions due to their unusually high piezoelectric coefficients and electromechanical coupling factors. Like PZT solid solutions, these ferroelectric systems have morphotropic phase boundaries (MPB) separating stable ferroelectric phases of tetragonal and rhombohedral structures. They have superior piezoelectric properties on compositions of the rhombohedral side of the MPB. Specifically, giant piezoelectric coefficients (>2500 pm/V) have been achieved on (001) oriented xPb($Mg_{1/3}Nb_{2/3}$)O_3-(1-x)$PbTiO_3$ ($x \leq 0.33$) [11] and xPb($Zn_{1/3}Nb_{2/3}$)O_3-(1-x)$PbTiO_3$ ($x \leq 0.09$) single crystals. [9], [61]

After the discoveries of these superior piezoelectric crystals, it is desirable to integrate them into MEMS devices. For a better design and performance of MEMS devices, the electrical and mechanical engineers need to have $e_{31,f}$ and $d_{33}^{f,C}$ values instead of bulk properties of these materials and they seek answers from materials engineers. The availability of complete sets of electromechanical constants for relaxor-PT single crystals [15], [16], [61],[75] -[77] has made it possible a theoretical study of $e_{31,f}$ and $d_{33}^{f,C}$ on relaxor ferroelectric films.

There are two types of single crystal database in literature. One is for single-domain single crystal, which may be used to predict the orientation dependence of physical properties for bulk and film materials. [16], [76] The other is for single crystals with specific multi-domain configurations (or so called “Engineered domain structure”),

which may only be used to predict the properties of bulk or film materials under the same domain configurations. [15], [61], [75], [77] The available single domain single crystal data for rhombohedral $0.67Pb(Mg_{1/3}Nb_{2/3})O_3$-$0.33PbTiO_3$ [16] and tetragonal $0.58Pb(Mg_{1/3}Nb_{2/3})O_3$-$0.42PbTiO_3$ [76] are used here for a complete study of $e_{31,f}$ and $d_{33}^{f,C}$ as functions of crystalline orientation. In addition, piezoelectric properties for multi-domain [001] films of PMN-PT [15], [75], PZN-PT [61] and $BiScO_3$-$PbTiO_3$ [77] are also calculated for comparison.

The orientation dependence of $e_{31,f}$ in a single domain $0.67Pb(Mg_{1/3}Nb_{2/3})O_3$-$0.33PbTiO_3$ film is visualized in Fig. 2.18 (a), where the distance between the surface of the graph and the origin represents the magnitude of $e_{31,f}$ in that orientation. Fig. 2.18 (b) shows the orientation dependence of $d_{33}^{f,C}$ in a similar manner as in Fig 2.18 (a), while Fig.2.18 (c) and (d) shows the cross section curve of a pseudo-cubic (1 -1 0) plane for $e_{31,f}$ and $d_{33}^{f,C}$, respectively. The orientation dependence of single crystal e_{31} and d_{33} are also plotted in Fig 2.18 (c) and (d) for comparison with the film data and evaluation of the clamping effect. It can be seen that $e_{31,f}$ and $d_{33}^{f,C}$ each has similar orientation dependence as the bulk coefficients. The calculated orientation for maximum $e_{31,f}$ is in a direction 65^o degree away from the polar direction [1 1 1] (155^o away from [1 1 -2], as denoted in Fig. 1 c), coinciding with the direction calculated for maximum $d_{33}^{f,C}$ (Fig. 1 d) while in the bulk single crystal the orientation for maximum piezoelectric coefficients are calculated to be 71^o (161^o away from [1 1 -2]) and 63^o (153^o away from [1 1 -2]) for e_{31} and d_{33}, respectively. However, the maximum piezoelectric

coefficients for $e_{31,f}$ and $d_{33}^{f,C}$ are -332.4 C/m^2 and 1690 pm/V, while those for bulk e_{31} and d_{33} are -210C/m^2 and 2411 pm/V, respectively. These differences reflect the important role clamping plays on the effective intrinsic piezoelectric coefficients of relaxor ferroelectric films.

In addition, the piezoelectric anisotropy reflected on Fig 2.18 may be used to explain the large differences observed between piezoelectric properties of [0 0 1] and [1 1 1] oriented relaxor ferroelectric films or bulk materials. W. Cao et al [17] has shown that a [0 0 1] oriented 0.67PMN-0.33PT single crystal can have much higher d_{33} than that of a [1 1 1] oriented 0.67PMN-0.33PT single crystal. They attributed this difference to the large shear piezoelectric coefficient, which can contribute to longitudinal piezo-electric response when the single crystal is rotated to a non-polar orientation. Here their conclusion on single crystals is verified by our calculation and is further extended to epitaxial films. It can be seen from Fig. 2.18 (d) that $d_{33}^{f,C}$ is ~1400pm/V along a [0 0 1] direction (close to the direction of maximum $d_{33}^{f,C}$), while $d_{33}^{f,C}$ is only ~70pm/V along the polar direction [1 1 1]. Moreover, calculations on in-plane piezoelectric coefficients e_{31} and $e_{31,f}$ showed that they have a similar anisotropy as that of the longitudinal piezoelectric coefficients. The calculated $e_{31,f}$ is -269 C/m^2 for a [0 0 1] oriented single domain film, while it is only -10.8 C/m^2 for a [1 1 1] oriented single domain film. From our calculations, it is suggested that a [0 0 1] oriented 0.67Pb($Mg_{1/3}Nb_{2/3}$)O_3-0.33$PbTiO_3$ epitaxial film will have superior electromechanical properties, as compared with those of a [1 1 1] oriented film.

Similarly, the orientation dependence of $e_{31,f}$ and $d_{33}^{f,C}$ for a 0.58Pb($Mg_{1/3}Nb_{2/3}$)

O_3-0.42$PbTiO_3$ epitaxial tetragonal film, are shown in Fig 2.19. As can be seen from Fig 2.19 (c) and (d), the orientations for maximum $e_{31,f}$ and $d_{33}^{f,C}$ coincide in the polar direction [0 0 1], just as those for bulk e_{31} and d_{33}. $e_{31,f}$ and $d_{33}^{f,C}$ are -11.7C/m^2 and 116pm/V for a [0 0 1] oriented film, while for a [1 1 1] oriented film they are -2.4 C/m^2 and 51pm/V, respectively. Both $e_{31,f}$ and $d_{33}^{f,C}$ decrease monotonously with the angle of the orientation away from the polar direction [0 0 1].

In Fig. 2.20, calculated $e_{31,f}$ and $d_{33,f}$ values for some relaxor films are plotted as function of Curie temperature by using available single crystal data.[15],[16], [75]-[77] It shows that:

(1) For the same relaxor ferroelectric material, a (001) oriented film have higher $e_{31,f}$ and $d_{33,f}$ values than those of a (111) oriented film.

(2) In general, a (001) oriented relaxor ferroelectric film has superior piezoelectric properties ($e_{31,f}$ ~-20C/m^2 and $d_{33,f}$ >150pm/V).

(2) Single domain (001) oriented PMN-33%PT has much larger $e_{31,f}$ (-269C/m^2) and $d_{33,f}$ (1390pm/V) than those of a multi-domain film ($e_{31,f}$ =-23C/m^2 and $d_{33,f}$ =261pm/V), probably because the inter-clamping of domain variants reduces the contributions from shear piezoelectric effect in a multi-domain film. [78]

(4) $BiScO_3$-$PbTiO_3$ (BSO-PT) material has much higher Curie temperature (~400 ^{o}C) than those of PMN-PT and PZN-PT (<200^{o}C). The piezoelectric coefficients $e_{31,f}$ and $d_{33,f}$ of BSO-PT are comparable with those of PMN-

PT and PZN-PT, which makes it a promising candidate for high-temperature electromechanical applications.

In summary, two important parameters characterizing the piezoelectric performance of ferroelectric films, $e_{31,f}$ and $d_{33}^{f,C}$, have been calculated for various relaxor ferroelectric systems, taking into account the effect of substrate clamping. It is found that as (001) oriented relaxor ferroelectric films generally have sound piezoelectric properties (calculated $e_{31,f}$ ~ 20C/m^2 and $d_{33}^{f,C}$ >150pm/V), a (001) oriented single domain rhombohedral film on the morphotropic phase boundary of PMN-PT system can have very high piezoelectric coefficients (calculated $e_{31,f}$ =-269C/m^2 and $d_{33}^{f,C}$ = 1390 pm/V), which suggests an optimal design for relaxor ferroelectric-based MEMS devices.

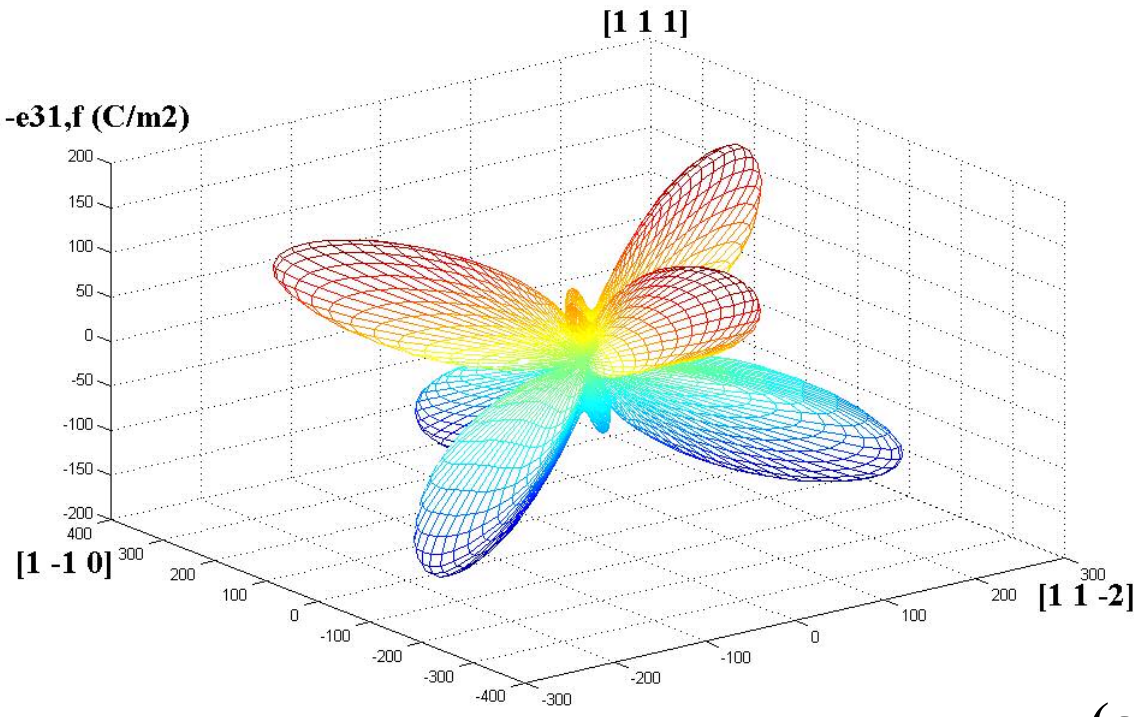
[1 1 1]
-e31,f (C/m2)
200
150
100
50
0
-50
-100
-150
-200
400
300
200
100
0
-100
-200
-300
-400
[1 -1 0]
300
200
100
0
-100
-200
-300
[1 1 -2]

(a)

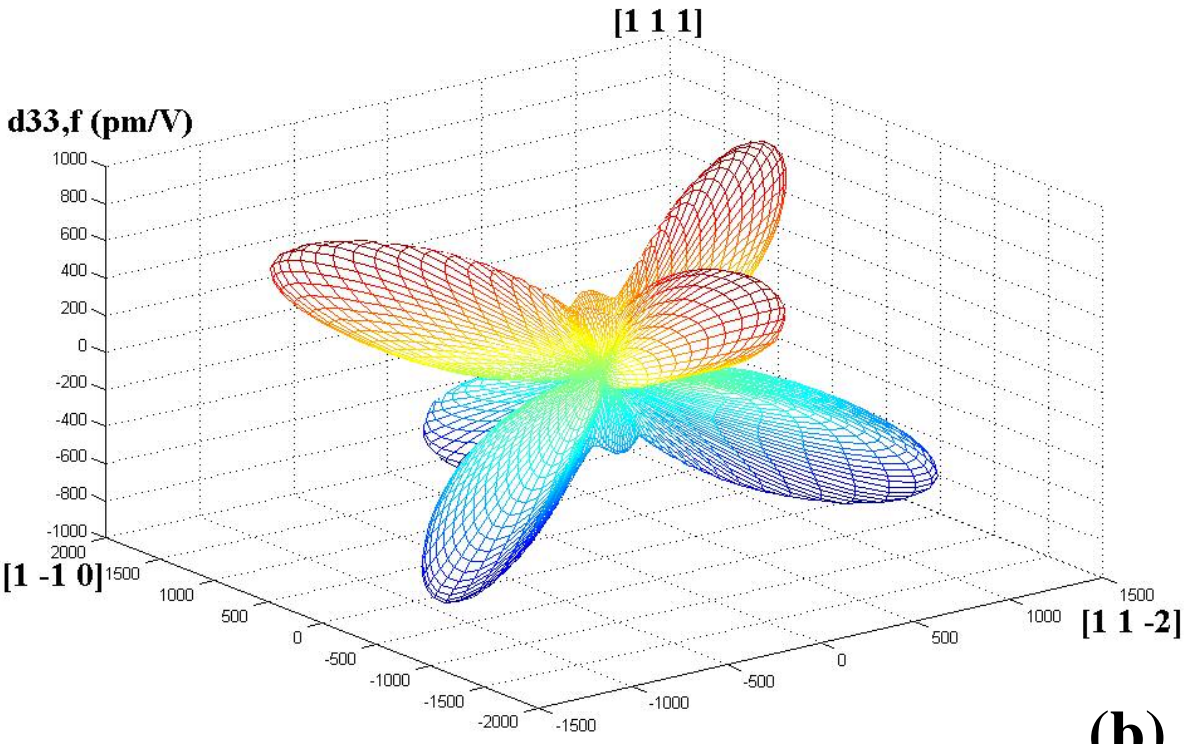
[1 1 1]
d33,f (pm/V)
1000
800
600
400
200
0
-200
-400
-600
-800
-1000
2000
1500
1000
500
0
-500
-1000
-1500
-2000
[1 -1 0]
1500
1000
500
0
-500
-1000
-1500
[1 1 -2]

(b)

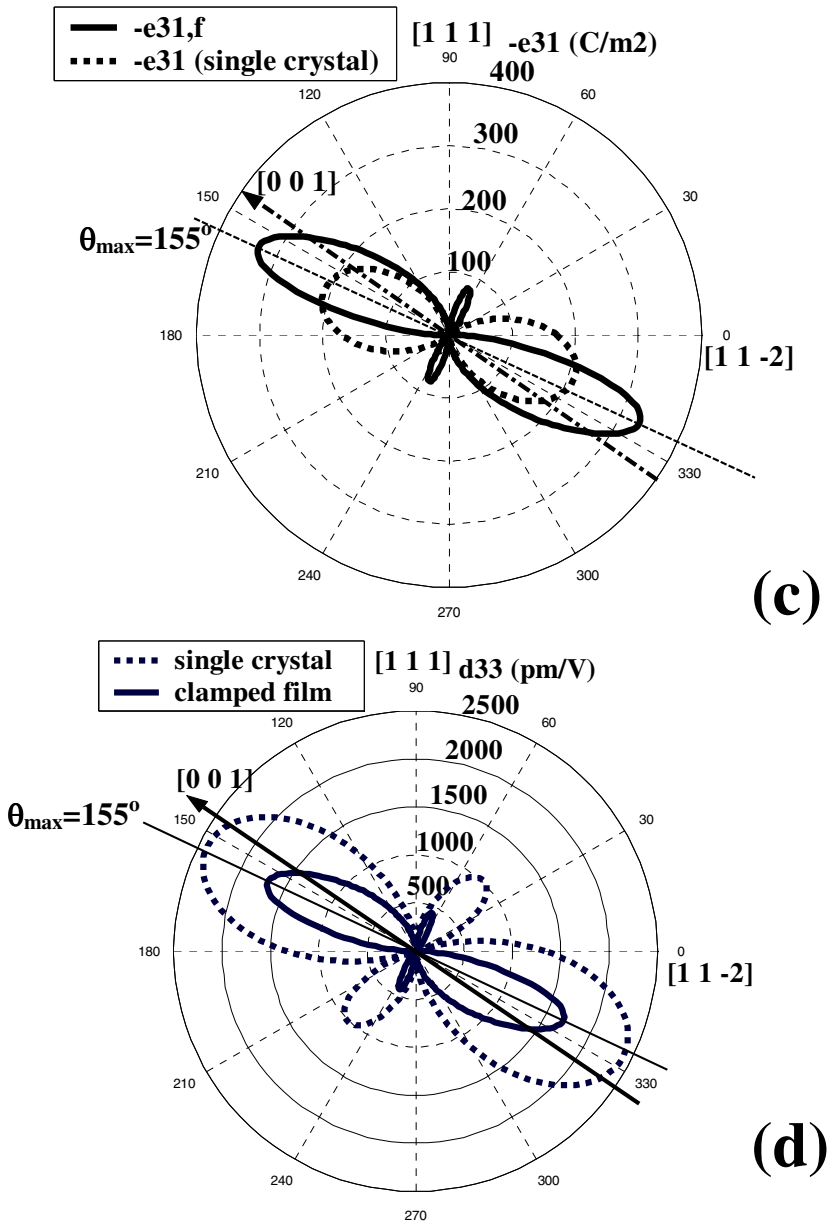

Figure 2.18. (a) Calculated piezoelectric coefficients $e_{31,f}$ and (b) $d_{33,f}$ of a single domain rhombohedral 0.67Pb($Mg_{1/3}Nb_{2/3}$)O_3-0.33$PbTiO_3$ film as function of crystalline orientation of the film normal. (c) Cross section curves of piezoelectric coefficients $e_{31,f}$ and (d) $d_{33,f}$ of a single domain rhombohedral 0.67Pb($Mg_{1/3}Nb_{2/3}$)O_3-0.33$PbTiO_3$ film when Fig. 2.18 (a), (b) are cut by a pseudo-cubic (1 -1 0) plane.

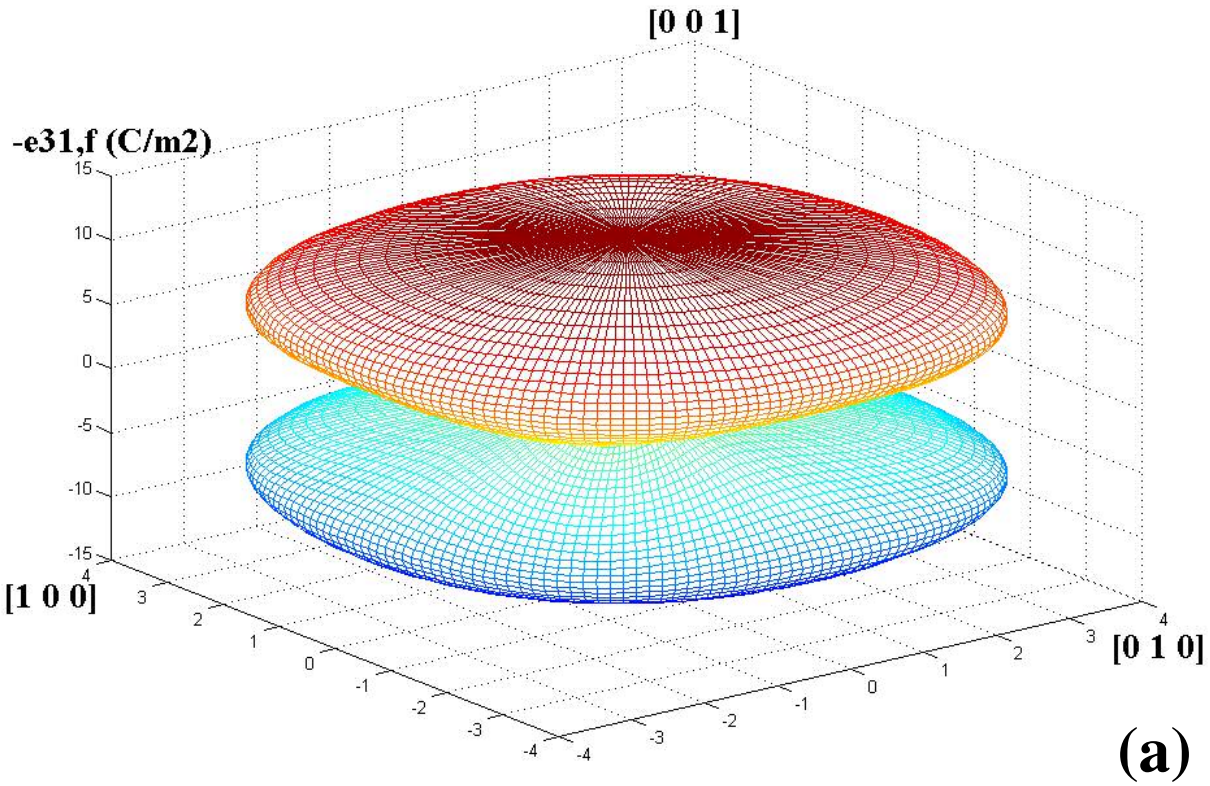
[0 0 1]
-e31,f (C/m2)
15
10
5
0
-5
-10
-15
[1 0 0]
4
3
2
1
0
-1
-2
-3
-4
-4
-3
-2
-1
0
1
2
3
4
[0 1 0]

(a)

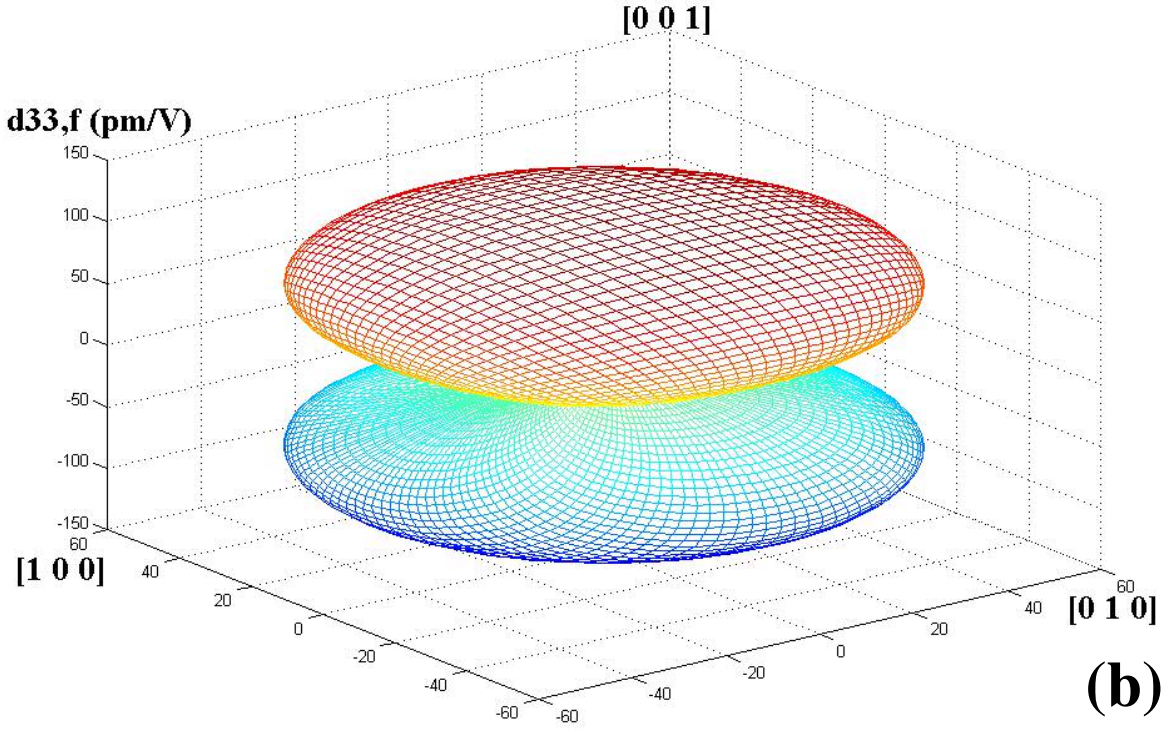
[0 0 1]
d33,f (pm/V)
150
100
50
0
-50
-100
-150
[1 0 0]
60
40
20
0
-20
-40
-60
-60
-40
-20
0
20
40
60
[0 1 0]

(b)

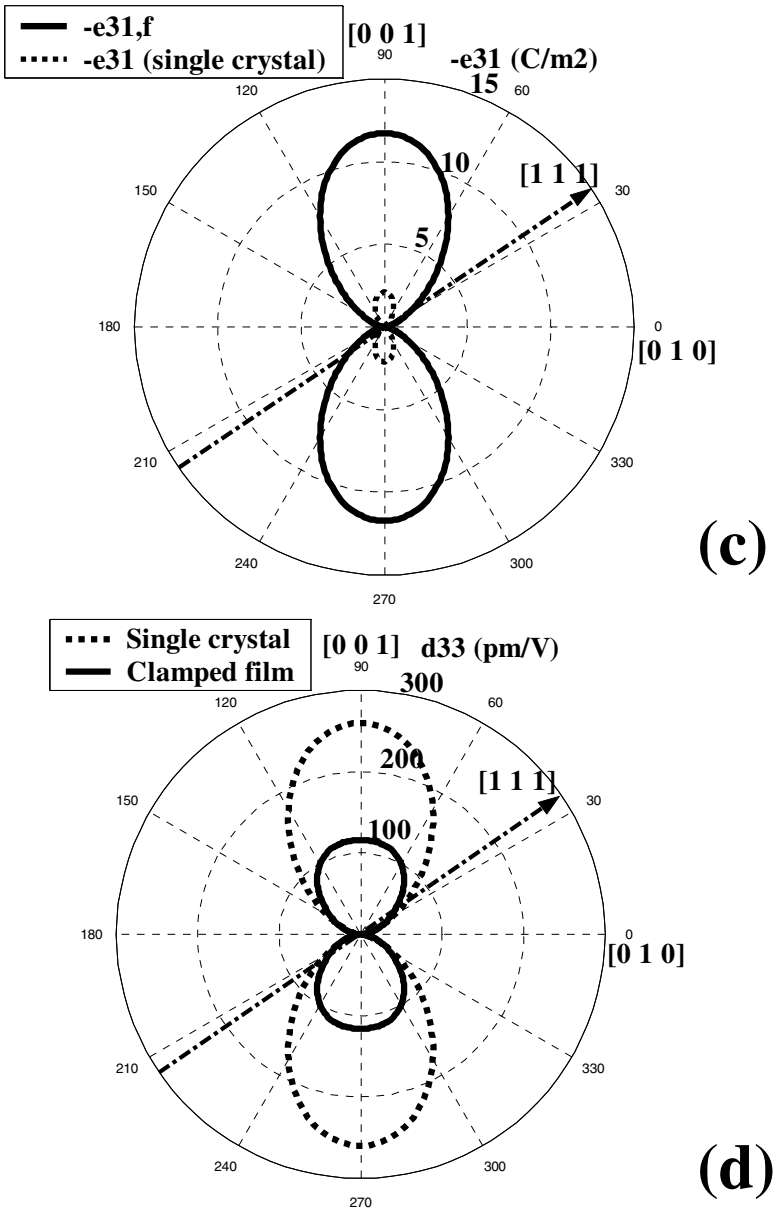

Figure 2.19. (a) Calculated piezoelectric coefficients $e_{31,f}$ and (b) $d_{33,f}$ of a single domain tetragonal $0.58Pb(Mg_{1/3}Nb_{2/3})O_3$-$0.42PbTiO_3$ film as function of crystalline orientation of the film normal. (c) Cross section curves of piezoelectric coefficients $e_{31,f}$ and (d) $d_{33,f}$ of a single domain tetragonal $0.58Pb(Mg_{1/3}Nb_{2/3})O_3$-$0.42PbTiO_3$ film when Fig. 2.19 (a) (b) are cut by a pseudo-cubic (1 0 0) plane.

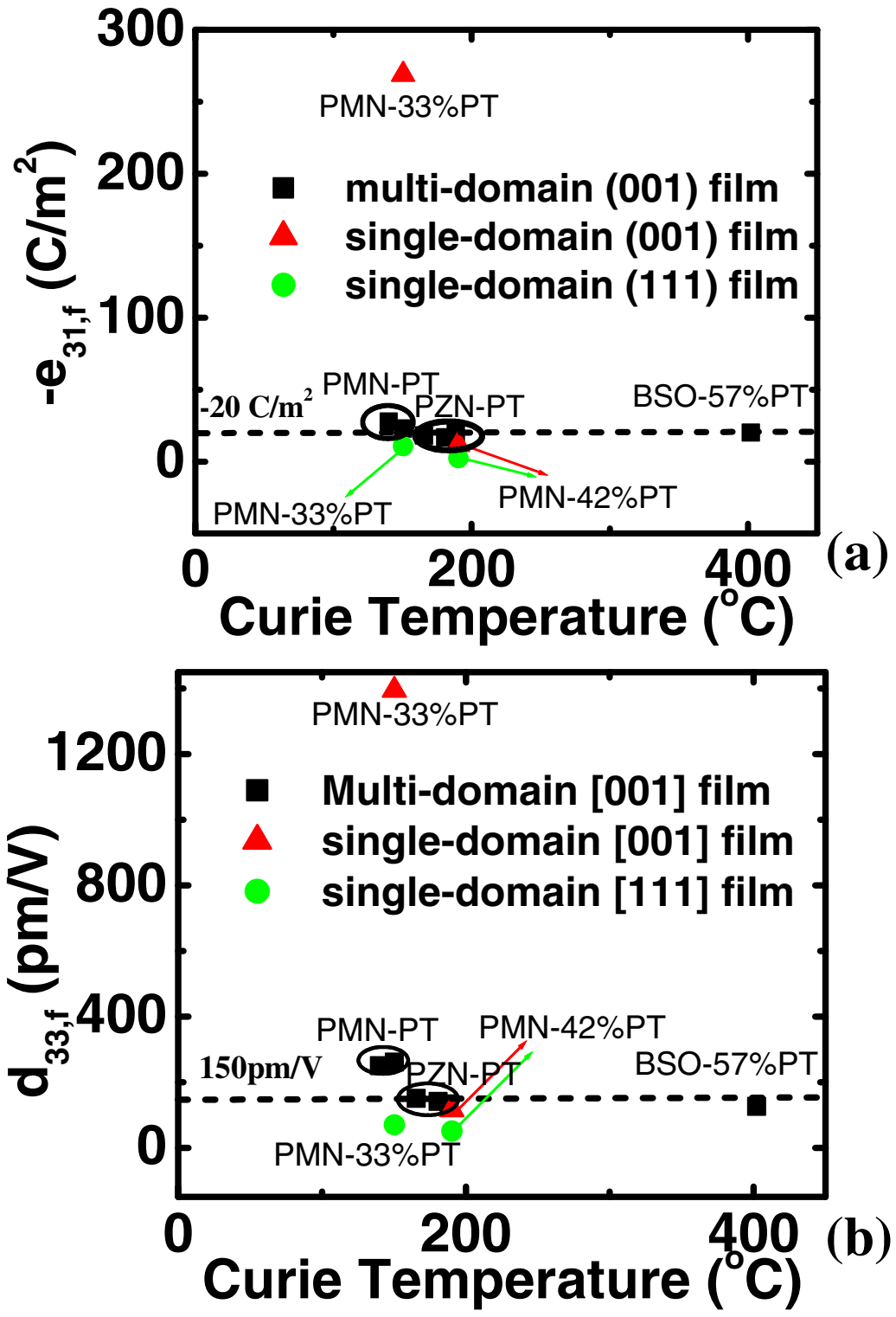

Figure 2.20. (a) Calculated piezoelectric coefficients $e_{31,f}$ and (b) $d_{33,f}$ of various relaxor ferroelectric films.

2.5 Experiment measurement on longitudinal piezoelectric coefficient $d_{33,f}$

2.5.1 Piezoelectric force microscopy

Piezoelectric force microscopy is a voltage-modulated scanning probe microscopy technique.[79]-[80] In this technique, a conductive tip is biased by an ac field in contact mode,[80] and the tip field can be written as:

$$E_{tip}=E_{dc}+E_{ac}\sin(\omega t) \tag{2.18}$$

When ω is the voltage modulation frequency, which is much smaller than the cantilever resonance frequency. The tip deflection δ as a function of applied bias can be written as:[79]

$$\delta=A_0+A_1\sin(\omega t+\varphi_1)+A_2\sin(2\omega t+\varphi_2) \tag{2.19}$$

Where A_0 is static response, and A_1, A_2, φ_1, φ_2 are amplitudes and phase shifts of first and second harmonic responses. Magnitudes of A_o, A_1, and A_2 are relatively small and only the latter two components along with corresponding phase shifts can be determined by lock-in technique.[81] Separation of the first and second harmonic response will allow quantification of the electromechanical properties of the materials being tested.

If the longitudinal tip deflection signal is recorded and separated, the first harmonic signal will be the longitudinal piezoelectric response. A_1 , the amplitude of first harmonic response, is in proportion with longitudinal piezoelectric constant d_{33} at small ac field, and can be used to measure d_{33} indirectly. For example, for a fully poled tetragonal ferroelectric plate with polarization aligned along the longitudinal direction "3", the longitudinal piezoelectric displacement can be written as:

$$\delta(E)=\varepsilon(E)h=Q_{11}[P(E)^2-P_0^2]*h=Q_{11}h[P(E)^2-P_0^2]=Q_{11}h[(P_0+\chi E)^2-P_0^2]$$

$$=2Q_{11}P_0\chi Eh+Q_{11}h(\chi E)^2 \tag{2.20}$$

Where Q_{11} is the effective eletrostrictive coefficient, P(E) and P_0 are the polarization at field E and in the remnant state. h is the thickness of the plate and χ is the dielectric constant. Substitute E with E_{tip} in Eq. (2.18) and keep only items which depend on frequency ω (therefore can be detected by the lock-in technique), then we have:

$$\delta(\omega) = 2Q_{11}P_0\chi E_{ac}\sin(\omega t) + \frac{1}{2}Q_{11}\chi^2 E_{ac}^2\cos(2\omega t) \qquad (2.21)$$

Compare Eqs (2.19) and (2.21), it is found that $A_1=2Q_{11}P_0\chi E_{ac}=d_{33}E_{ac}$ (Eq. 1.3). It should be noted that this technique for measuring d_{33} is good only at small ac electric field when piezoelectric response is strictly a "linearized electrostriction". [6]

Fig. 2.21 (a) schematically shows the set-up of piezoelectric force microscopy. The output of the circuit can be either a topography (contact mode imaging by Z (height)-feedback of the piezo scanner[79], [80]), a d_{33}-DC bias loop, or a piezoelectric force microscopy image (local measurement of d_{33}).

As shown in Fig. 2.21 (b), the d_{33}-DC bias loop was made by detecting the DC-biased piezoelectric response of a ferroelectric thin film capacitor under an alternating ac field.[82], [83] A X-cut quartz (d_{11}=2.3pm/V) coated with top and bottom Au electrodes was used to calibrate the out-of-plane tip displacement at a given AC amplitude and therefore the d_{33} of a ferroelectric film. In this setup, a ferroelectric film (in this figure, "PZT") is sandwiched between a uniform layer of bottom electrode and top electrode pads. A direct current (dc) field is applied to the top electrode through the AFM tip to write the domain state while the applied ac signal is used to read the piezoelectric response of the domain state by the lock-in technique.[81] A hysteresis loop is traced out by plotting the calibrated d_{33} coefficients as a function of the dc field.

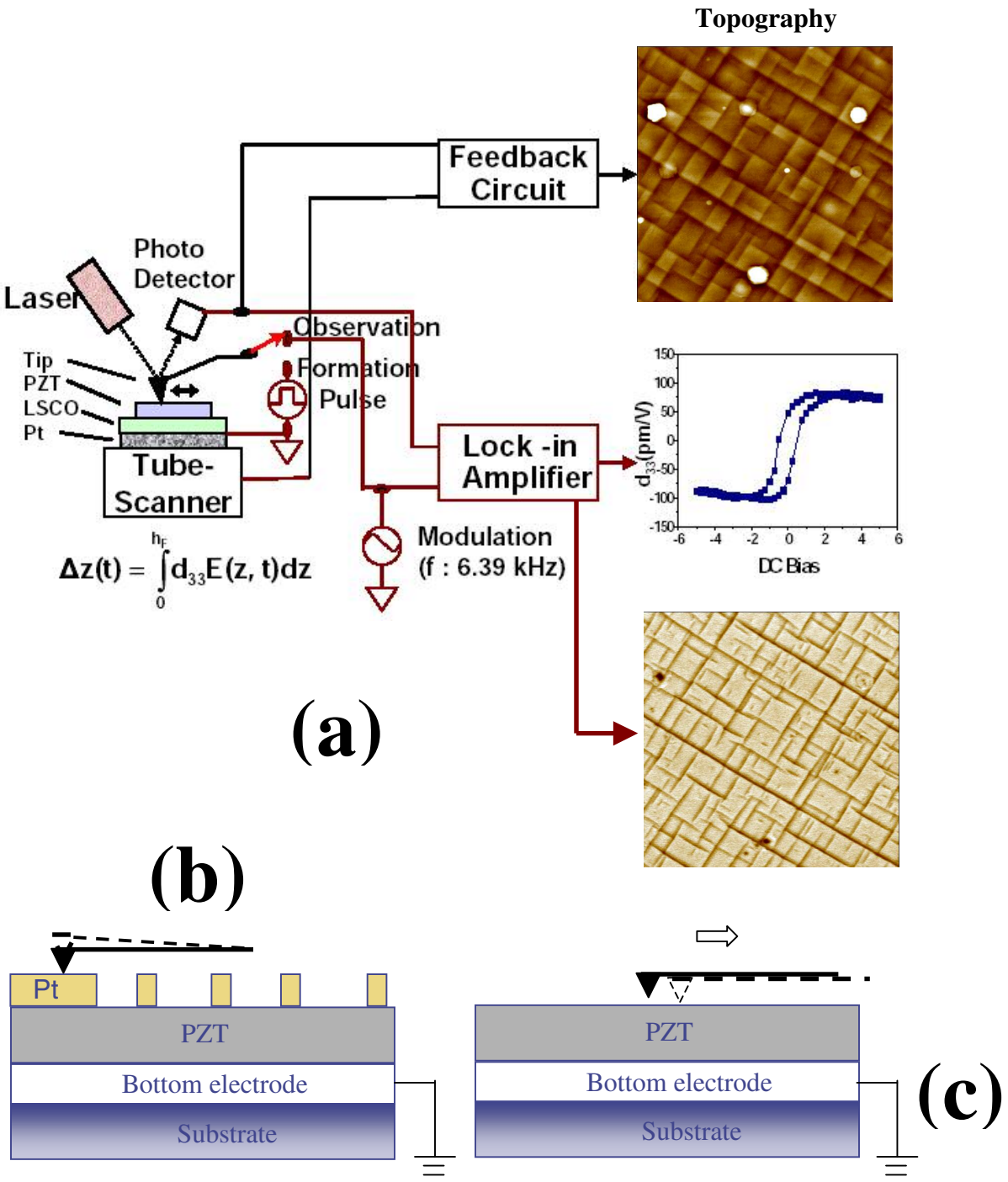

Fig. 2.21 (a) Schematics of the set-up of piezoelectric force microscopy (PFM); Figure adapted from Ref. [80]. (b) Measurement of d_{33} amplitude under a uniform tip field by covering the film with Pt top electrode pads. (c) local piezoelectric response measurement (imaging).

Fig. 2.21 (c) shows the piezoelectric imaging technique. In this technique, an ac-biased AFM probe is scanning on the surface of a "naked" ferroelectric film, the amplitude and phase information of local piezoelectric responses are recorded during the scan to simultaneously form contours of domain patterns. The amplitude of piezoelectric response is recorded by a position-sensitive detector (PSD),[79], [80] which is shown in Fig. 2.22. The PSD is a four-quadrant (A, B, C, D) laser photo detector. The difference in laser throughput intensity between the two upper detectors (A+B) and the two lower detectors (C+D) is in proportion with the vertical displacement of the tip (therefore the longitudinal piezoelectric response of the film since the tip is in contact with film), while the difference in laser throughput intensity between the two left-side detectors (B+D) and the two right-side detectors (A+C) is in proportion with the lateral displacement of the tip (therefore the shear piezoelectric response of the film).

At the same the amplitude information is detected, the phase information is also detected and separated by the lock-in amplifier (Fig 2.23 a). When the polarization vector inside a ferroelectric domain is aligned along the electric field direction, the phase angle between the piezoelectric response and the ac field is zero, and this domain is said to be "in phase" with the ac signal applied to the tip. On the other hand, if the polarization vector inside a ferroelectric domain is aligned against the electric field direction, the phase angle between the piezoelectric response and the ac field is 180^{o}, and this domain is said to be "out-of-phase" with the ac signal. There is a strong contrast between neighboring 180^{o} domains as shown in Fig 2.23 (b) and (c).

In a 90^{o} domain with polarization vector aligned in-plane (usually called "*a*" domain), the longitudinal piezoelectric response is zero while its shear piezoelectric

response reaches a maximum (Fig. 2.23 b and c). On the other hand, for a 90° domain with polarization vector aligned out-of-plane (usually called "*c*" domain), the amplitude of longitudinal piezoelectric response is maximum while its shear piezoelectric response is zero (Fig. 2.23 b and c).

$$\Delta z(t) \approx \int_0^{h_F} d_{33} E(z,t)\,dz \qquad \Delta\theta \approx \frac{1}{\sqrt{2}t_F}\int_0^{t_F} d_{15} E_{AC}(t)\,dt$$

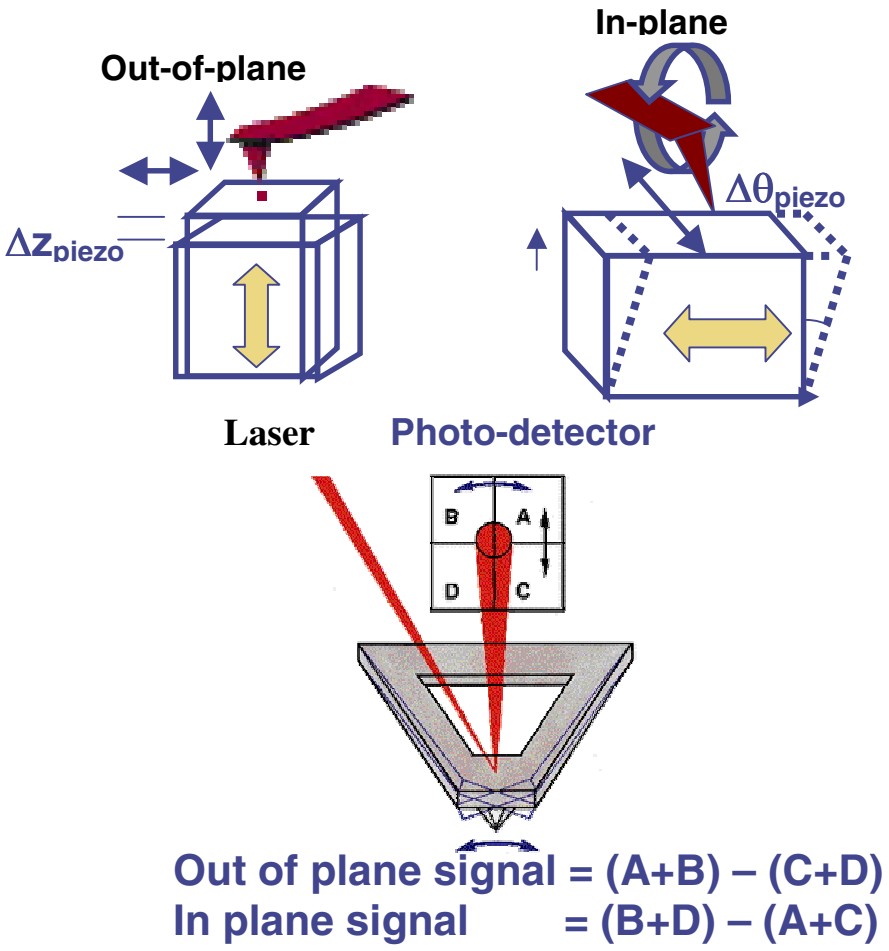

Fig. 2.22. Recording the amplitude of a piezoelectric response by a position-sensitive detector (PSD).

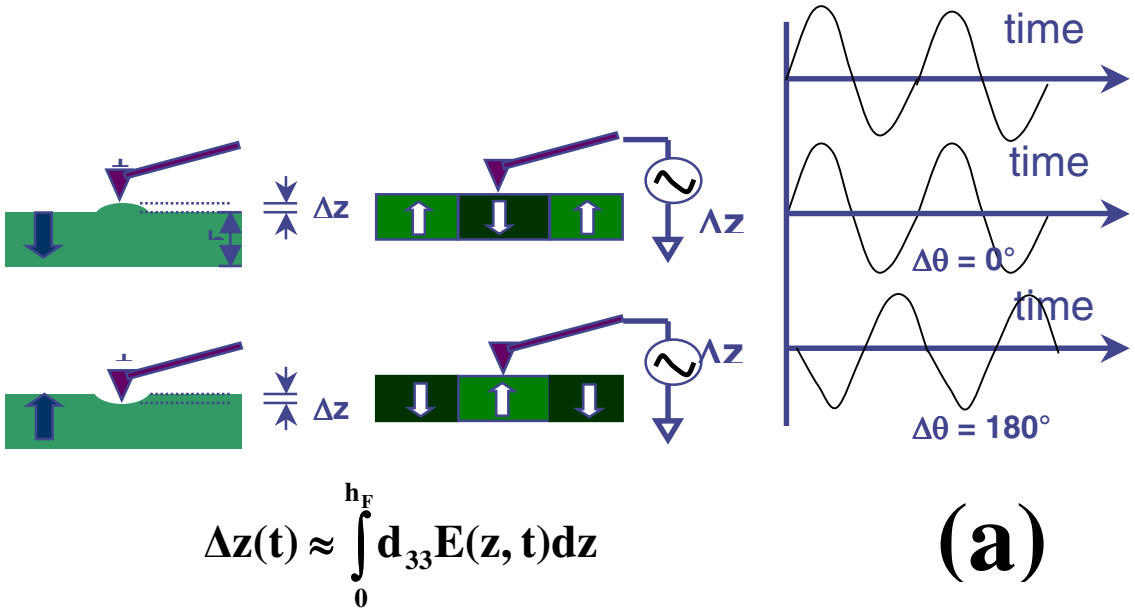

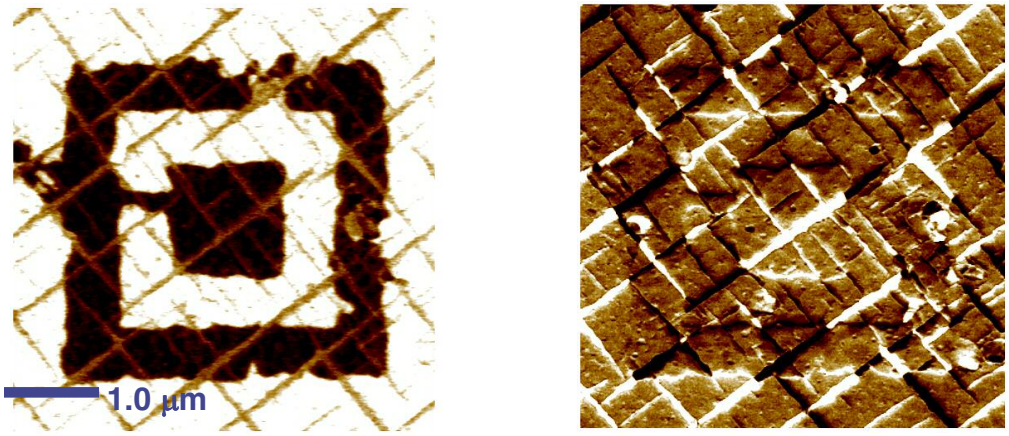

Fig. 2.23. (a) Detection of 180° domains by finding the phase angle between the longitudinal piezoelectric response and the tip ac signal. (b) Out-of-plane; (c) in-plane PFM image of a 400nm PZT(20/80)/LSCO/STO ferroelectric film showing both 180° (by writing) and 90° domain (grown in-situ) patterns. Figure adapted from [80].

2.5.2 Lead zirconate titanate thin films

Longitudinal piezoelectric constant $d_{33,f}^{C}$ were measured experimentally for ferroelectric $Pb(Zr_{0.2}Ti_{0.8})O_3$ thin films, which were prepared by liquid delivery metalorganic chemical vapor deposition (MOCVD) on $SrTiO_3$ substrate (a layer of $SrRuO_3$ bottom electrode was pre-deposited on $SrTiO_3$ by pulsed laser deposition). The details of MOCVD and pulsed laser deposition processes are described in Ref [84] and [85], respectively. The composition of the ferroelectric film is chosen to obtain best matching of lattice parameters of $Pb\,[Zr_x\,Ti_{(1-x)}]O_3$ and $SrRuO_3/SrTiO_3$ heterostructures. In our experiments, 0.3 mol/L $Pb(thd)_2$ in THF, 0.3 mol/L $Ti(OiPr)_2(thd)_2$ in THF and 0.3 mol/L $Zr(dmhd)_4$ in THF (all from Mitsubishi Materials Corporation) were used as precursors. Pt was deposited as the top electrode on 32 μm diameter circular pads patterned by standard lithography processes.

Film thickness was 130 nm for all films. X-ray results showed very good cube on cube epitaxy (Fig. 2.24). All films demonstrated small FWHM widths (Table 2.7), which indicates good crystalline quality. There was no evidence of multi-domain structures for all films, as verified by piezoresponse microscopy on image mode.[86] Quantitative $d_{33,f}^{C}$ (d_{nn}^{f})-*E* loops (Fig. 2.25) were obtained by recording the feedback Z output when applying a DC sweep bias.[82], [83] For each film, ten capacitors were tested and results averaged. Special precautions (fixing exterior surface of substrates and using full coverage of substrates by the films) were undertaken to minimize effects of substrate deformation on measuring d_{nn}^{f}. The remnant d_{nn}^{f} values (d_{nn}^{f} at zero field) are listed in Table 2.7 and compared with the theoretical calculations. Piezoelectric and elastic

constants necessary for calculations are taken from Refs [6] and [56], respectively. It is seen that the theoretical calculations agree well with experiment results.

Table 2.7. Experiment results for $Pb(Zr_{0.2}Ti_{0.8})O_3$ films. d_{nn}^{f} values are the equilibrium ones at zero electric field. Film thickness is kept at 130 nm for all films.

Orientation	(001)	(011)	(111)
Bulk d_{nn} (pm/v)	87.2	41.7	28.6
Theory d_{nn}^{f} (pm/v)	78	37	27
Experiment d_{nn}^{f} (pm/v)	67±7	35±4	25±3
FWHM for X-ray	0.26^{o}	0.50^{o}	0.71^{o}
peaks (in parenthesis)	(002)	(011)	(111)

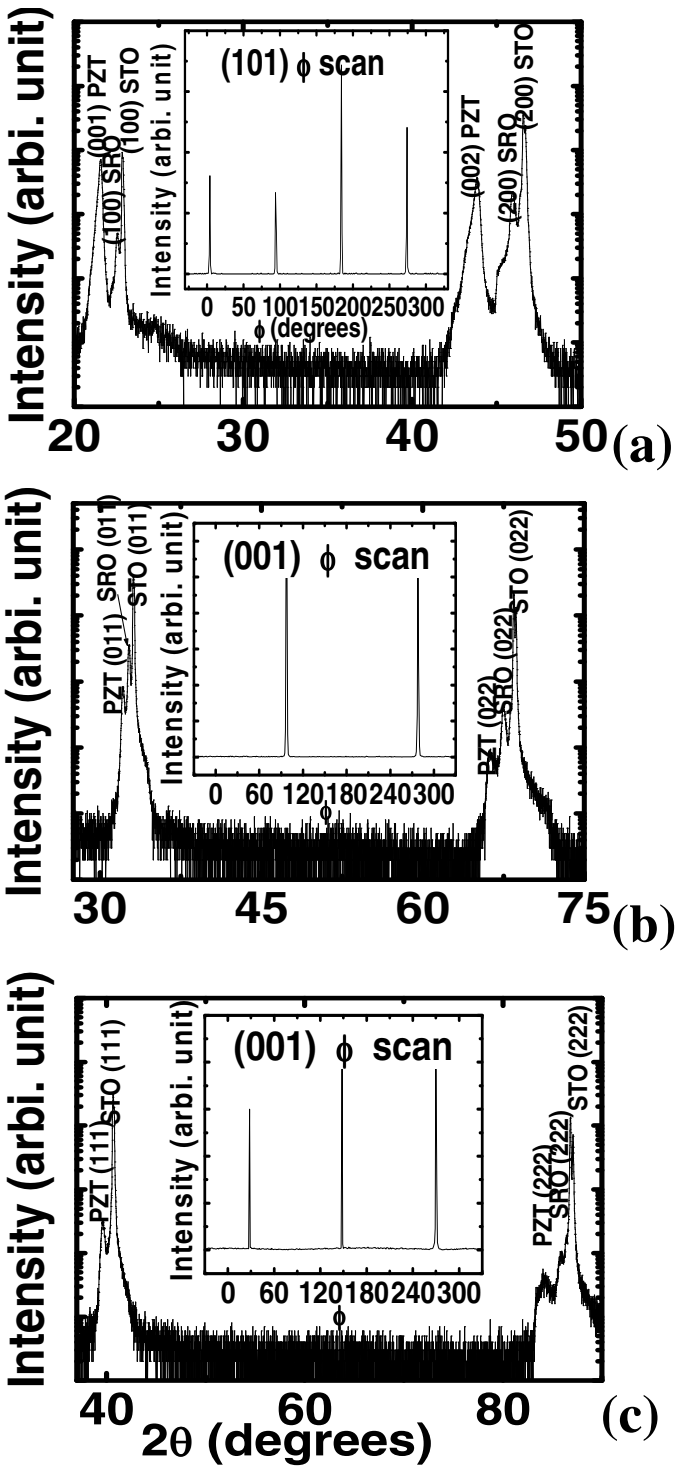

Figure 2.24 X-ray spectrum and ϕ-scans for (001)-(a), (011) - (b) and (111)- (c) for $Pb(Zr_{0.2}Ti_{0.8})O_3$ films.

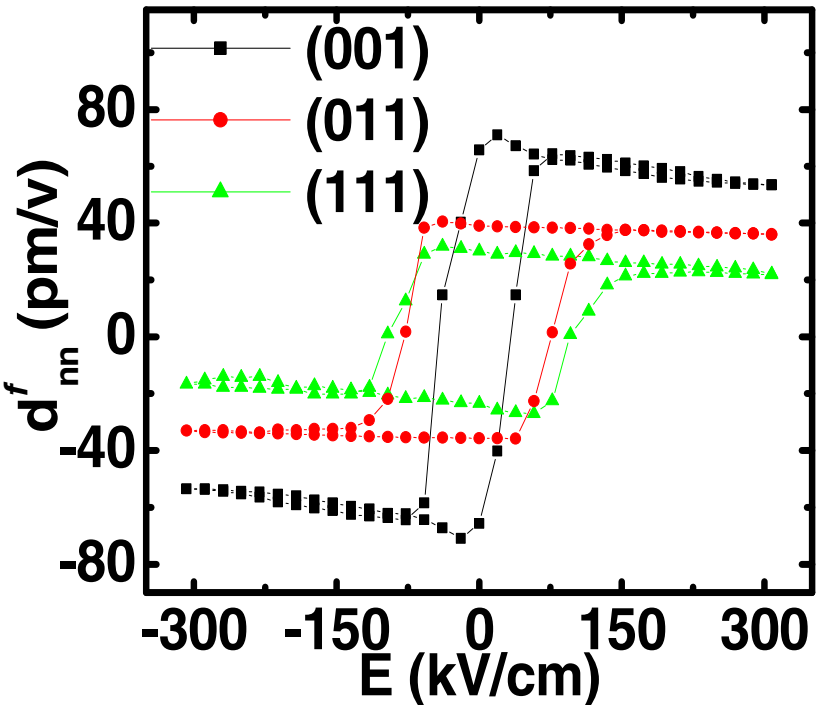

Figure 2.25 Effective longitudinal piezoelectric constants as function of DC Bias for (001), (011) and (111) oriented $Pb(Zr_{0.2}Ti_{0.8})O_3$ films.

2.5.2 Lead Magnesium Niobate –lead titanate ferroelectric films

Method of domain engineering, which aims at enhancing the piezoelectric properties of ferroelectric materials by applying the electric field in a non-polar direction across the crystal, has been investigated intensively for the past decade.[8]-[12] For relaxor based ferroelectrics on the rhombohedral side of their morphotropic phase boundaries, such as $x\text{Pb}(\text{Mg}_{1/3}\text{Nb}_{2/3})\text{O}_3\text{-}(1\text{-}x)\text{PbTiO}_3$ (x<0.35), and $x\text{Pb}(\text{Zn}_{1/3}\text{Nb}_{2/3})\text{O}_3\text{-}(1\text{-}x)\text{PbTiO}_3$ (x<0.09), giant piezoelectric constants (>2500 pm/V) can be achieved by poling the crystal in a pseudo-cubic (001) direction.[9] Recently, Cao et al. studied both multi-domain (001 oriented crystal) and single domain (111 oriented crystal) properties of $0.67\text{Pb}(\text{Mg}_{1/3}\text{Nb}_{2/3})\text{O}_3\text{-}0.33\text{PbTiO}_3$ single crystals.[15]-[17] They attributed the origin of the superior electromechanical properties in the (001) direction to the large d_{15} of the single-domain properties, as they reproduced the large piezoelectric constants in multi-domain (001) crystals from single domain properties in the rotated coordinated system.[17] Further theoretical study[18], [19] showed that the low field piezoelectric constants for the engineered configuration are very close to those obtained for the corresponding single domain state and the domain wall influence is not significant. Therefore, it is possible to estimate the piezoelectric constants of a multi-domain single crystal with an arbitrary orientation by knowing those calculated in a rotated coordinated system.

Our recent theoretical work[44] on lead zirconate titanate thin films ($\text{PbZr}_x\text{Ti}_{1-x}\text{O}_3$, x=0.2) completed the orientation dependence of the intrinsic converse piezoelectric constants in epitaxial single domain tetragonal films, which was initially proposed in Ref. [36] for a partial case of a (001) oriented tetragonal film. Here we calculate the orientation dependence of the intrinsic converse longitudinal piezoelectric constant for a

rhombohedral film, and apply the theoretical results to 0.67Pb $(Mg_{1/3}Nb_{2/3})O_3$-$0.33PbTiO_3$ relaxor ferroelectric films.

The tensor Π_{ik} for epitaxial rhombohedral films of (001), (011) and (111) orientations are shown in Table 2.2. Expressions for the intrinsic converse longitudinal piezoelectric constants d_{nn}^{f} ($d_{33,f}^{C}$) of these three orientations are list in Table 2.4, in comparison with those for d_{nn} of single crystals. It should be noted here that for (001) orientation, a calculated value of d_{nn}^{f} for a multi-domain film (which has a macroscopic symmetry of pseudo-tetragonal 4mm [15]) is also listed for comparison. Since all the necessary single crystal properties were given in Ref. [15] and [16] (note that the d_{22} in Ref. [16] should take a negative sign by using the current coordinate system), we calculated d_{nn}^{f} as a function of orientation and the results are visualized in Fig.2. 18 (b) (d). It can be seen that in both film and single crystal case, the [001] pseudo cubic direction (the dash-dot line with an arrow in the figure) is close to the direction of maximum longitudinal converse piezoelectric constants, which accounts for the large piezoelectric response in a [001] oriented single crystal or film.

The converse longitudinal piezoelectric constants were measured experimentally for epitaxial $0.67Pb(Mg_{1/3}Nb_{2/3})O_3$-$0.33PbTiO_3$ films, which were prepared by an on-axis radio-frequency magnetron sputtering technique on $SrTiO_3$ substrates with 3 different pseudo cubic orientations, namely, (001), (110) and (111). Prior to the film deposition, 200nm thick epitaxial $SrRuO_3$ bottom electrodes were deposited on the substrate. The details of the sputtering can be found in Ref [87]. The cube on cube epitaxy and good crystallinity of the films are confirmed by the X-ray results (θ-2θ scan and ϕ-scan results

in Fig 2.26, FWHM results in Table 2.8, all results were obtained by using a Siemens D 5000 four-circle diffractometer). For the purpose of electric and piezoelectric measurements, Pt was deposited as the top electrode on 54 μm diameter circular pads patterned by standard lithography processes.

Film thickness was 3.3 μm for all films.[88], [89] Quantitative d_{nn}^{f}-E loops (Fig. 2.27) were obtained by piezoelectric force microscopy[82], [83] in a commercial Dimension 3000™ AFM (Veeco Metrology). For each film, ten capacitors were tested and results averaged. Test capacitors were pre-poled in order to obtain d_{nn}^{f} of stabilized domain structures. Special precautions (fixing exterior surface of substrates and using full coverage of substrates by the films) were undertaken to minimize effects of substrate deformation on measuring d_{nn}^{f} [43]. The remnant d_{nn}^{f} values (d_{nn}^{f} at zero field) are listed in Table 2.8 and compared with the theoretical calculations.

It is seen that the piezoelectric constants of (110) and (111) oriented films agreed fairly well with our calculations based on single-domain bulk properties. However, while the large piezoelectric constants in multi-domain (001) crystals can be reproduced from the single domain piezoelectric properties in a rotated coordinated system, it is not the case in a clamped film- the intrinsic converse longitudinal piezoelectric constant of the (001) oriented film agreed well with that calculated for a clamped multi-domain film, which was several times less than that calculated for a clamped single-domain film. This can be explained as follows: In an engineered multi-domain single crystal or free film, since the deformation is free of bound, shear piezoelectric deformation of each individual domain variant can equally contribute to the longitudinal piezoelectric strain. Therefore a multi-domain single crystal or free film deforms like a “single-domain” crystal. [17], [18]

However, when the film is constrained by a thick substrate, the shear deformations of neighboring individual domain variants are interlocked due to the clamping of the substrate. For (1 1 1) oriented film, it has only one domain variant after poling, therefore its d_{nn}^{f} should be close to that of a single-domain film. For a (001) oriented film, it has four equivalent <1 1 1> domains after poling ([1 1 1], [-1 1 1], [1 -1 1] and [-1 -1 1]), therefore its small d_{nn}^{f} values as compared with that of a single domain film may be explained by the interlocking of shear piezoelectric deformations among domain variants. For the (110) orientation, its d_{nn}^{f} value (152pm/V) for a single domain film is much smaller than its bulk value (937 pm/V), which indicates a much reduced contribution to longitudinal piezoelectric response from the film's shear piezoelectric deformation. In addition, a poled (110) oriented film only has two domain variants ([1 1 1] and [1 1 -1]), therefore the interlocking of shear deformation may be much less effective in the poled (110) film, as compared with that of a (001) film.

In summary, the general expression for the intrinsic converse longitudinal piezoelectric constant (d_{nn}^{f}) of a substrate-clamped single-domain rhombohedral film is obtained as function of the film orientation. The d_{nn}^{f} for epitaxial $0.67Pb(Mg_{1/3}Nb_{2/3})O_3$-$0.33PbTiO_3$ films of three different crystallographic orientations, (001), (110), and (111), are calculated and compared with measured results using piezoelectric force microscopy. It is shown that the orientation for maximum d_{nn}^{f} is close to the pseudo cubic [001] direction. The measured d_{nn}^{f} for a $0.67Pb(Mg_{1/3}Nb_{2/3})O_3$-$0.33PbTiO_3$ film of this orientation is about 250pm/V, which makes it a promising candidate for MEMS devices.

It should be notified that, as the (111) and (110) oriented films showed d_{nn}^{f} values close to calculated results for single domain films, the (001) oriented film showed a much lower value than that of a single domain film. This discrepancy may be understood on the basis of an interlocking mechanism of shear deformations among different domain variants.

Table 2.8. Experiment results for 0.67Pb($Mg_{1/3}Nb_{2/3}$) O_3-0.33$PbTiO_3$ films. d_{nn}^{f} values are the equilibrium ones at zero electric field. Film thickness is kept at 3.3 μm for all films.

Orientation **n**	(001)	(110)	(111)
Bulk d_{nn} (pm/v)	2309	937	190
Theory d_{nn}^{f} (pm/v)	1395/261*	152	70
Experiment d_{nn}^{f} (pm/v)	251±47	130±10	73±7
FWHM for X-ray	0.28°	0.4°	0.3°
peaks (in parenthesis)	(002)	(011)	(111)

* Calculation based on the piezoelectric and mechanical properties of a multi-domain (001) oriented rhombohedral single crystal.[6]

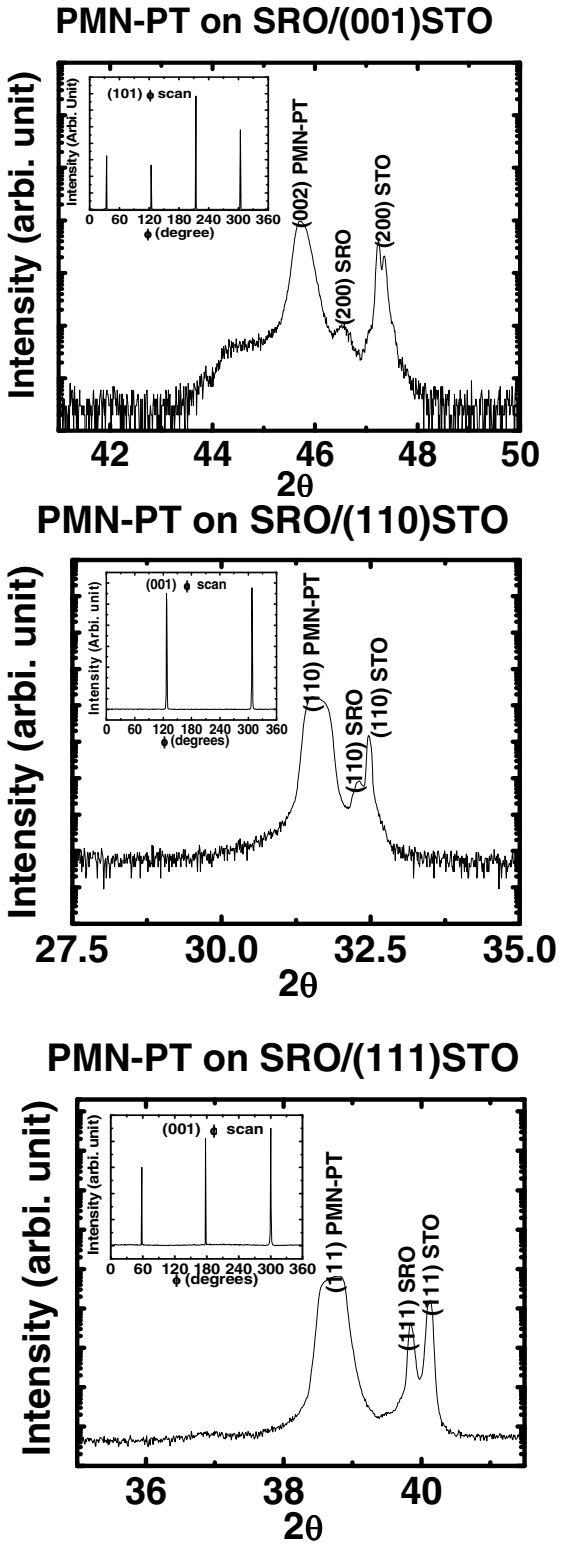

Figure 2.26. X-ray spectrum and ϕ-scans for (001) (top), (110) (middle) and (111) (bottom) oriented $0.67Pb(Mg_{1/3}Nb_{2/3})O_3$-$0.33PbTiO_3$ films.

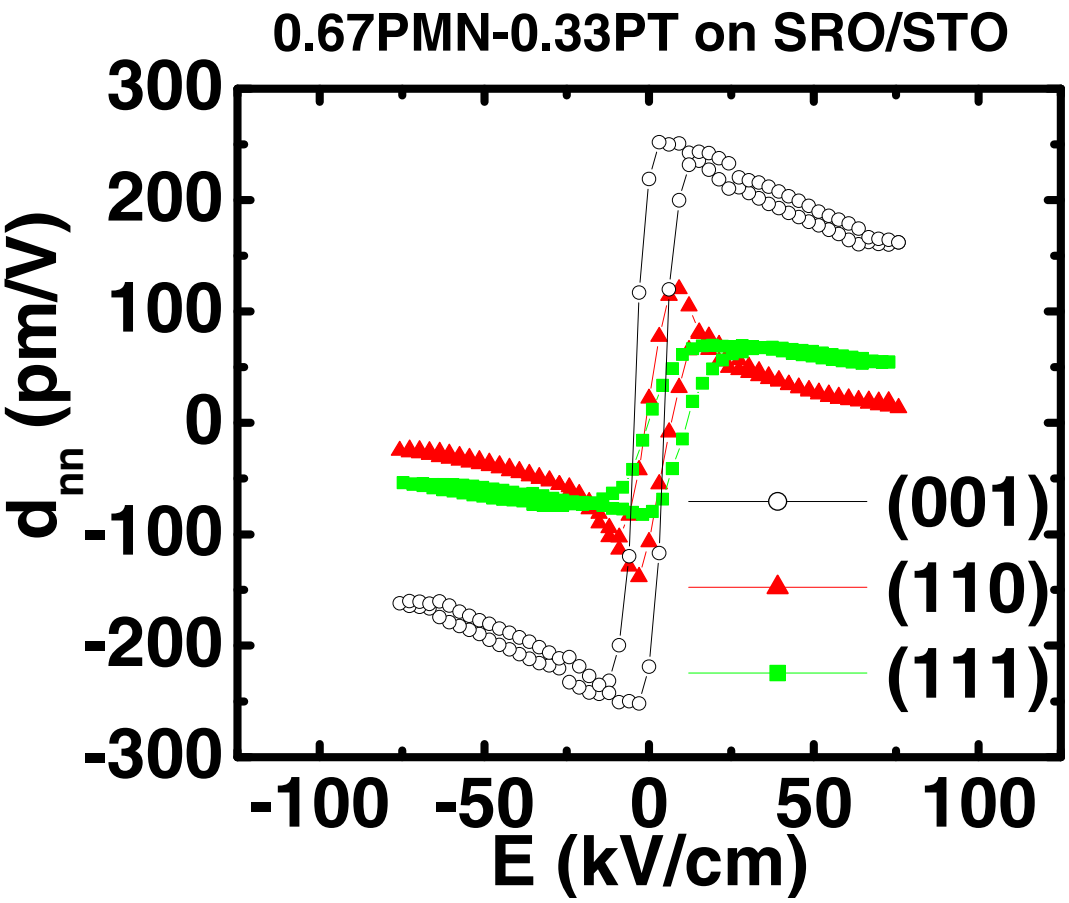

Figure 2.27. Measured effective longitudinal piezoelectric constants as function of DC Bias for (001), (110) and (111) oriented $0.67Pb(Mg_{1/3}Nb_{2/3})O_3$-$0.33PbTiO_3$ films.

2.6 Conclusion

The following points summarize this chapter:

(1) The converse piezoelectric property of a ferroelectric film is characterized by a field induced invariant-plane strain. There are longitudinal and shear piezoelectric strain components, which are characterized by two effective piezoelectric coefficients:

$$d_{\ln}^{f} = \Pi_{ik}\, C_{kt\alpha\beta}\, d_{\gamma\alpha\beta}\, n_t n_i l_\gamma \quad (2.3a)$$

$$d_{l\tau}^{f} = \Pi_{ik}\, C_{kt\alpha\beta}\, d_{\gamma\alpha\beta}\, n_t \tau_i l_\gamma \quad (2.3b)$$

Equations (2.3a) and (2.3b) allow one to compute the effective piezoelectric coefficients for arbitrary orientations of a film and the electric field, if the intrinsic piezoelectric coefficient and the elastic moduli are known. For tetragonal and rhombohedral epitaxial films with electric field applied along the normal, exact solutions of the longitudinal piezoelectric coefficients d_{nn}^{f} ($d_{nn}^{f} = d_{33,f} = \Pi_{ik}\, C_{kt\alpha\beta}\, d_{\gamma\alpha\beta}\, n_t n_i n_\gamma$) are provided and compared with experiment measured results by piezoelectric force microscopy.

(2) The direct piezoelectric coefficients are different from their corresponding converse ones, not only on that it has a non-zero d_{31} component, but the apparent d_{33} value are quantitatively different from the converse d_{33} coefficient. It is shown that these two d_{33} coefficients are equivalent only when the film/substrate couple is studied as a whole, instead of measuring the film's physical quantities alone.

(3) The effective piezoelectric properties, which are characterized by direct and converse effective piezoelectric coefficients - $d_{33}^{f,D}$, $d_{31}^{f,D}$, $e_{31}^{f,D}$, $d_{33}^{f,C}$ (measured by film strain), $\overline{d}_{33}^{f,C}$ (measured by total strain), $e_{31}^{f,C}$ and $d_{3\tau}^{f,C}$ are studied in a general theoretical framework by studying the film-substrate in-plane stresses induced by piezoelectric stimuli (mechanical or electrical). The modification on piezoelectric responses of a ferroelectric film by in-plane stresses are a longitudinal polarization Δp_3 in a direct piezoelectric mode and a longitudinal strain $\Delta\varepsilon_{33}$ in a converse piezoelectric mode:

$$\Delta p_3 = d_{klm}\sigma_{lm}n_k^{(3)} \quad \text{or} \quad \Delta\varepsilon_{33} = s_{ijpq}^{E,f}\,\sigma_{pq}n_i^{(3)}n_j^{(3)} \tag{2.15}$$

It is shown that effective piezoelectric coefficients can be obtained by taking into account of the above additional terms in the apparent piezoelectric responses.

(3) For a single domain ferroelectric film, the clamping from a rigid substrate will make the converse longitudinal piezoelectric coefficient $d_{33}^{f,C}$ different from the direct coefficient $d_{33}^{f,D}$. $d_{33}^{f,C}$ is also reduced by clamping as compared with the bulk value. Experiment measurements of $d_{33,f}$ by piezoelectric force microscopy (PFM) on tetragonal lead titanate zirconate ($Pb(Zr_xTi_{1-x})O_3$ with x=0.2) and rhombohedral lead magnesium niobate-lead titanate (xPb($Mg_{1/3}Nb_{2/3}$)O_3-(1-x)$PbTiO_3$ with x=0.67) epitaxial ferroelectric films with various crystalline orientations have shown good agreement with theoretical prediction on the reduction of $d_{33,f}$ by the substrate-clamping effect. While it is shown that a pseudo cubic (001) orientation in $Pb(Zr_xTi_{1-x})O_3$ (from x=0 to x=0.6) and xPb($Mg_{1/3}Nb_{2/3}$) O_3-(1-x)$PbTiO_3$ (x=0.58 and 0.67)

epitaxial single domain films will have the maximum $d_{33,f}$ coefficient, it is a (111) oriented epitaxial film that have the maximum $d_{33,f}$ in $BaTiO_3$ system. It should be noted that all piezoelectric coefficients calculated and compared in this dissertation refer to those at room temperature.

(5) On the other hand, the transverse piezoelectric coefficients ($e_{31,f}$) will be enhanced in thin films as compared with those in bulk materials, which is good for an ferroelectric film to be used in transverse piezoelectric applications. $e_{31,f}$ has a similar orientation dependence to that of $d_{33,f}$, i.e., a (001) pseudo-cubic orientation for maximum $e_{31,f}$ in $Pb(Zr_xTi_{1-x})O_3$ (from x=0 to x=0.6) and xPb($Mg_{1/3}Nb_{2/3}$) O_3-(1-x)$PbTiO_3$ (x=0.58 and 0.67) epitaxial single domain films, while a (111) oriented epitaxial film will have the maximum $e_{31,f}$ in $BaTiO_3$ system.

(6) Piezoelectric force microscopy can be used to characterize piezoelectric responses of ferroelectric films. In the quantitative d_{33} measurement, the effective longitudinal piezoelectric coefficient of a ferroelectric film can be indirectly measured by calibrating the raw signal of the piezoelectric response with a X-cut quartz plate (d_{11}=2.3pm/V).[80],[82], [83] On the other hand, the contours of domain patterns on the surface can be detected by imaging the local piezoelectric response with both amplitude and phase information, with the aid of a lock-in amplifier.[86]

CHAPTER 3, EXTRINSIC PIEZOELECTRIC RESPONSE IN THIN EPITAXIAL FERROELECTRIC FILMS

3.1 Orientation dependence of 90^o domain pattern

In tetragonal ferroelectric films, 90^o domains form as elastic domains to release the internal growth stresses. For (001) oriented film, the neighboring elastic domains have polar vectors aligned out-of-plane and in plane, alternatively, which is usually called a "*c/a/c/a*" 90^o domain pattern. Under an applied electric field, the extrinsic contribution to d_{33} from the 90^o domain wall movement can be comparable to or even larger than the intrinsic d_{33}, as has been calculated by Yu and Roytburd et al.[90] N. Pertsev et al. also calculated the extrinsic piezoelectric response from domain wall motion for a tetragonal ferroelectric thin film with a dense c*/a* domain structure.[91] In apparent piezoelectric coefficient d_{33} for a (001) oriented tetragonal lead titanate thin film, their calculation showed an increase of ~70pm/V, which is about the same as the intrinsic d_{33}. It can be expected that, as the composition of the tetragonal $PbZr_{1-x}Ti_xO_3$ film approaches the morphotropic phase boundary (x~0.5), the extrinsic contribution to d_{33} from the 90^o domain wall movement will be enhanced, as both the intrinsic piezoelectric properties and the softness of the material with respect to the change of polar state peak at the MPB.

Furthermore, there is an orientation dependence of the 90^o domain patterns. For a (001) oriented tetragonal film, a 3-domain pattern will form due to the symmetrical biaxial in-plane stress (Fig 3.1 a, b).[92] The two sets of *a* domains are orthogonal and therefore are pinned by each other. They are not as easy to move under the electric field as a *c/a* 2-domain pattern which has been theoretically modeled aforementioned. For a (111) oriented tetragonal film, all three variants of the tetragonal phase are equivalent

under an applied electric film along the film normal ("Engineered Domain Configuration"), therefore there will be no extrinsic contribution from domain wall movement toward the longitudinal piezoelectric response. For a (101) oriented tetragonal film, the in-plane stress is close to a uniaxial one due to the anisotropy in misfit strains (Section 3.2), a dominant *c/a* 2-domain pattern (may still contain the third domain variants in minor fractions) with canted and in-plane polar vectors alternatively aligned in neighboring domains is expected (Fig 3.1 c, d). As the film composition approaches the MPB, the softness of the PZT material in shear directions[27],[29] also eases the 90° domain movement in a non-polar (101) orientation in addition to the domain pattern. Unlike the c/*a* two-domain pattern calculated by Perterv et al. in a (001) orientation[91], which is in a stressed state, the two-domain pattern in (101) is a fully relaxed structure. Therefore it is possible that the (101) orientation can have a larger extrinsic contribution to d_{33} from its 90° domain wall movement than the (001) orientation for MPB-PZT films.

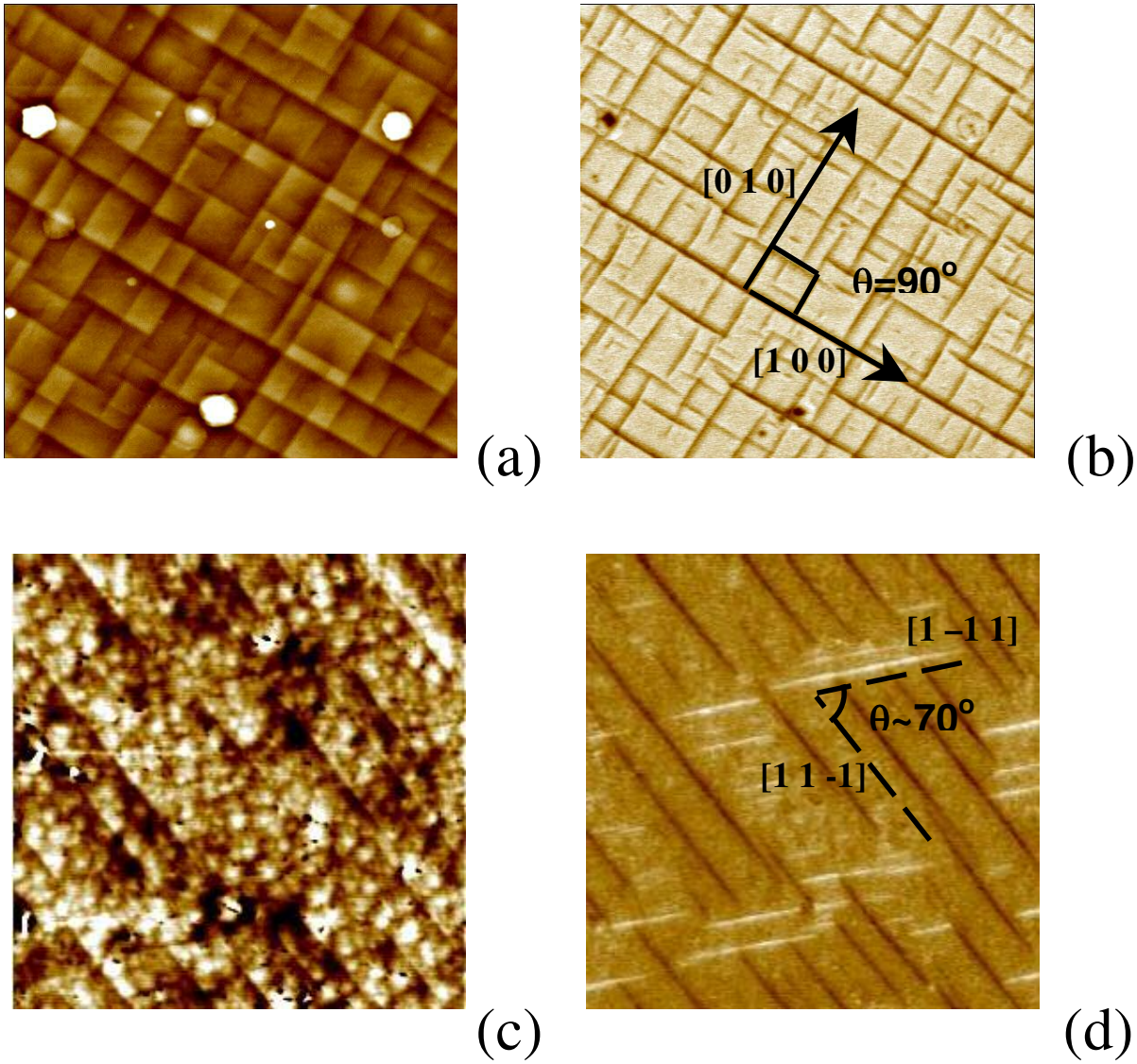

Fig. 3. 1 (a) topography, (b) out-of -plane piezoelectric force microscopy (PFM) for illustration of the domain structure of a tetragonal (001) film: (PZT 20/80, 5 μm × 5 μm, the bright matrix areas are c domains while the orthogonal gray strips are *a* domains which have zero longitudinal piezoelectric response); (c) topography, (d) in-plane PFM for illustration of the domain structure of a tetragonal (101) film (PZT 52/48, 10 μm × 10 μm, the areas with grey contrast are *c* domains which have small piezoelectric shear deformation; while the strips with white and dark contrasts are *a* domains which have large shear piezoelectric deformation. The opposite contrasts in *a* domains indicate the opposite signs of the in-plane polarizations).

3.2 Anisotropic misfit in a (011) oriented epitaxial film

For a tetragonal phase with self strain $\varepsilon_1=(a_T- a_c)/a_c$, $\varepsilon_3=(c_T-a_c)/ a_c$ (a_T and c_T are the lattice constants of tetragonal *c* and *a* axis, respectively, and a_c is the lattice constant of the cubic phase, therefore $\varepsilon_1<0$ and $\varepsilon_3>0$,), $\varepsilon_1=Q_{12}P_s^2$ and $\varepsilon_3=Q_{11}P_s^2=-\kappa Q_{12}P_s^2$.[6] $\kappa=-Q_{11}/Q_{12}=2.1\sim 2$.

For a (101) plane, the self strain for *a* and *c* domains are:

$$\hat{\varepsilon}_a=\begin{bmatrix}\varepsilon_1 & 0 & 0\\ 0 & \varepsilon_3 & 0\\ 0 & 0 & \varepsilon_1\end{bmatrix}=-Q_{12}P_s^2\begin{bmatrix}-1 & 0 & 0\\ 0 & \kappa & 0\\ 0 & 0 & -1\end{bmatrix}$$

$$\hat{\varepsilon}_c=\begin{bmatrix}\frac{\varepsilon_1+\varepsilon_3}{2} & 0 & \frac{-(\varepsilon_3-\varepsilon_1)}{2}\\ 0 & \varepsilon_1 & 0\\ \frac{-(\varepsilon_3-\varepsilon_1)}{2} & 0 & \frac{\varepsilon_1+\varepsilon_3}{2}\end{bmatrix}=-Q_{12}P_s^2\begin{bmatrix}\frac{-1+\kappa}{2} & 0 & -\frac{1+\kappa}{2}\\ 0 & -1 & 0\\ -\frac{1+\kappa}{2} & 0 & \frac{-1+\kappa}{2}\end{bmatrix}$$

For a *c/a/c/a* two domain structure with α being the *a* domain fraction, the average self-strain is:

$$\hat{\varepsilon}_0(\alpha)=\alpha\hat{\varepsilon}_a+(1-\alpha)\hat{\varepsilon}_c=\begin{bmatrix}\varepsilon_1(\alpha) & 0 & \varepsilon_4(\alpha)\\ 0 & \varepsilon_2(\alpha) & 0\\ \varepsilon_4(\alpha) & 0 & \varepsilon_4(\alpha)\end{bmatrix}=-Q_{12}P_s^2\begin{bmatrix}\frac{\kappa-1}{2}\frac{\kappa+1}{2}\alpha & 0 & \frac{1+\kappa}{2}(1-\alpha)\\ 0 & (1+\kappa)\alpha-1 & 0\\ \frac{1+\kappa}{2}(1-\alpha) & 0 & \frac{\kappa-1}{2}(1-\alpha)-\alpha\end{bmatrix}$$

For the equilibrium *a* domain fraction ~$(1+\kappa)^{-1}$,[92] it can be seen that $\varepsilon_2(\alpha)=0$ and it is uniaxial strain in the (101) film growth plane. In reality, the *a* domain fractions in a tetragonal film is directly related with the ratio of effective misfit strain ($\bar{\varepsilon}_M$) and its tetragonality (ε_T) by $\alpha_a=-\bar{\varepsilon}_M/\varepsilon_T$.[92] If we consider that the film is fully relaxed (for

thick films) on the substrate in its cubic paraelectric phase, then $\bar{\varepsilon}_M \sim \varepsilon_a$, the compressive tetragonal strain, and $\varepsilon_T \sim \varepsilon_a + \varepsilon_c$ with ε_c being the elongational tetragonal strain. An estimation for the *a* domain fraction in thick tetragonal films can be made by substituting $\varepsilon_a = Q_{12} P_s^2$ and $\varepsilon_c = Q_{11} P_s^2$, which results $\alpha_a \sim (1+\kappa)^{-1}$, where $\kappa = -Q_{11}/Q_{12}$ is characteristic of the anisotropy in electrostrictive effects. This gives $\alpha_a \sim 30\%$ for PZT 50/50 films in a fully relaxed state. For PZT films epitaxial grown on STO substrate, $\bar{\varepsilon}_M$ is smaller than ε_a due to the compressive state in the film from thermal mismatch, [92] therefore $\alpha_a \sim 30\%$ is the upper bound for the *a* domain fraction. In our experiment, $\alpha_a \sim 20\%$is estimated from X-ray rocking curve and PFM results (Fig 3.4) for the films in remnant state, which is also supported by the remnant polarization measurement results.[6]

3.3 Experiment discovery of highly mobile 90^o domain walls and ultra high extrinsic piezoelectric responses due to 90^o domain wall movement

BACKGROUND

Lead Zirconate Titanate solid ceramics ($PbZr_{1-x}Ti_xO_3$) with compositions close to the morphotropic boundary are used in sensors, actuators, etc., because of their high piezoelectric coefficients. Due to the substrate clamping effect, the extrinsic contributions to the piezo-response are reduced and the effective piezoelectric coefficients of $PbZr_{1-x}Ti_x O_3$ films are degraded relative to bulk materials (typically on the order of 100 pm/V). We recently discovered reversible strain as high as 0.35% (longitudinal) in the (101) oriented epitaxial $PbZr_{0.52}Ti_{0.48}O_3$ films under applied ac

electric fields of <30kV/cm, resulting in the effective piezoelectric coefficients on the order of 1000 pm/V. Transmission electron microscopy, X-ray diffraction analysis, and atomic force microscopy revealed that the (101) film features a self-assembled polydomain structure, consisting of two domain sets of a tetragonal phase. Thermodynamic analysis suggests the high strain level in this film may be understood on the basis of a field-induced 90^o domain wall movement, which is greatly enhanced due to the special domain pattern and softness of the film material.

$PbZr_{1-x}Ti_xO_3$ (abbreviated as PZT) solid solution system is of many practical applications, among which piezoelectric transducers (sensors, actuators) are major application fields especially for PZT materials with compositions near its morphotropic phase boundary (abbreviated as MPB-PZT, x~0.5). One of the important piezoelectric constants is the converse longitudinal piezoelectric coefficient, namely, d_{33}, which is a measure of how much normal strain the piezoelectric material can achieve per unit of applied electric field and hence a measure of the performance of piezoelectric actuators. MPB-PZT bulk ceramic materials show large d_{33} coefficients (~300-800pm/V), which has long been known to have a dominant extrinsic contribution from 90^o domain movement.[93]-[95] However, for ferroelectric films which are widely used in integrated systems such as micron-electrical-mechanical-systems (MEMS), it was found that clamping of substrate greatly reduces the d_{33} coefficient. [36], [96] Particularly, it was reported that the extrinsic contributions by 90^o domain wall movement to the piezoelectric response are strongly suppressed in most films under a micron in thickness.[97], [98] There are many reports on the d_{33} coefficient of ferroelectric films by different measurement techniques and most of them showed similar results on the order

of 100 pm/V for films less than a micron in thickness. [38], [99]-[103] However, most of these measurements were carried out under relatively small signal excitation of the film with applied electric field along the polar axis, or in films with polycrystalline quality. Therefore, it is interesting to ask whether or not larger piezoelectric responses can be generated for epitaxial films of different orientations under excitation field of variable strengths.

EXPERIMENT RESULTS

In this study, epitaxial $PbZr_{1-x}Ti_xO_3$ films were grown on $SrTiO_3$ substrates with 2 different crystallographic orientations, (100) and (101), using an on-axis radio-frequency magnetron sputtering technique. The nominal Zr/Ti ratio of the sputtering target was 52/48. Prior to the PZT film deposition, 200nm thick epitaxial $SrRuO_3$ bottom electrodes were deposited on the substrate by a 90° off-axis sputtering technique.[83] During the PZT film deposition, the substrate temperature was maintained at 600°C with an oxygen pressure of 400 mTorr, followed by cooling under an oxygen pressure of 300 Torr. The thicknesses of the PZT films were about 700~1000 nm. The composition of the PZT films is the same as the target as confirmed by the Energy Dispersion Spectroscopy. For the purpose of electric and piezoelectric measurements, Pt electrodes were fabricated via UV lithography and pulsed laser deposition. X-ray diffraction analysis showed good epitaxy and tetragonally distorted structures for both (001) and (101) films. As an example, Fig 3.2 shows the different scans used to verify the crystalline structure of the (101) film, the splitting in the {002} peak in Fig 3.2 (b) and the non-splitting (222) peak in Fig 3.2 (c) support a tetragonal symmetry against a rhombohedral one. The *a* domain fractions for both (001) and (101) films are estimated to be ~20% from x-ray rocking

curves (not shown here).

Cross-section and plain view transmission electron microscopy (TEM) were performed for the (101) films. In Fig 3.3 (a) (b), it clearly showed that two sets of strip-like parallel domains were formed in this film with a <111> type domain boundary trace lying on the (101) growth plane. The TEM results were interpreted in Fig. 3.3 (c). A tetragonal polydomain structure with alternating c and *a* domains has a {101} domain boundary. This domain boundary will have a <111> trace when the film is grown on a (101) crystalline plane. Imaging-mode piezoresponse microscopy [81] was performed for the (101) film. A dominant 2-domain pattern with two sets of plane parallel large domains was discovered in this film from the topography and in-plane piezoelectric images as shown in Fig. 3.1 (c) (d). It was also illustrated that the angle between the traces of the *a* domains is ~ 68^{o}, which is in a good agreement with the angle between two <111> traces (~70^{o}). This observation supported the X-ray and TEM analysis results. Furthermore, in Fig 3.4 (a)-(c), it is illustrated that these a-domains are easy to move under a local writing field provided by the PFM tip, which was not discovered for (001) oriented films with symmetrical 3-domain architectures. Therefore, it is interesting to know how the domain wall movement will contribute to a global measured strain under an uniform field applied through a top electrode pad.

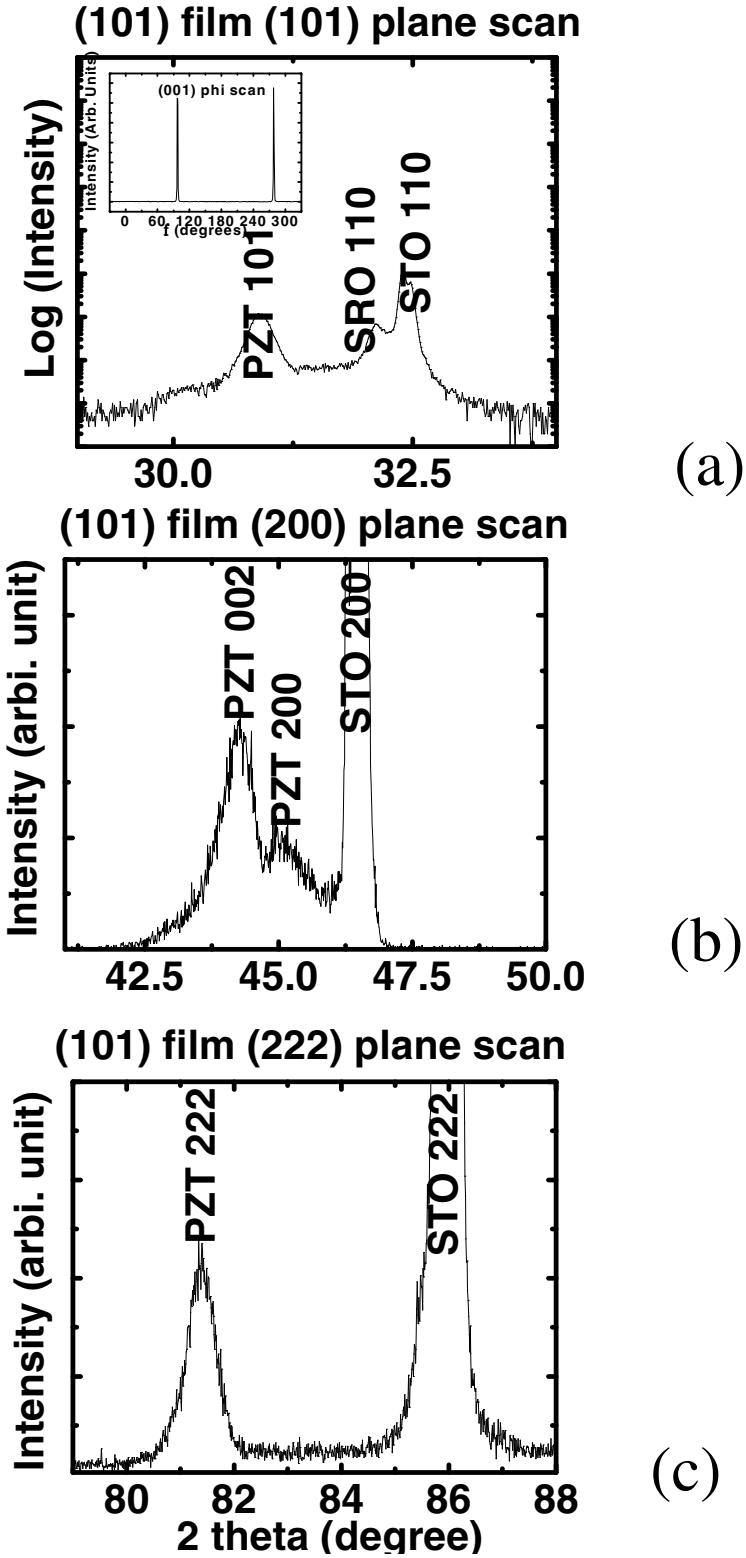

Fig. 3. 2 (a)-(c) X-ray result for (101) PZT 52/48 film showing a tetragonal distorted structure.

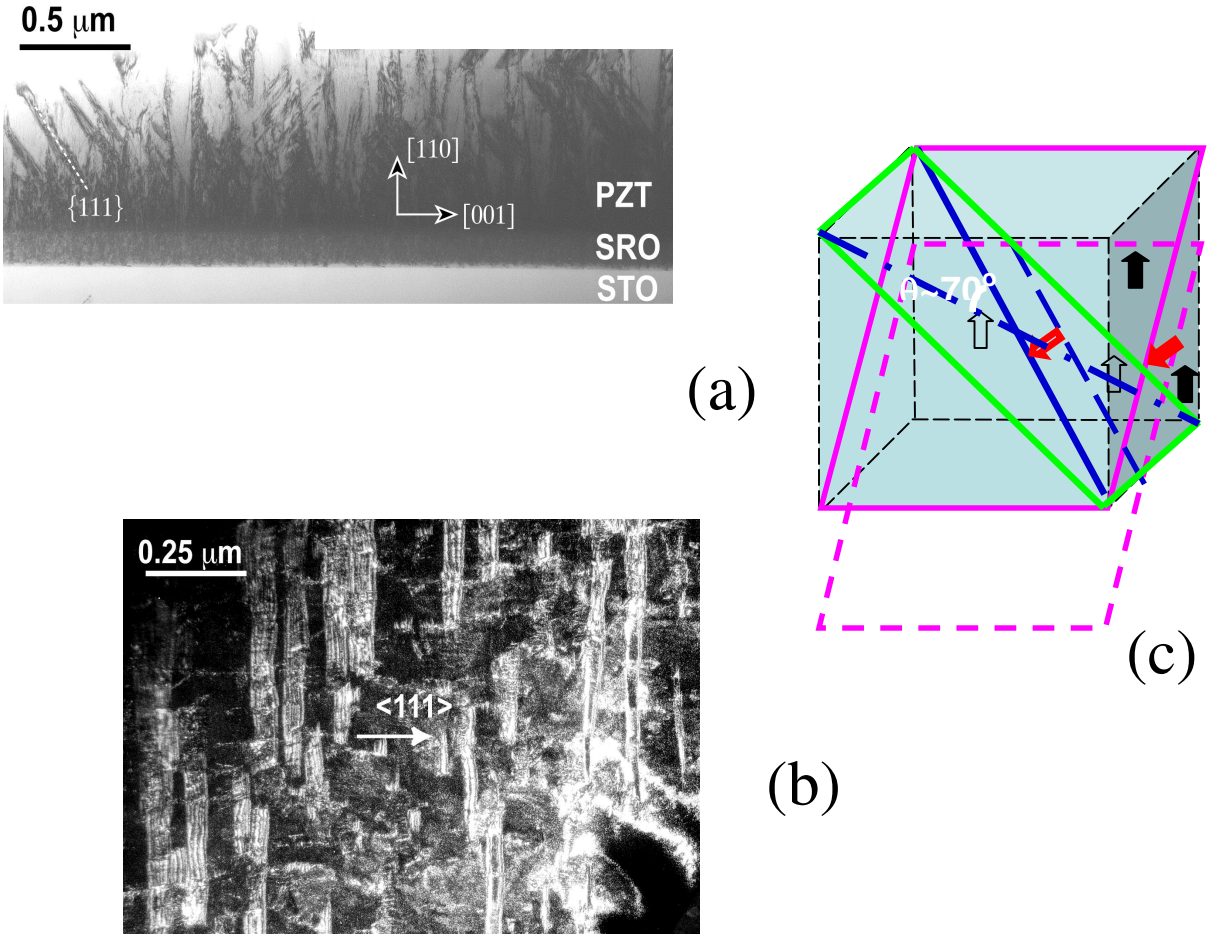

Fig. 3.3 (a) Cross-sectional TEM image (twin traces are // <111>); (b) Plain-view TEM image (dark-field image near <110> zone axis.; the twin traces are // <111>) for (101) oriented PZT 52/48 film. (c) Schematics of 90° domain pattern in a (101) film.

(a)

Fig. 3.4 Piezoelectric Force Microscopy (PFM) results of (101) PZT 52/48 film (6μm×6μm), Top: topography, center: out-of –plane PFM, bottom: in-plane PFM: (a) Original.

Fig. 3.4 Piezoelectric Force Microscopy (PFM) results of (101) PZT 52/48 film (6μm×6μm), Top: topography, center: out-of –plane PFM, bottom: in-plane PFM: (b) After writing –10V in a 3μm×3μm area.

Fig. 3.4 Piezoelectric Force Microscopy (PFM) results of (101) PZT 52/48 film (6μm×6μm), Top: topography, center: out-of –plane PFM, bottom: in-plane PFM: (c) Poling back using +10V in the same 3μm×3μm area.

The piezoelectric measurements were made by piezoelectric response microscopy[41], [86], [106]. During the strain measurements, the ac signal gradually increased from zero to its maximum amplitude and then went back to zero. The strains were recorded at each step. The maximum ac amplitude used for each film was limited to less than half of its coercive field in order to minimize the possible contribution to piezoelectric response from 180^o domain movement.[103] For each film, ten continuous capacitors were measured and for each capacitor, the strain measurements were repeated for 5 times. In Fig 3.5 (a), it is shown that (001) film has linear piezoresponse to electric field and has no hysteresis. The maximum strains for (001) film is ~0.04% at 30kV/cm, resulting in an effective d_{33} of 120pm/V. For the (101) films, as the field increased from zero to less than 5kv/cm, the piezoresponse is close to be a liner one with effective d_{33} ~110pm/V; however, as the field is further increased, the (101) films showed a strong non-liner piezoelectric response. At 30kV/cm, about 0.35% strain were obtained for the (101) films, which resulted in an effective d_{33}~ 1200pm/V. As the field went back to zero, the measured strains were in a different trace, resulting in a small hysteresis.

Fig. 3.5 (b) shows the polarization hysteresis measurement results using a ferroelectric tester (RT66A, Radiant Tech.) in the virtual ground mode. It shows that the remnant polarizations for these two films are in the order of (101) < (001), as what can be expected for a tetragonal structure. The remnant polarizations (P_r) for the (001) and (101) films are 0.4 C/cm^2 and 0.30 C/cm^2, respectively (leakage current densities for these films are less than 0.05 A/m^2 for the maximum field applied).

In order to understand the origin of the extrinsic contributions to the piezoelectric strains, sub-coercive polarization measurements were carefully performed and P_{max} values

were recorded as a function of applied field (Fig. 3.5 (c)). The frequency of the pulse signal and the maximum field amplitude for the polarization measurements were kept the same as those for the strain measurements. It shows that there is a small hysteresis in the P_{max}-E curve of the (101) film and the change of polarization is about 0.04C/m^2 at the field of 30kV/cm, while the P_{max}-E curves for the (001) film is linear and the maximum polarization change is only 0.015 C/m^2 at the same field. This is consistent with the strain-field cycling data. Although it is clear that an unipolar polarization hysteresis should be related with a change in polar state of the material, the change in polarization here was far too small to be characteristic of a change of the entire film from tetragonal to orthorhombic symmetry.[27] Therefore, the small hysteresis is very likely to be related with 90^o domain movement.

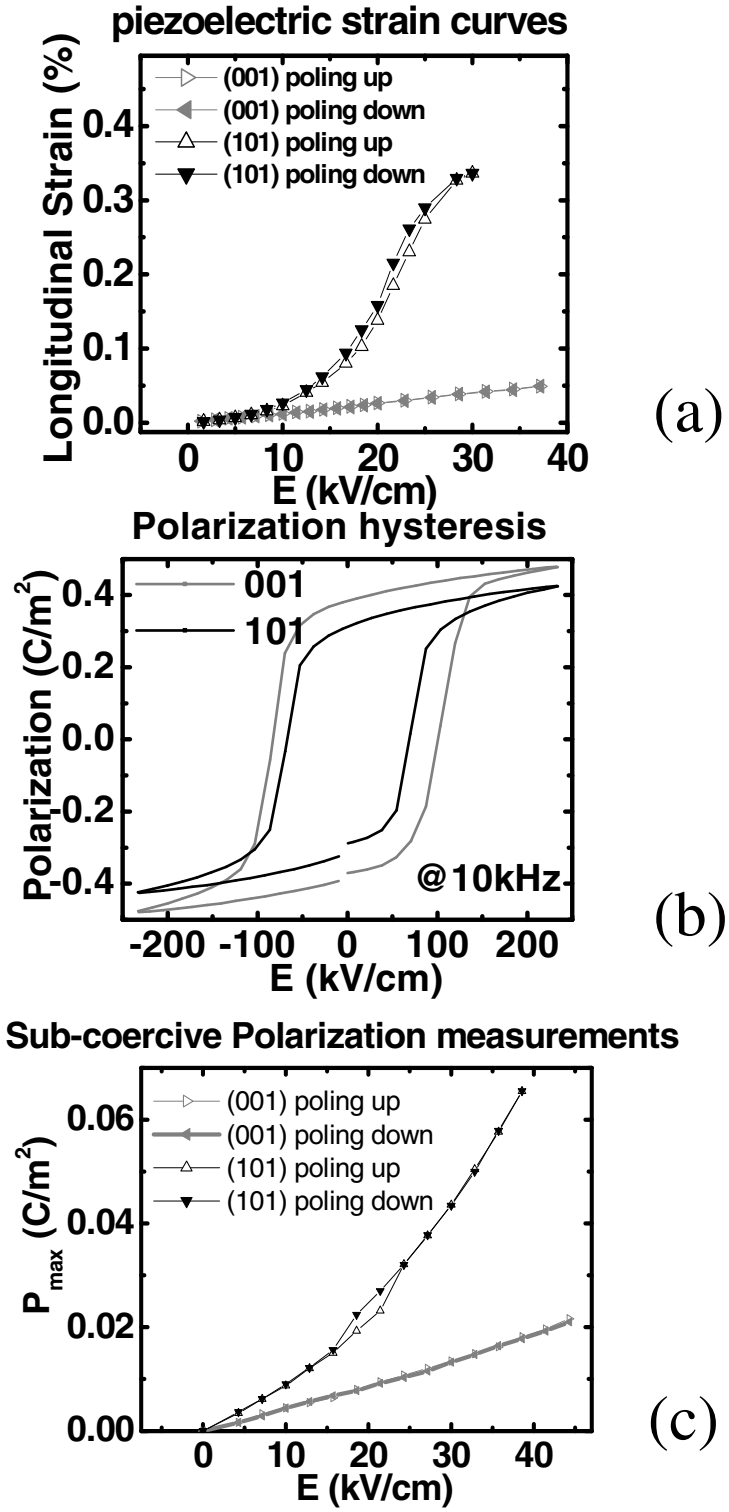

Fig. 3.5 (a) Longitudinal strain measurements under AC field; (b) Polarization hysteresis; (c) Subcoercive polarization measurements for (001) and (101) oriented PZT 52/48 films.

3.3 Theoretical analysis, and the importance of elasticity

Recent first principle calculations [27],[28], [104] have shown that PZT is soft with respect to shear in both tetragonal and rhombohedral structures near the MPB, therefore the large piezoelectric properties in bulk ceramics may be interpreted as from the shear contributions, which can be either intrinsic shear piezoelectric response[108] or extrinsic contribution from phase transition or domain wall movement due to shear deformation. [27], [28] In our recent works, the orientation dependence of intrinsic d_{33} of single domain ferroelectric thin films were calculated for $PbZr_{1-x}Ti_xO_3$ (PZT) solid solution systems by taking into account of intrinsic shear contribution in a non-polar orientation .[44], [71] However, it was found that a pseudo cubic (001) orientated film has the largest intrinsic d_{33} for both tetragonal and rhombohedral compositions, similar to the results calculated for bulk materials.[7]-[8] The maximum intrinsic d_{33} calculated near the morphotropic phase boundary (MPB) are still on the order of 100 pm/V.[71] The calculated intrinsic d_{33} for PZT 50/50 tetragonal films are 120pm/V for 101 orientation and 167pm/V for 001 orientation.

If the fractions of *c* domains in both films are 80%, then the contribution from *c* domain's piezoresponse to d_{33} are 96pm/V and 132 pm/V for (101) and (001) films, respectively. The remnant polarizations (measured normal charge density) are 0.4 C/m^2 and 0.28C/m^2 (P_r=0.5 C/m^2 is taken from Ref. [6]) since *a*-domains are aligned in-plane. By comparing these calculation results with experiment data, it is found that there are negligible contributions from 90^o domain wall movement to the d_{33} and polarization of the (001) film, or the 90^o domains can be treated as "immobile" in the (001) films throughout the strength spectrum of the ac excitation field. On the other hand, although

the small signal d_{33} (E<5kV/cm) and remnant polarization of the (101) film agreed fairly well with theoretical values by considering the 90° domains walls as "immobile" under small excitation signal, the large non-linear longitudinal piezoresponse under larger excitation field can not be explained without considering contribution from 90° domain wall movement, which is the extrinsic shear contribution in this case.

Based on all these experiment results, our proposed mechanism for the large piezoelectric response of the (101) film is as follows. The 90° domains in (001) oriented film has low mobility, which can be seen clearly from the piezoelectric strain and polarization results. While for the (101) film, the 90° domains are highly mobile due to the 2-D domain pattern. Under the ac exciting field ±E, there will be shrink and expansion of *a* domain walls in the film (Fig 3.6), which will lead to large extrinsic contribution to the piezoelectric response. In this case, the mobility of 90° domain walls is higher than that of the 180° domain walls. To prove that this model is consistent with experiment results, a thermodynamic analysis is performed as follows.

Consider a fully relaxed film, the transformation from *a* domain to *c* domain will result in a self strain $\hat{\varepsilon} = \hat{\varepsilon}_c - \hat{\varepsilon}_a = \begin{bmatrix} 0 & 0 & 0 \\ 0 & -\varepsilon & 0 \\ 0 & 0 & \varepsilon \end{bmatrix}$, where $\varepsilon = \varepsilon_3 - \varepsilon_1 = -(\kappa + 1) Q_{12} P_r^2 = 3.6\%$ (Appendix A, Ref. [6]). The change of total free energy associated with a reversible domain wall movement characterized by a shift of $\Delta\alpha$ fraction of *a*-domains under applied electric field E is written in Eq (3.1). $\hat{\varepsilon}(\Delta\alpha) = \Delta\alpha \hat{\varepsilon}$ is the self strain change of the film. $\hat{\hat{G}}(n, E)$ is the planar elastic modulus tensor at constant electric field of the (101) polydomain film, which is a function of film orientation, film elastic modulus, as well as

the field strength E due to the highly non-linear electromechanical behavior of MPB-PZT materials. $\hat{\hat{G}}(n,E) = \hat{\hat{C}}(E) - \hat{\hat{C}}(E)\hat{n}[\hat{n}\hat{\hat{C}}(E)\hat{n}]^{-1}\hat{n}\hat{\hat{C}}(E)$, $\hat{\hat{C}}(E)$ is the tensor of elastic moduli of the polydomain film. [46]-[48] $\hat{n} = \frac{1}{\sqrt{2}}(101)$ here and ΔP is the difference in net polarization between neighboring 90^o domains given by $\Delta P = P_r \cos 45^o$.

$$F_{total}(\Delta\alpha) = F_{elastic}(\Delta\alpha) + F_{electric}(\Delta\alpha) = \frac{1}{2}\hat{\varepsilon}(\Delta\alpha)\hat{\hat{G}}(n,E)\hat{\varepsilon}(\Delta\alpha) - \Delta P(\Delta\alpha)E$$

$$= \frac{(\Delta\alpha)^2}{2}\hat{\varepsilon}\hat{\hat{G}}(n,E)\hat{\varepsilon} - \Delta P(\Delta\alpha)E \qquad (3.1)$$

Minimization of Eq. (3.1) with respect to electric field E results in the equilibrium $\Delta\alpha$ at a given field E, and subsequently the equilibrium change in normal polarization ΔP_{eq} and normal strain $\Delta\varepsilon_{eq}$:

$$\Delta\alpha_{eq}(E) = P_r \cos(45^o)E / [\hat{\varepsilon}\hat{\hat{G}}(n,E)\hat{\varepsilon}] \qquad (3.2.1)$$

$$\Delta P_{eq}(E) = P_r \cos 45^o \Delta\alpha_{eq}(E) \qquad (3.2.2)$$

$$\Delta\varepsilon_{eq}(E) = \varepsilon \cos 45^o \Delta\alpha_{eq}(E) \qquad (3.2.3)$$

Due to lack of elastic modulus data for a polydomain film, Eqs. (3.2) can not be accurately solved. However, the experimentally measured ΔP_{eq} and $\Delta\varepsilon_{eq}$ can be compared to see if consistent results are obtained. It is found that these two quantities have a good fitting throughout the applied field. For example, at E=30kV/cm, $\Delta P_{eq}=0.04 C/m^2$, $\Delta\alpha_{eq}(E=30kV) = \Delta P_{eq}/(P_r \cos 45^o) = 0.113 = 11.3\%$. While at the same field, $\Delta\varepsilon_{eq} = 0.35\% - 96*10^{-12}*30*10^5 \sim 0.32\%$, $\Delta\alpha_{eq}(E=30kV) = = \Delta\varepsilon_{eq}/(\varepsilon\cos 45^o) = 0.32\%/(3.6\%*\cos 45^o) = 12.7\%$.

On the other hand, we can estimate the lower bound of the extrinsic piezoelectric strain by taking $\hat{\hat{G}}(n,E)$ as that in the *c*-domain film near zero electric field. That this estimation is the lower bound are because:

(1) *c*-domain has its hard axis (010) being clamped on the film plane (101), while the same axis in *a*-domain is the soft axis (001). Therefore, it can be expected that pure c-domain film is harder than the mixture on the (101) film plane, which means that the dominator in Eq. (3.2.1) $\hat{\varepsilon}\hat{\hat{G}}(n,E)\hat{\varepsilon}$ is overestimated. By Eq. (3.2.1)-(3.2.3), it can be seen that the extrinsic piezostrain $\Delta\varepsilon_{eq}$(E) is underestimated in this case.

(2) It is well known that MPB-PZT materials have highly non-linear electromechanical behavior. Specifically, they become extremely soft with respect to a shear deformation. In this case, the transformation from *a*-domain to *c*-domain is a shear process along the {101} plane. Once this process is trigged, it can effectively soften the lattice of PZT materials (reducing the elastic energy $\propto \hat{\varepsilon}\hat{\hat{G}}(n,E)\hat{\varepsilon}$ as the energy barrier) as the field is further increased, which in return facilitates the *a*-*c* transformation by 90^o domain wall movement.

By taking the elastic compliance data for tetragonal PZT 52/48 from Ref. [57] and follow the calculation of $\hat{\hat{G}}$ (n) for a tetragonal film from Ref. [44], it is obtained that $\hat{\varepsilon}\hat{\hat{G}}(n,E)\hat{\varepsilon} = 74\,\varepsilon^2$ Gpa, and the small signal $\Delta\alpha_{eq}$(E)= $P_r \cos(45^o)E/[\hat{\varepsilon}\hat{\hat{G}}(n,E)\hat{\varepsilon}]$=(3.6* 10^{-2}*E) %, where E is in the unit of kV/cm. The effective small signal d_{33} it can produce can be obtained by $\Delta\varepsilon_{eq}(E)/E = \varepsilon \cos 45^o \Delta\alpha_{eq}(E)/E = 3.6\% * \cos(45^o) * 3.6 * 10^{-2}\% = 9.2 * 10^6$

cm/kV=92pm/V. This value plus the intrinsic d_{33} from *c*-domain's piezoresponse (96pm/V) account for the ~200pm/V measured d_{33} in the field range of 5kV/cm~10kV /cm. However, it is an order of magnitude smaller than the measured large signal effective d_{33} (E>10kV/cm), which characterizes a large non-linear extrinsic piezoelectric response. This may be explained by the field induced softening of the MPB-PZT lattice.

The large extrinsic d_{33} (~1000pm/V) can also be reproduced by replacing the relatively small elastic compliance s_{11}^E and s_{33}^E in Ref. [57] with the large compliance data of poled soft PZT materials[105]-[109]. The effect of poling on the softening of the elastic modulus provides another piece of evidence for the observed large d_{33} on the poled films.

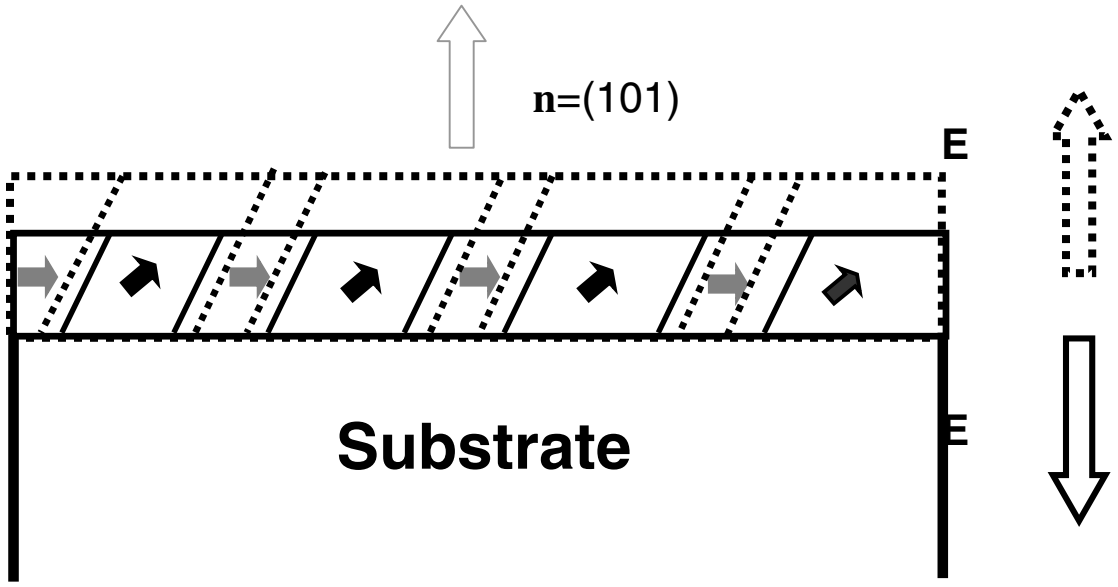

Fig. 3.6 Schematics of a field-induced 90° domain movement in the (101) PZT 52/48 film.

3.4 Conclusion

In a summary, we report for the first time the discovery of effective piezoelectric coefficients on the order of 1000pm/V under high ac driving field for continuous ferroelectric films. The material we used was PZT 52/48 epitaxially grown on SRO/(101) STO substrate. Longitudinal strains of ~0.35% were achieved when the film was excited with an ac electric field of V_{pp}~60kV/cm. The high piezoelectric response can be excited repeatedly and are accessible in a frequency range from 100Hz to at least100k (the up limit of our lock-in amplifiers). This makes our film a promising candidate for next generation MEMS devices.

A model of field-induced 90^{o} domain wall movement is proposed to explain the experiment observations. The main statement of this model is that a 2-domain *c/a* structure on the (101) oriented tetragonal film can be much more mobile than the 3-domain *c/a* structure in the (001) oriented film, especially when the film material is endowed extraordinary softness by the composition (MPB) and the (101) non-polar orientation. It should be noted that the formation of the 2-domain *c/a* structure is a natural consequence of the asymmetric misfit of a (101) crystalline plane in a tetragonal phase during its growth from a cubic structure. This result suggests an optimized design of ferroelectric thin film heterostructures for better electro-mechanical performance. It should also be viable to other ferroic (ferroelectric, ferromagnetic and ferroelastic) materials, whose domain structures (and hence properties) can be engineered by changing the epitaxial relations with a substrate, and as such our work should impact a broad range of materials research.

CONCLUSIONS AND FUTURE WORK

This work is the first study on the general orientation dependence of the piezoelectric properties of epitaxial ferroelectric thin films, which includes both theoretical and experiment work on intrinsic and extrinsic piezoelectric properties of epitaxial ferroelectric films.

(1) For a single domain epitaxial ferroelectric film, it is shown that elastic clamping from a substrate has broken the equivalence between "direct" and "converse" intrinsic piezoelectric coefficients.

(2) On evaluating piezoelectric properties of ferroelectric films for applications in MEMS transducers,[35] the two most important coefficients are the longitudinal piezoelectric coefficient $d_{33,f}$, and the transverse piezoelectric coefficient $e_{31,f}$. $d_{33,f}$ is the ratio between a longitudinally generated mechanical strain ε_{33} and a longitudinally applied electric field E_3, while $e_{31,f}$ is the ratio between an induced longitudinal polarization ΔP_3 (electric charge density) and the sum of laterally applied mechanical strains ε_{11} and ε_{22} (subscripts "1" and "2" indicate the in-plane axies while "3" the longitudinal axis). Excellent piezoelectric transducers either can produce large electric charge signal at small mechanical strains (large $e_{31,f}$) or large mechanical strains at a small electric field (large $d_{33,f}$), therefore $e_{31,f}$

and $d_{33,f}$ are essential quantities describing the performance of ferroelectric-film based MEMS transducers. Due to the clamping from substrate, these two piezoelectric coefficients for ferroelectric films can be very different from their counterparts in bulk materials.[44], [52]

(3) For a single domain ferroelectric film, the clamping from a rigid substrate will make the converse longitudinal piezoelectric coefficient $d_{33}^{f,C}$ different from the direct coefficient $d_{33}^{f,D}$. $d_{33}^{f,C}$ is also reduced by clamping as compared with the bulk value. Experiment measurements of $d_{33,f}$ by piezoelectric force microscopy (PFM) on tetragonal lead titanate zirconate ($Pb(Zr_xTi_{1-x})O_3$ with x=0.2) and rhombohedral lead magnesium niobate-lead titanate ($xPb(Mg_{1/3}Nb_{2/3})O_3$-$(1-x)PbTiO_3$ with x=0.67) epitaxial ferroelectric films with various crystalline orientations have shown good agreement with theoretical prediction on the reduction of $d_{33,f}$ by the substrate-clamping effect. While it is shown that a pseudo cubic (001) orientation in $Pb(Zr_xTi_{1-x})O_3$ (from x=0 to x=0.6) and $xPb(Mg_{1/3}Nb_{2/3})O_3$-$(1-x)PbTiO_3$ (x=0.58 and 0.67) epitaxial single domain films will have the maximum $d_{33,f}$ coefficient, it is a (111) oriented epitaxial film that have the maximum $d_{33,f}$ in $BaTiO_3$ system.

(4) On the other hand, the transverse piezoelectric coefficients ($e_{31,f}$) will be enhanced in thin films as compared with those in bulk materials, which is good for an ferroelectric film to be used in transverse piezoelectric applications. $e_{31,f}$ has a similar orientation dependence to that of $d_{33,f}$, i.e., a (001) pseudo-cubic orientation for maximum $e_{31,f}$ in $Pb(Zr_xTi_{1-x})O_3$ (from x=0 to x=0.6) and xPb($Mg_{1/3}Nb_{2/3}$) O_3-(1-x)$PbTiO_3$ (x=0.58 and 0.67) epitaxial single domain films, while a (111) oriented epitaxial film will have the maximum $e_{31,f}$ in $BaTiO_3$ system.

(5) A complete theoretical analysis of piezoelectric responses in a single domain ferroelectric film, which are characterized by effective longitudinal, transverse and shear piezoelectric coefficients, is presented as a summary of this theoretical work.

(6) On the part of extrinsic piezoelectric properties, movement of elastic domains has long been known to have a large contribution to apparent piezoelectric coefficients in ferroelectric bulk materials. It has also long believed that elastic domains in thin films are immobile due to the substrate clamping and inter-domain pinning. Our work on the piezoelectric properties of epitaxial thick lead titanate zirconate ($Pb(Zr_xTi_{1-x})O_3$ with x=0.52) films with tetragonal distorted structures has shown that (011) oriented epitaxial films had much enhanced

piezoelectric responses as compared with those of (001) and (111) oriented films. Detailed structure analysis showed that instead of an interconnected 3-domain (3-D) architecture that is usually found in a (001) oriented thick film, the (011) films consisted of a dominant 2-domain (2-D) architecture, by which the pinning between neighboring domain walls is much reduced and domains walls become mobile. This study demonstrate the possibility of achieving high extrinsic piezoelectric responses by optimizing the epitaxial relationship between the film and substrate with respect to the domain mobility, and should also be instructive to the design of ferromagnetic and ferroelastic thin film devices used for transducer applications. Future work is being carrying out on tetragonal lead zirconate titanate ($Pb(Zr_xTi_{1-x})O_3$ with x=0.2) epitaxial films with different orientations.

(7) Another important source of extrinsic piezoelectric response is from phase boundary movement and it will be the focus of future study. The coexistence of tetragonal and rhombohedral phases as elastic domains is being studied for lead zirconate titanate ferroelectric films near its morphotropic phase boundary. The volume fraction of the phases and different twin components will be obtained as functions of misfit strain and film orientation. It will be illustrated that, instead of the explanation by an “ultra flexible” monoclinic phase which can easily change its polarization direction under poling field and produce

large piezoelectric response, the superior electromechanical properties of MPB-PZT films may be understood on the basis of a field-induced evolution of this tetragonal-rhombohedral heterophase polydomain structure.

My Ph.D. research work is supported by the NSF under Grant DMR 02-10512.

Principle results of this dissertation are published in several journals as listed below.

Journal papers published (or accepted)

1. Jun Ouyang, R. Ramesh and A. L. Roytburd, "Theoretical investigation of the intrinsic piezoelectric properties for tetragonal $BaTiO_3$ epitaxial films", Applied Surface Sciences (in press).

2. Jun Ouyang, D. M. Kim, C. B. Eom, R. Ramesh, and A. L. Roytburd, "Orientation dependence of the intrinsic converse longitudinal piezoelectric constant for 0.67Pb$(Mg_{1/3}Nb_{2/3})O_3$ - 0.33$PbTiO_3$ ferroelectric films with a rhombohedral structure". Smart Materials and Structures, 14, 524 (2005).

3. Jun Ouyang, R. Ramesh and A. L. Roytburd, "Theoretical predictions for the intrinsic converse longitudinal piezoelectric constants of lead zirconate titanate epitaxial films". Advanced Engineering Materials, **7**, 229 (2005).

4. Jun Ouyang, R. Ramesh and A. L. Roytburd, "Intrinsic effective piezoelectric coefficient $e_{31,f}$ for ferroelectric thin films ". Applied Physics Letters, **86**, 152901 (2005).

5. Jun Ouyang, S. Y. Yang, L. Chen, R. Ramesh, and A. L. Roytburd, "Orientation dependence of the converse piezoelectric constants for epitaxial single domain ferroelectric films". Applied Physics Letters, **85**, 278 (2004).

Conference paper(s) published

1. Jun Ouyang, R. Ramesh and A. L. Roytburd, "Effective piezoelectric constants in ferroelectric films as MEMS sensors", 2005 MRS Spring Meeting Proceedings, CC 5.7.

Journal papers in preparation

1. Jun Ouyang, and A. L. Roytburd, " Effective piezoelectric constants of epitaxial ferroelectric films", Applied Physics A (submitted).

2. Jun Ouyang, R. Ramesh and A. L. Roytburd, "Evaluation of piezoelectric properties of relaxor ferroelectric films for MEMS applications ", Thin Solid Films (submitted).

3. Jun Ouyang, Z. K. Ma, R. Ramesh, and A. L. Roytburd, "Theoretical modeling of coexisting tetragonal and rhombohedral heterophase polydomain structures in lead zirconate titanate ferroelectric films near the morphotropic phase boundary", Physical Review B, (submitted).

4. Jun Ouyang, D. M. Kim, I. Levin, S. Trolier-McKinstry, Z. K. Ma, S. Y. Yang, J. Melngailis, C. B. Eom, A. L. Roytburd, R. Ramesh "Ultrahigh piezoelectric response in epitaxial ferroelectric thin films" (in preparation for Nature Materials).

5. Jun Ouyang, D. M. Kim, Z. K. Ma, J. Melngailis, A. L. Roytburd, C. B. Eom and R. Ramesh, "Effect of micropatterning by focus ion beam milling on piezoelectric responses of 0.67 Pb ($Mg_{1/3}Nb_{2/3}$)-0.33 $PbTiO_3$ epitaxial films engineered for MEMS applications" (in preparation for Applied Physics Letters).

BIBLIOGRAPHY

[1] Haertling, G. H., "Ferroelectric Ceramics: History and Technology", J. Am. Ceram. Soc., vol. 82, No. 4, pp. 797-818 (1999).

[2] Lines, M. E. and Glass, A. M., Principles and Applications of Ferroelectrics and Related Materials, Oxford, 1977.

[3] Damjanovic, D., "Ferroelectric, dielectric and piezoelectric properties of ferroelectric thin films and ceramics", Rep. Prog. Phys., vol. 61, pp. 1267-1324 (1998).

[4] T. Tybell et al, Phys. Rev. Lett. **89**, 097601 (2002).

[5] Intellmat: www.intellimat.com

[6] M. J. Haun et al. Ferroelectrics 99, 13 (1989).

[7] X. Du, U. Belegundu, and K. Uchino, Jpn. J. Appl. Phys., Part 1 **36**, 5580 (1997).

[8] X. Du, J. Zheng, U. Belegundu, and K. Uchino, Appl. Phys. Lett. 72, 2421 (1998).

[9]. S.-E. Park and T. R. Shrout, J. Appl. Phys. 82 (4), 1804 (1997).

[10]. S. Wada, S. Suzuki, T. Noma, T. Suzuki, M. Osada, M. Kakihana, S-E. Park, L. E. Cross and T. R. Shrout, Jpn. J. Appl. Phys. 38, Part 1, No. 9B, 5505 (1999).

[11]. D. V. Taylor and D. Damjanovic, Appl. Phys. Lett. 76 (12), 1615 (2000).

[12]. M. Budimir, D. Damjanovic and N. Setter, J. Appl. Phys. 94(10), 6753 (2003).

[13] D. Damjanovic, F. Brem, and N. Setter, Appl. Phys. Lett. **80**(4), 652, (2002).

[14] Jun Ouyang, R. Ramesh and A. L. Roytburd, "Theoretical investigation of the intrinsic piezoelectric properties for tetragonal $BaTiO_3$ epitaxial films", Applied Surface Sciences (accepted).

[15]. R. Zhang, B. Jiang and W. Cao, J. Appl. Phys. 90(7), 3471 (2001). The following elastic and piezoelectric constants are used in our calculation: $\mathbf{C}_{13}^{E}$=10.2 GPa, $\mathbf{C}_{33}^{E}$=10.3 GPa, $d_{31}^{m} = -1330\,\text{pm/V}$, $d_{33}^{m} = 2895\,\text{pm/V}$.

[16]. R. Zhang, B. Jiang and W. Cao, Appl. Phys. Lett, 82 (5), 787 (2003). The

following elastic constants are used in our calculation: $\mathbf{C}_{11}^{E}$=201.2 GPa, $\mathbf{C}_{12}^{E}$=73.6 GPa, $\mathbf{C}_{13}^{E}$=115 GPa, $\mathbf{C}_{14}^{E}$=41.5 GPa, $\mathbf{C}_{33}^{E}$=171.2 GPa, $\mathbf{C}_{44}^{E}$=29 GPa, $d_{15} = 4100\,\text{pm/V}$, $d_{12} = -1340\,\text{pm/V}$. $d_{31} = -90\,\text{pm/V}$, $d_{33} = 190\,\text{pm/V}$.

[17]. R. Zhang, B. Jiang and W. Cao, Appl. Phys. Lett, 82 (21), 3737 (2003).

[18]. R. Ahluwalia, T. Lookman, A. Saxena and W. Cao, Appl. Phys. Lett, 84 (18), 3450 (2004).

[19]. D. Damjanovic, M. Budimir, M. Davis and N. Setter, Appl. Phys. Lett, 83 (3), 527 (2003).

[20]. C. Kittel, Introduction to solid state physics, 6th edition, John Wiley & Sons, New York, 1986.

[21]. B. A. Strukov, A. P. Levanyuk, Ferroelectric Phenomena in Crystals, Springer, New York, 1998.

[22]. Lang Chen, J. Ouyang, Z.-K. Ma and A. L. Roytburd (submitted).

[23]. M. Iwata and Y. Ishibashi, Jpn. J. Appl. Phys. 39, Part 1, No. 9A, 5156 (2000).

[24]. M. Iwata, H. Orihara, and Y. Ishibashi, Jpn. J. Appl. Phys. 40, Part 1, No. 2A, 703 (2001).

[25]. B. Noheda, D. E. Cox, and G. Shirane, R. Guo, B. Jones, and L. E. Cross, Phys. Rev. B, **63,** 014103 (2000), and the associated references.

[26]. H. Fu and R. E. Cohen, Nature, 403, 281-283 (2000).

[27]. L. Bellaiche, A. García and D.Vanderbilt, Phys. Rev. B **64**, 060103(R) (2001)

[28]. R. E. Cohen, E. Heifets and H. Fu, Fundamental Physics of Ferroelectrics 2001, 11-22.

[29]. E. Heifets and R. E. Cohen, Fundamental Physics of Ferroelectrics 2002, 150-159.

[30]. W. G. Cady: *Piezoelectricity*, **Vol. 1** (Dover Publications, New York, 1964).

[31]. K. R. Udayakumar, J. Chen, A. M. Flynn, S. F. Bart, L. S. Tavrow, D. J.

Ehrlich, L. E. Cross, and R. A. Brooks: Ferroelectrics, **160**, 347 (1994).

[32]. Y. Nemirovsky, A. Nemirovsky, P. Muralt, and N. Setter: Sens. Actuators A, **56**, 239 (1996).

[33]. D. L. Polla, L. F. Francis: Annu. Rev. Mater. Sci. 28 (1998).

[34]. P. Muralt: J. Micromech. Microeng. **10**, 136 (2000).

[35]. S. Trolier-Mckinstry, P. Muralt: J. Electroceramics, **12**, 7 (2004).

[36]. K. Lefki and G. J. M. Dormans: J. Appl. Phys. **76**, 1764 (1994).

[37]. A. Barzegar, D. Damjanovic, N. Ledermann and P. Muralt: J. Appl. Phys. **93**, 4756 (2003).

[38]. F. Xu, F. Chu, and S. Trolier-McKinstry: J. Appl. Phys. **86**, 588 (1999).

[39]. J. F. Shepard Jr., P. J. Moses, S. Trolier-Mckinstry: Sens. Actuators A, **71**, 133 (1998).

[40]. Q. F. Zhou, Q. Q. Zhang, T. Yoshimura and S. Trolier-McKinstry: Appl. Phys. Lett. **82**, 4767 (2003).

[41]. J. A. Christman, R. R. Woolcott, Jr., A. I. Kingon and R. J. Nemanich: Appl. Phys. Lett. 73, 3851 (1998).

[42]. J. F. Li, D. D. Viehland, T. Tani, C. D. E. Lakeman, and D. A. Payne: J. Appl. Phys. **75**, 442 (1994).

[43]. L. Chen, J-H. Li, J. Slutsker, J. Ouyang and A. L. Roytburd: J. Mater. Res. **19**, 2853 (2004).

[44]. Jun Ouyang, S.-Y. Yang, L. Chen, R. Ramesh and A. L. Roytburd: Appl. Phys. Lett. **85,** 278 (2004).

[45]. D-J. Kim, J-P Maria A. I. Kingon and S. K. Streiffer, J. Appl. Phys. **93**, 5568 (2003).

[46]. A. L. Roytburd and N. S. Kosenko, Phys. Stat. Sol. (a) **35**, 735(1976).

[47]. A. L. Roytburd, Phys. Stat. Sol. (a) **37**, 329 (1976).

[48]. A. L. Roytburd, J. Appl. Phys. **83**, 228 (1998).

[49]. J. F. Nye, Physical Properties of Crystals, Oxford Press, 1957.

[50]. D. L. Polla, L. F. Francis, MRS Bull., July, 59, (1996).

[51]. J. J. Bernstein, S. L. Finberg, K. Houston, L. C. Niles, H. D. Chen, L. E. Cross, K. K. Li, and K. Udayakumar, IEEE Trans. Ultrason. Ferroelectr. Freq. Control **44**, 960 (1997).

[52]. Jun Ouyang, R. Ramesh and A. L. Roytburd, Appl. Phys. Lett. **86**, 152901 (2005).

[53]. An unusual substrate bending effect may dramatically change the apparent piezoelectric constants of a ferroelectric film if the substrate is not thick enough and its bottom surface is not fixed, as has been discussed by Barzegar et al. in measurement of "direct" piezoelectric constants, [37] and by Chen et al. in measurement of "converse" piezoelectric constants.[43]

[54]. V. Nagarajan, A. Stanishevsky, L. Chen, T. Zhao, B.-T. Liu, J. Melngailis, J. Finder, Z. Yu, R. Droopad, and K. Eisenbeiser, A. L. Roytburd, and R. Ramesh, *Appl. Phys. Lett.* **2002**, *81*, 4215.

[55]. D. Fu, H. Suzuki, T. Ogawa and K. Ishikawa, *Appl. Phys. Lett.* **80**, 3572 (2002).

[56]. J. D. Freire and R. S. Katiyar, *Phys. Rev. B*, **1988**, *37*, 2074. The following elastic constants are used for calculation: $\mathbf{C}_{11}^{E}$=143.3 GPa, $\mathbf{C}_{12}^{E}$=32.2 GPa, $\mathbf{C}_{13}^{E}$=24.1 GPa, $\mathbf{C}_{33}^{E}$=131.6 GPa, $\mathbf{C}_{44}^{E}$=55.8 GPa, $\mathbf{C}_{66}^{E}$=55.6 GPa.

[57]. T. Mitsui, S. Nomura, M. Adachi, J. Harada, T. Ikeda, E. Nakamura, E. Sawaguchi, T. Shigenari, Y. Shiozaki, I. Tatsuzaki, K. Toyoda, T. Yamada, K. Geshi, Y. Makita, M. Marutake, T. Shiosaki, and K. Wakino, in *Landolt-Börnstein*, Vol. 16 (Eds: K.-H. Hellwege and A. M. Hellwege), Springer, **Berlin, 1981**, Group III: Crystal and Solid State Physics: Ferroelectrics and Related Substances. Pseudo-tetragonal elastic compliances were given as function of x for bulk $Pb(Zr_xTi_{1-x})O_3$ ceramics near the morphotropic boundary (x=0.48~0.6). For rhombohedral PZT (x≥0.52), the compliance data were obtained by the following procedures:[7] The average value of s_{11}^{E} and s_{33}^{E} was used as s_{11}^{E}, the average value of s_{12}^{E} and s_{13}^{E} was used as s_{12}^{E}, and the average value of s_{44}^{E} and s_{66}^{E} was used as s_{44}^{E} in the axis system for the cubic phase. Then the cubic axis system was rotated to the rhombohedral axis system and the elastic compliance data were obtained by rules of tensor operations.[49]

[58]. N. Ledermann, P. Muralt, J. Baborowski, S. Gentil, K. Mukati, M. Cantoni, A. Seifert, and N. Setter, Sens. Actuators, A **105**, 162 (2003).

[59]. K.-H. Hellwege and A. M. Hellwege Springer, *Numerical Data and*

Functional Relationship in Science and Technology, Landolt-Bőrnstein, Berlin, 1981, **16**, 3. The following elastic compliances are used: $\mathbf{s}_{11}^{E}$=7.74 TPa^{-1}, $\mathbf{s}_{12}^{E}$=-2.17 TPa^{-1}, $\mathbf{s}_{44}^{E}$= 12.6 TPa^{-1}.

[60]. K.-H. Hellwege and A. M. Hellwege Springer, *Numerical Data and Functional Relationship in Science and Technology*, Landolt-Bőrnstein, Berlin, 1981, **Vol. 16**, 64, the following elastic compliances are used for a $SrTiO_3$ substrate: $\mathbf{s}_{11}$=3.772 TPa^{-1}, $\mathbf{s}_{12}$=-0.926 TPa^{-1}, $\mathbf{s}_{44}$=8.233TPa^{-1}.

[61]. R. Zhang, B. Jiang and W. Cao, J. of Mater. Sci. Lett. **21**, 1877, (2002).

[62]. A. Garcia and D. Vanderbilt, Appl. Phys. Lett. **72**(23), 2981, (1998).

[63]. A. G. Luchaninov, V.I.Aleshin and L.A.Shuvalov, Phys. of Solid State, **41**(6), 984, (1999).

[64]. D. Liu and J.-Y. Li, Appl. Phys. Lett. **83**(6), 1193, (2003).

[65]. R. A. Mckee, F. J. Walker, J. R. Conner, D. E. Zelmon, and E. D. Specht, Appl. Phys. Lett. **59**(7), 782, (1991).

[66]. K. Nashimoto and D. K. Fork, Appl. Phys. Lett. **60**(10), 1199, (1992).

[67]. T. Zhao, H. Lu, F. Chen, G. Yang, and Z. Chen, J. Appl. Phys. **87**(10), 7448, (2000).

[68]. Yu. A. Boikov and T. Claeson, Phys. of the Solid State, **43**(2), 337, (2001).

[69]. Yu. A. Boikov and T. Claeson, J. Appl. Phys. **89**(9), 5053, (2001).

[70]. K. J. Choi, M. Biegalski, Y. L. Li, A. Sharan, J. Schubert, R. Uecker, P. Reiche, Y. B. Chen, X. Q. Pan, V. Gopalan, L.-Q. Chen, D. G. Schlom, C. B. Eom, Science **306**, 1005, (2004).

[71]. Jun Ouyang, R. Ramesh and A. L. Roytburd, Advanced Engineering Materials, **7**, 229 (2005).

[72]. D. Berlincourt and H. Jaffe, Phys. Rev. **111**, 143 (1958).

[73]. A. Schaefer, H. Schmitt, and A. Dorr, Ferroelectrics **69**, 253, (1986).

[74]. Z. Li, S.-K. Chan, M. H. Grimsditch, and E. S. Zouboulis, J. Appl. Phys. **70**(12), 7327, (1991).

[75]. R. Zhang, W. Jiang, B. Jiang and W. Cao, in: R. Cohen (Eds.), Fundamental

Physics of Ferroelectrics, Williamsburg, VA, U.S.A., February 6-9, 2002.

[76]. H. Cao, V.-H. Schmidt, R. Zhang, W. Cao and H. Luo, J. Appl. Phys. 96 549 (2004).

[77]. S. Zhang, C.-A. Randall, and T. R. Shrout, J. Appl. Phys. 95, (2004) 4291.

[78]. Jun Ouyang, D. M. Kim, C. B. Eom, R. Ramesh, and A. L. Roytburd, Smart Materials and Structures, 14, 524 (2005).

[79]. D. Bonnell, Scanning Probe Microscopy and Spectroscopy, 2nd Edition, Wiley-VCH, New York, 2000.

[80]. C. S. Ganpule, Ph.D. dissertation, 2001, University of Maryland.

[81]. Manual for SR-830 Lock-in Amplifier, Stanford Research System.

[82]. C. S. Ganpule, A. Stanishevsky, Q. Su, S. Aggarwal, J. Melngailis, E. Williams, and R. Ramesh, Appl. Phys. Lett. **75**, 409 (1999).

[83]. J. A. Christman, R. R. Woolcott Jr., A. I. Kingon and R. J. Nemanich, Appl. Phys. Lett. **73**, 3851 (1999).

[84]. S. Y. Yang, B. T. Liu, J. Ouyang, V. Nagarajan, V. N. Kulkarni, R. Ramesh J. Kidder, R. Droopad & K. Eisenbeiser, J. of Electroceramics, **14**, 37 (2005).

[85]. V. Nagarajan, I. G. Jenkins, S. P. Alpay, H. Li, S. Aggarwal, L. Salamanca-Riba, A. L. Roytburd and R. Ramesh, J. Appl. Phys. **86**, 595 (1999).

[86]. A. Gruverman, O. Auciello and H. Tokumoto, Annu. Rev. Mater. Sci., 1998, 28: 101.

[87]. C. B. Eom, R. J. Cava, R. M. Fleming, J. M. Phillips, R. B. Vandover, J. H. Marshall, J. W. P. Hsu, J. J. Krajewski, and W. F. Peck, Science, **258**, 1766 (1992).

[88]. According to our experience[85], large internal stresses present in sub-micron PMN-PT films and lead to degradation of electromechanical properties. Thick films have higher degree of relaxation and better crystallinity, therefore a large film thickness like this one was chosen in this work.

[89]. V. Nagarajan, C. S. Ganpule, B. Nagaraj, S. Aggarwal, S. P. Alpay, A. L. Roytburd, E. D. Williams, and R. Ramesh, Appl. Phys. Lett. **75**, 4183 (1999).

[90]. Y. Yu and A. L. Roytburd, TMS, "Twinning in advanced Materials", 1994.

[91]. N. A. Pertsev and A. Yu. Emelyanov, Appl. Phys. Lett. **71**, 3646 (1997).

[92]. A. L. Roytburd, S. P. Alpay, L. A. Bendersky, V. Nagarajan, and R. Ramesh, J. Appl. Phys. **89**, 553 (2001)

[93]. Q. M. Zhang, W. Y. Pan, S.J. Jang, L. E. Cross, J. Appl. Phys. **64**, 6445 (1988).

[94]. R. Herbeit, U. Robels, H. Dederichs, G. Arlt, Ferroelectrics, **98**,107 (1989).

[95]. Q. M. Zhang, H. Wang, N. Kim and L. E. Cross, J. Appl. Phys. **75**, 454 (1994).

[96]. L. Chen, V. Nagarajan, R. Ramesh and A. L. Roytburd, J. Appl. Phys. **94**, 5147 (2003).

[97]. A. L, Kholkin, M. L. Calzada, P, Ramos, J, Mendiola, N. Setter, *Appl. Phys. Lett.* **69** (23), 3602 (1996).

[98]. F. Xu, S. Trolier-McKinstry, W. Ren, and B. Xu, J. Appl. Phys. **89** (2) 1336 (2001).

[99]. O. Kuffer, I. M. Aprile, J.-M Triscone, Q. Fischer, and Ch. Renner, Appl. Phys. Lett. **77**, 1701 (2000).

[100]. S. Buhlmann, B. Dwir, J. Baborowski and P. Muralt, Appl. Phys. Lett. **80**, 3195 (2002).

[101]. D.-J. Kim, J.-P. Maria and A. I. Kingon, J. Appl. Phys. **93** (9), 5568 5575 (2003).

[102]. V. Nagarajan, A. Stanishevsky, L. Chen, T. Zhao, B.-T. Liu, J. Melngailis, J. Finder, Z. Yu, R. Droopad, and K. Eisenbeiser, A. L. Roytburd, and R. Ramesh, Appl. Phys. Lett. **81**, 4215 (2002).

[103]. S. Trolier-Mckinstry, private communication.

[104]. L. Bellaiche, A. Garcia, and D. Vanderbilt, Phys. Rev. Lett. **84**, 5427 (2000).

[105]. D. A. Berlincourt, C. Cmolik, and H. Jaffe, Proceedings of the IRE, **48**, 220 (1960).

[106]. Technical Publication TP-220, Piezoelectric Transducer Materials – Stress, Morgan Electro Ceramics.

[107]. Technical data (typical values), PZT piezoelectric materials, CTS wireless Components (2000).

[108]. Materials Characteristic for BM 500 PZT, Sensor Technology Limited.

[109]. Typical Parameters of Piezoelectric Ceramics, PI Inc. Germany.